

# **ANALYTICAL PERFORMANCE EVALUATION OF OFDM IN PRESENCE OF CHANNEL ESTIMATION ERROR AND CARRIER FREQUENCY OFFSET**

A

Thesis Report

Submitted to

**The Dipartimento di Elettronica, Informazione e Bioingegneria**

**POLITECNICO DI MILANO, MILANO, ITALY**



**In partial fulfilment for the award of degree of**

**MASTER OF SCIENCE**

**IN**

**ELECTRONICS ENGINEERING**

Supervisor:

**Prof. Maurizio Magarini**

Co-Supervisor:

**Atul Kumar**

Submitted By:

**Sarvraj Singh Ranhotra**

**10475594**



## **POLITECNICO DI MILANO**

P.zza L. da Vinci, 32, 20133 Milano, Italy

Phone: 800.02.2399 Fax: +39.02.2399.2206

Website: [www.polimi.it](http://www.polimi.it)

---

### **CERTIFICATE**

This is to certify that “Sarvraj Singh Ranhotra 835942 (10475594)” student of **Electronics Engineering** from “POLITECNICO DI MILANO, ITALY” has done Thesis at “**Politecnico di Milano, Milano, ITALY**” in the partial fulfilment for the award of degree of “**Master of Science**” under the guidance of “**Prof. Maurizio Magarini**” and “**Phd. Atul Kumar**”

The project work entitled as “**ANALYTICAL PERFORMANCE EVALUATION OF OFDM IN PRESENCE OF CHANNEL ESTIMATION ERRORS AND CARRIER FREQUENCY OFFSET**” embodies the original work done for Thesis. This work has not been submitted partially or wholly to any other university or institute for the award of this or any other degree.

**Prof. Maurizio Magarini**  
**Dipartimento di Elettronica, Informazione e**  
**Bioingegneria (DEIB)**

**Atul Kumar**  
**PhD, DEIB**

# ACKNOWLEDGEMENT

The thesis on “*Analytical Performance Evaluation of OFDM in Presence of Channel estimation Errors and carrier frequency offset*” is presented here.

I would like to express my deepest appreciation to all those who provided me the possibility to complete this report. A special and sincere gratitude I give to Professor Maurizio Magarini, whose contribution in problem formulation, development of a methodological approach towards it and in stimulating suggestions and encouragement, helped me to coordinate my project especially in writing this report.

Furthermore I would also like to acknowledge with much appreciation the crucial role of my co-supervisor Atul Kumar, who gave the permission to use all required equipment and the necessary material to complete the chapter on channel Estimation errors with frequency offsets.

I have to appreciate the guidance given by other supervisor as well as the panels especially in our project presentation that has improved our presentation skills thanks to their comment and advices.

.....  
Sarvraj Singh Ranhotra

## List of Abbreviations

S.No.	Abbreviation	Description
1	1G	First Generation
2	2 G	Second Generation
3	2.5 G	Third Generation
4	3GPP	3G Partnership Project
5	4G	Fourth Generation
6	5G NOW	5th Generation Non-Orthogonal Waveforms for Asynchronous Signalling
7	ADC	Analog-to-digital converter
8	ADSL	Asymmetric Digital subscriber lines
9	AMPS	Advanced Mobile Phone System
10	AMTS	Advanced Mobile Telephone System
12	AWGN	Additive White Gaussian Noise
12	BER	Bit Error Rate
13	BW	Band Width
14	CCDF	Complementary Cumulative Distributive Function
15	CDMA	Code Division Multiple Access
16	CFO	Carrier Frequency Offset
17	CP	Cyclic Prefix
18	DAB	Digital Audio Broadcasting
19	DAC	Digital-to-Analog converter
20	DFTFT	Discrete Fractional Fourier Transform
21	DFT	Discrete Fourier Transform
22	FFT	Fast Fourier Transform
23	DSP	Digital Signal Processing
24	DVB-T	Terrestrial Digital Video Broadcasting
25	FDD	Frequency Division Duplex
26	FDM	Frequency Division multiplexing
27	FDMA	Frequency Division multiplexing Access

28	FEQ	Frequency Domain Equalizer
29	FFO	Fractional Frequency Offset
30	FM	Frequency Modulation
31	FrFT	Fractional Fourier Transform
32	FT	Fourier Transform
33	Gbps	Giga bit per second
34	HDSL	High Bit Rate Digital Subscriber line
35	HPA	High Power Amplifier
36	ICI	Inter Carrier Interference
37	IDFT	Inverse Discrete Fourier Transform
38	IFFT	Inverse Fast Fourier Transform
39	IFO	Integer Frequency Offset
40	Kbps	Kilobit Per Sec
41	MB-OFDM	Multiband OFDM
42	MC	Multi Carrier
43	MCM	Multi Carrier Modulation
44	MC-CDMA	Multi Carrier CDMA
45	MMSE	Minimum Mean-Square Error
46	M-PSK	M-ary Phase shift keying
47	M-QMA	M-ary Quadrature Amplitude Modulation
48	OFDM	Orthogonal Frequency Division Multiplexing
49	OFDMA	Orthogonal Frequency Division Multiplexing Access
50	PAPR	Peak to Average Power Ratio
51	SC	Single Carrier
52	SIR	Signal to interference Ratio
53	SNR	Signal to Noise Ratio
54	TDD	Time Division Duplex
55	TDM	Time Division Multiplexing
56	TDMA	Time Division Multiplexing Access
57	W-CDMA	Wideband CDMA
58	DSP	Digital Signal Processing

<b>59</b>	<b>FPGA</b>	Field Programmable Gate Array
<b>60</b>	<b>SDR</b>	Software Defined Radio
<b>61</b>	<b>ZED</b>	Zynq™ Evaluation and Development
<b>62</b>	<b>EPP</b>	Extensible Processing Platform
<b>63</b>	<b>PS</b>	Processing System
<b>64</b>	<b>PL</b>	Programmable Logic
<b>65</b>	<b>ISI</b>	Inter-Symbol Interference
<b>66</b>	<b>FBMC</b>	Filter Bank Multi-Carrier
<b>67</b>	<b>GFDM</b>	Generalized Frequency Division Multiplexing
<b>68</b>	<b>UFMC</b>	Unified Frequency Multi-Carrier
<b>69</b>	<b>HST</b>	High-speed trains
<b>70</b>	<b>RTL</b>	Register-Transfer Level
<b>71</b>	<b>STO</b>	Symbol Timing Offset
<b>72</b>	<b>VHDL</b>	VHSIC Hardware Description Language
<b>73</b>	<b>BFDM</b>	Bi-orthogonal Frequency Division Multiplexing
<b>74</b>	<b>MIMO</b>	multiple-input multiple-output
<b>75</b>	<b>Fi</b>	Fixed point representation
<b>76</b>	<b>HDL</b>	Hardware Description Language
<b>77</b>	<b>LTE-A</b>	Long Term Evolution - Advanced
<b>78</b>	<b>MTC</b>	Machine-Type-Communication
<b>79</b>	<b>M2M</b>	Machine-To-Machine
<b>80</b>	<b>RF</b>	Radio Frequency
<b>81</b>	<b>ESM</b>	Emission Spectrum Mask
<b>82</b>	<b>PHY</b>	Physical Layer
<b>83</b>	<b>CoMP</b>	Coordinated Multipoint
<b>84</b>	<b>UMTS</b>	Universal Mobile Telecommunications System
<b>85</b>	<b>MAC</b>	Medium Access Layers

## List of Symbols

S. No	Symbols	Description
1	$\varepsilon$	Carrier-frequency offset normalized by sub-carrier spacing
2	$\Re$	Real part
3	$\Im$	Imaginary part
4	$\gamma$ or $\varrho$	Average SNR
5	$\alpha$	Angle parameter in FRFT
6	$\xi$	Conditional BER
7	$\tau_l$	Propagation Delay of the $l^{th}$ path
8	$\sigma_l^2$	Variance of each $l^{th}$ path
9	$\sigma_w^2$	Variance of AWGN
10	$\sigma_{ICI}^2$	ICI Power of the $q^{th}$ Sub-Carrier
11	$\tau_{max}$	Maximum channel delay spread
12	$\Delta f$	Carrier-frequency offset (CFO)
13	$E[.]$	Expectation average
14	$f_k = k/T_u$	Sub-carrier Frequency of the $k^{th}$ sub-carrier
15	$G$ or CP	total Number of sub-carrier in Guard Band (CP)
16	$h(\tau, t)$	Multipath fading channel impulse response
17	$h_l(t)$	complex amplitude or tap coefficient of the $l^{th}$ path
18	$H(k)$ or $\beta(k)$	Channel Response in frequency domain
19	$L$	Total number of path
20	$N_0/2$	Noise variance
21	$N$	Total Number of sub-carrier
22	$r(i, t)$	Received signal in time domain
23	$r(i, n)$	Received signal in frequency domain
24	$S(k - p + \varepsilon)$	ICI Coefficient
25	$SIR_q$	Signal to interference ratio on $q^{th}$ sub-carrier
26	$T_s$	Sampling time
27	$T_u$	Uses full symbol duration

28	$T_g$	Guard band time
29	$T_{sym}$	Symbol time
30	$T_{th}$	Threshold time
31	$w(i, t)$	AWGN noise
32	$\varphi(\omega)$	Output of characteristic function
33	$P_b(\xi)$	Conditional BER
34	$P_b$	Unconditional BER
35	$\beta_k$	Real part of ICI term
36	$\delta_k$	Imaginary part of ICI term
37	$\Delta \theta$	Symbol timing offset
38	$g(\cdot)$	Raised cosine impulse response
39	$sgn(\cdot)$	Signum function
40	$H(\cdot)$	Hermitian transpose
41	$\overline{(\cdot)}$	Complex conjugate

## List of Tables

S. No.	Table no.	Title of the Table	Page No.
1.	Table-2.1	Complexity analysis for OFDM(with switching) and OFDM(without switching)	13
2.	Table-3.1	Physical Signals in both Uplink(UL) and Downlink(DL)	36
3.	Table-3.2	EPA, EPA, ETU propagation fading model description	41
4.	Table-3.3	Complexity of Least Squares(LS) and Least Minimum Mean Square Error(LMMSE)	46
5.	Table-3.4	Complexity of DFT based interpolation and Linear interpolation	48
6.	Table-3.5	Parameters of LTE downlink System	49
7.	Table-3.6	Resource Allocation for Synchronization Signals and Reference signals using both normal and Extended Cyclic prefix	49
8.	Table-4.1	Summary of OFDM	60
9.	Table-4.2	Summary of OFDM based system with CFO	64

## List of Figures

S. No.	Figure no.	Caption of the Figure	Page No.
1.	Fig. 1.1.1	Frequency spectrum of OFDM subcarrier signals	2
2.	Fig. 1.1.2.1	Roadmap of Channel Estimation Techniques	3
3.	Fig. 1.1.2.2	Mapping sub carriers to transferred modulated OFDM symbols	4
4.	Fig. 1.1.2.3	Frequency and Phase Response	5
5.	Fig. 2.1.1	Time/frequency offset correction and channel estimation/equalization in an OFDM receiver	10
6.	Fig. 2.1.2	Time-frequency grid for an OFDM system with three pilot patterns: entirely known OFDM symbols Block type, pilot subcarriers- Comb Type and scattered pilots .	12
7.	Fig. 2.2.1	Digital implementation of Baseband OFDM system	13
8.	Fig. 2.4.2.2.1	Block Diagram of training process for ANN based method	25
9.	Fig. 2.4.2.3.1	Comparison of PAPR's CCDF with number of subcarriers $N = 64$ (Wireless LAN standard) and $N =$	26

		256 (WiMAX standard)	
10.	Fig. 2.5.1.1	Artificial Neural Network Structure	29
11.	Fig. 2.6.1.	SER Performance versus SNR for Block-Type Pilot Channel Estimation Based on LS, MMSE, and OLR-MMSE algorithms	30
12.	Fig. 2.6.2	SER Performance versus SNR for the Channel Estimators Based On LS with Block-Type and Comb-Type Pilot Arrangements	31
13.	Fig. 2.6.3	16QAM Modulation with Rayleigh fading- Comparison of conventional channel estimates techniques with those implemented with Artificial Neural Network	32
14.	Fig. 2.6.4	BPSK Modulation with Rayleigh fading -Comparison of conventional channel estimates techniques with those implemented with Artificial Neural Network	33
15.	Fig. 2.6.5	Comparison of BER performance for Wireless LAN standard.	33
16.	Fig. 2.6.6	Comparison of BER performance for WiMAX standard	34
17.	Fig. 3.2.1.1	Frame structure of LTE in FFD mode	35
18.	Fig. 3.2.1.2	1 <sup>st</sup> slot of LTE radio frame	36
19.	Fig. 3.2.1.2.1	Cell-specific reference signals	37
20.	Fig. 3.2.1.3.1.1	Correlation between the different roots	38
21.	Fig. 3.2.1.3.2	SSS signal of 62 symbols	39
22.	Fig. 3.2.5.1	Averaging Channel estimates at pilot symbol locations	43
23.	Fig. 3.2.5.1.2	Scenario for virtual Pilots Subsystem. P-Pilot, dashed array- Resource elements (RE) which cannot be determined by interpolation	43
24.	Fig. 3.2.5.1.3	Virtual Pilot Placement	44
25.	Fig. 3.2.5.1.4	Calculating Virtual Pilot Symbol values	45
26.	Fig. 3.2.6.1	Transmit Resource Grid with 72 subcarriers	50
27.	Fig. 3.2.6.2	Transmit waveform	51
28.	Fig. 3.2.6.3	Received Resource Grid passed through Extended Typical Urban model(ETU) multipath fading propagation condition	52
29.	Fig.3.2.6.4	Noisy Received Waveform	53
30.	Fig.3.2.6.5	Perfect Channel surface for Extended Typical Urban model(ETU) multipath fading propagation condition	54
31.	Fig.3.2.6.6	Estimated Channel Surface for Extended Typical	54

		Urban model(ETU) multipath fading propagation condition, Type of Channel Estimator LMMSE.	
32.	Fig.3.2.6.7	Perfect Channel surface for Extended Pedestrian A model(EPA) multipath fading propagation condition	55
33.	Fig.3.2.6.8	Estimated Channel Surface for Extended Pedestrian A model(EPA) multipath fading propagation condition	55
34.	Fig.3.2.6.9	Perfect Channel Surface for Extended Vehicular A model multipath fading propagation condition	56
35.	Fig.3.2.6.10	Estimated Channel surface for Extended Vehicular A model multipath fading propagation condition	56
36.	Fig.3.2.6.11	Equalized Resource Grid, Type of Equalizer: MMSE	58
37.	Fig.3.2.6.12	Error In Equalization	58
38.	Fig.4.3.1	OFDM System Model	65
39.	Fig.4.4.1	(a)QPSK constellation with Grey coding, (b)16-QAM constellation with grey coding	74
40.	Fig.4.4.2	16-QAM bit by bit demapping	76
41.	Fig.4.5.1	BER expression of FFT based- OFDM system in presence of CFO and channel estimation error for BPSK in Rayleigh channel with $N = 8$ .	80
42.	Fig.4.5.2	BER expression of FFT based- OFDM system in presence of CFO and channel estimation error for QPSK in Rayleigh channel with $N = 8$	80
43.	Fig.4.5.3	BER expression of FFT based- OFDM system in presence of CFO and channel estimation error for 16 QAM in Rayleigh channel with $N = 8$ .	81
44.	Fig.4.5.4	BER expression of FFT based- OFDM system in presence of CFO and channel estimation error for BPSK in Rayleigh channel with tap filter length=5.	81
45.	Fig.4.5.5	BER expression of FFT based- OFDM system in presence of CFO and channel estimation error for QPSK in Rayleigh channel with tap filter length=5.	82
46.	Fig.4.5.6	BER expression of FFT based- OFDM system in presence of CFO and channel estimation error for 16-QAM in Rayleigh channel with tap filter length=5.	82

# ABSTRACT

ABSTRACT(English): In this thesis, channel Estimation techniques have been summarized according to their performance index in terms of Bit error rate and implementation complexity, furthermore a comparison of performance is made with the estimators simulated using soft computing method, namely Artificial Neural Networks. Channel Estimation techniques are further extended to OFDM based Long Term Evolution(LTE). Followed by introducing analytical expression and performance comparison for OFDM based systems in presence of channel estimation error and Carrier Frequency Offset.

SOMMARIO(Italian):

In questa tesi, tecniche di stima di canale sono state analizzate in base al loro indice di prestazioni, in termini di tasso di errore sul bit e complessità di realizzazione, inoltre, un confronto tra le prestazioni è stato fatto tra gli stimatori simulati utilizzando un metodo soft computing chiamato Artificial Neural Networks. Tecniche di stima di canale sono ulteriormente estese alla tecnologia Long Term Evolution (LTE) basata su modulazione OFDM. In seguito si sono introdotte espressioni analitiche ed effettuato un confronto di prestazioni tra sistemi basati su OFDM in presenza di errore sulla stima di canale e offset sulla frequenza portante.

# CONTENTS

<b>Certificate .....</b>	<b>i</b>
<b>Acknowledgement .....</b>	<b>ii</b>
<b>Declaration by Scholars .....</b>	<b>iii</b>
<b>List of Abbreviations .....</b>	<b>iv</b>
<b>List of Symbols .....</b>	<b>vii</b>
<b>List of Tables .....</b>	<b>ix</b>
<b>List of Figures .....</b>	<b>x</b>
<b>Abstract (English and Italian).....</b>	<b>xii</b>
<b>1. INTRODUCTION AND MOTIVATION</b>	<b>1-9</b>
<b>1.1. Introduction</b>	
<b>1.1.1 Origin of OFDM</b>	<b>1-4</b>
<b>1.1.2 Thesis Objective and Contributions</b>	
<b>1.2. Motivation</b>	<b>5</b>
<b>1.3 Advantages &amp; Disadvantages of OFDM based on FFT/FrFT</b>	<b>7</b>
<b>1.3. Application</b>	<b>7-8</b>
<b>1.4 Organization of Thesis</b>	<b>8-9</b>
<b>2. CHANNEL ESTIMAION IN OFDM SYSTEMS</b>	<b>10-34</b>
<b>2.1. Literature Survey on techniques for Channel Estimation</b>	<b>10-12</b>
<b>2.2. System Model</b>	<b>13-14</b>

<b>2.3.</b>	<b>Channel Estimation Techniques</b>	<b>14</b>
<b>2.3.1.</b>	<b>Block Type Pilot Channel Estimation</b>	<b>15-17</b>
<b>2.3.1.1.</b>	<b>LS Estimator</b>	
<b>2.3.1.2</b>	<b>MMSE Estimator</b>	
<b>2.3.1.3</b>	<b>Modified MMSE Estimator</b>	
<b>2.3.1.4</b>	<b>Estimation with Decision Feedback</b>	
<b>2.3.2.</b>	<b>Comb- Type Pilot channel Estimation</b>	<b>18-19</b>
<b>2.3.2.1.</b>	<b>LS Estimator with 1 D Interpolation</b>	
<b>2.3.2.2.</b>	<b>Linear Interpolation(LI)</b>	
<b>2.3.2.3.</b>	<b>Second Order Interpolation (SOI)</b>	
<b>2.3.2.4.</b>	<b>Low Pass Interpolation(LPI)</b>	
<b>2.3.2.5.</b>	<b>Spline Cubic Interpolation(SCI)</b>	
<b>2.3.2.6.</b>	<b>Time Domain Interpolation (TDI)</b>	
<b>2.4.</b>	<b>Linking Artificial Neural Networks to OFDM systems</b>	<b>19</b>
<b>2.4.1.</b>	<b>System Model and PAPR Formulation</b>	<b>21</b>
<b>2.4.2.</b>	<b>Artificial Neural Networks</b>	<b>22</b>
<b>2.4.2.1.</b>	<b>Choice of efficient training algorithm</b>	
<b>2.4.2.2.</b>	<b>Practical Implementation</b>	
<b>2.4.2.3.</b>	<b>Complexity Analysis</b>	
<b>2.5.</b>	<b>Artificial Neural Network Channel estimation based on Levenberg-Marquardt for OFDM Systems</b>	<b>27</b>

2.6.	Simulated Results and Discussion	30
<b>3.</b>	<b>CHANNEL ESTIMATION IN LTE DOWNLINK</b>	34-61
3.1.	Introduction to 3GPP Specifications	34
3.2.	Design of Physical Layer LTE Downlink	35
3.2.1.	Frame Structure	35-39
3.2.1.1	Physical Signals	
3.2.1.2	Reference Signals	
3.2.1.3	Synchronization Signals	
3.2.1.3.1.	Primary Synchronization Signals(PSS)	
3.2.1.3.2.	Secondary Synchronization Signals(SSS)	
3.2.2.	OFDM Modulation	40
3.2.3.	Multipath fading propagation conditions	40-41
3.2.4.	OFDM Demodulation	42
3.2.5.	Channel Estimation for Downlink 3GPP-LTE systems	42-48
3.2.5.1	Pilot Signal Estimation	
3.2.5.2	Interpolation	
3.2.5.2.1.	Linear Interpolation	
3.2.5.2.2.	DFT based Interpolation	
3.2.5.3	Noise Estimation	
3.2.6.	Simulated Results and Discussion	49

3.3.	Development in Multicarrier Systems	59-59
<b>4.</b>	<b>OFDM SYSTEM IN PRESENCE OF CHANNEL ESTIMATION ERROR &amp; CARRIER FREQUENCY OFFSET</b>	<b>60-83</b>
4.1.	Historical Development of OFDM	60
4.2.	Literature Survey on OFDM System in Presence of Channel Estimation Error and Carrier Frequency Offset.	61-64
4.3	System Model	64
4.3.1.	Transmitter Model	65
4.3.1.1	Cyclic Prefix or guard band insertion	
4.3.2.	Channel Model	67
4.3.2.1	Frequency Selective Rayleigh Channel	
4.3.3.	Receiver Model	68-70
4.3.4.	Effect of Channel Estimation Error	70-71
4.4	BER Analysis of effects of Channel Estimation error in presence of Carrier Frequency Offset	71
4.4.1.	BPSK Modulation	72-74
4.4.2.	QPSK Modulation	74-75
4.4.3.	16 QAM Modulation	75-78
4.5	Simulation Results	79
4.5.1	Discussion of Results	

**5. CONCLUSION AND FUTURE SCOPE**

84-90

**5.1. Conclusion**

84

**5.2. Future Scope**

87

# CHAPTER-I

---

## INTRODUCTION AND MOTIVATION

Topics:

### 1.1. Introduction

#### 1.1.1 Origin of OFDM

#### 1.1.2 Thesis Objective and Contributions

### 1.2. Motivation

### 1.3. Advantages & Disadvantages of FFT/FrFT based- OFDM

### 1.4. Application

### 1.5. Organization of Thesis

---

This chapter consists of: the introduction of OFDM along with Thesis objective and contribution, the research motivation along with Advantage/Disadvantage, the applications of OFDM technique and the organization of thesis.

## 1.1. INTRODUCTION

Orthogonal frequency division multiplexing (OFDM) is one of the multi-carrier modulation (MCM) techniques that transmit signals through multiple carriers. These carriers (sub-carriers) have different frequencies and they are orthogonal to each other. Orthogonal Frequency Division Multiplexing based on Fast Fourier Transform (FFT -based OFDM) has drawn major attention in broad band wireless communication due to its various advantages like less complex equalizer, high data rate, efficient bandwidth utilization and robustness against multi-path fading channel *etc.* [1-5]. It has been adopted by many wireless communication standards such as IEEE 802.11, LTE, DVB-T2. The carrier frequency can go up to as high as 2.4 GHz or 5 GHz. Researchers tend to pursue OFDM operating at even much higher frequencies nowadays [6-10]. For example, the IEEE 802.16 standard proposes yet higher carrier frequencies ranging from 10 GHz to 60 GHz and terrestrial digital video broadcasting (DVB-T2) system [11-14].

### 1.1.1 Origin of OFDM

It is well known that **Chang** *et al.* [15] proposed the original OFDM principles in 1966, and successfully achieved a patent in January of 1970. Later on, **Saltzberg** *et al.* [18] analysed the OFDM performance and observed that the crosstalk was the severe problem in this system. Although each subcarrier in the principal OFDM systems overlapped with the neighbourhood subcarriers, the orthogonality can still be preserved through the staggered QAM technique. However, the difficulty will emerge when a large number of subcarriers are required. In some earlier OFDM applications [6-8], the number of subcarriers can be chosen up to 34. Such 34 symbols will be appended with redundancy of a guard time interval to eliminate inter-symbol interference (ISI) [9-14]. However, more subcarriers should be required and the modulation, synchronization and coherent demodulation would induce a very complicated OFDM requiring additional hardware cost. In 1971, **Weinstein** and **Ebert** *et al.* [18] proposed a modified OFDM system in which the discrete Fourier Transform (DFT)

was applied to generate the orthogonal subcarriers waveforms. Their scheme reduced the implementation complexity significantly, by making use of the inverse DFT (IDFT) modules and the digital-to-analog converters(DAC). In their proposed model, baseband signals were modulated by the IDFT at the transmitter and then demodulated by DFT at the receiver. Therefore, all the subcarriers were overlapped with others in the frequency domain, while the DFT modulation still assures their orthogonality, as shown in Fig. 1.1.1

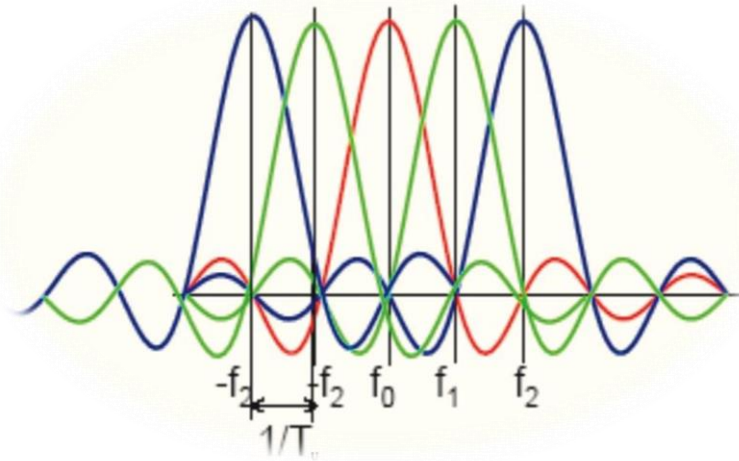


**Fig. 1.1.1** Frequency spectrum of OFDM subcarrier signals

Cyclic prefix (CP) was first introduced by **Peled** and **Ruiz** *et al.* [4] for OFDM systems. In their scheme, the conventional null guard interval is substituted by cyclic extension for fully-loaded OFDM modulation. As a result, the orthogonality among the subcarriers is guaranteed. Intercarrier Interference (ICI) is an impairment well known to degrade performance of Orthogonal Frequency Division Multiplexing (OFDM) transmissions. It arises from carrier frequency offsets (CFOs), from the Doppler spread due to channel time-variation and, to a lesser extent, from sampling frequency offsets (SFOs). With the trade-off of the transmitting energy efficiency, this new scheme[4] can result in a phenomenal ICI reduction. In 1980, **Hirosaki** *et al.* [24] introduced an equalization algorithm to suppress both ISI and ICI. In 1985, **Cimini** *et al.* [6] introduced a pilot-based method to reduce the interference emanating from the multipath and co-channels.

The many advantages responsible for the widespread application of OFDM systems are limited by the multipath fading. In OFDM systems, channel estimation is carried out by transmitting pilot symbols generally. In this thesis, an artificial neural network (ANN) channel estimation technique based on Levenberg-Marquardt training algorithm as an

alternative to pilot based channel estimation technique for OFDM systems over Rayleigh fading channels is described. Followed by application of channel estimation of OFDM based LTE systems Extending channel estimation to varying channels which produces channel estimation errors in the presence of Carrier Frequency offsets, An performance evaluation has been depicted.

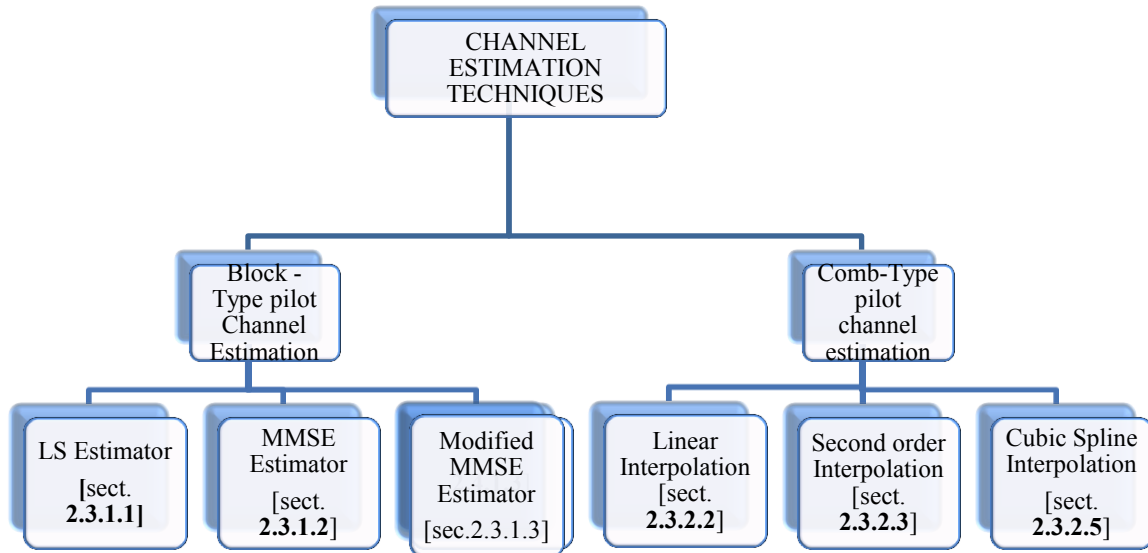


**Figure- 1.1.2.1** Roadmap of conventional Channel Estimation Techniques

### 1.1.2 Thesis Objective and Contribution

After the careful literature survey and study of OFDM system, and the foremost research area of channel estimation multicarrier system performance analysis is of my keen interest. In such a context for my M.S. Thesis I undertook the Thesis “Analytical Performance Evaluation of OFDM in Presence of Channel Estimation Errors and Carrier Frequency Offset”. Channel Estimation and its techniques have been realized and a comparison has been made on the performance analysis to start with. The Figure 1.1.2.1., displays most of the channel estimation techniques covered. Among main contributions I extended work done in [my paper] to multicarrier modulation schemes. An attempt has been made to simulate OFDM based multicarrier system using Artificial Neural Networks for IEEE802.11a wireless LAN (WLAN) and IEEE 802.11e WiMax standards. It is based on the scheme of replacement of data subcarriers with the null subcarriers to improve the Peak to average power ratio. Using Levenberg- Marquardt algorithm for the update rule of the weights in the neural network. Levenberg-Marquardt algorithm blends the steepest descent method and Gauss-

Newton algorithm and therefore it inherits advantage of faster convergence of Gauss-Newton algorithm and stability of steepest descent. It is one of the best choice as a learning method to train a feed- forward neural network. The network is trained using data patterns with low PAPR from null subcarrier switching scheme. In both OFDM standards the scheme with switching outperforms the scheme without switching. The performance of the described neural network based approach mainly depends on the training patterns, originated through conventional method.

Many advantages responsible for the widespread application of OFDM systems are limited by multipath fading. Frequency Selective fading caused by multipath could lead to carriers used, being heavily attenuated due to destructive interference at the receiver. This can result in carriers being lost in the noise. Figure 1.1.2.2 shows the behaviour of OFDM systems under Rayleigh frequency selective fading, Figure 1.1.2.3 depicts the frequency and phase response. To increase OFDM system performance under frequency selective channels, a channel estimation is required before the demodulation of OFDM signals. Here channel estimation comparison has been drawn between the performances of conventional and those based on Neural Network using Levenberg-Marquardt algorithm.

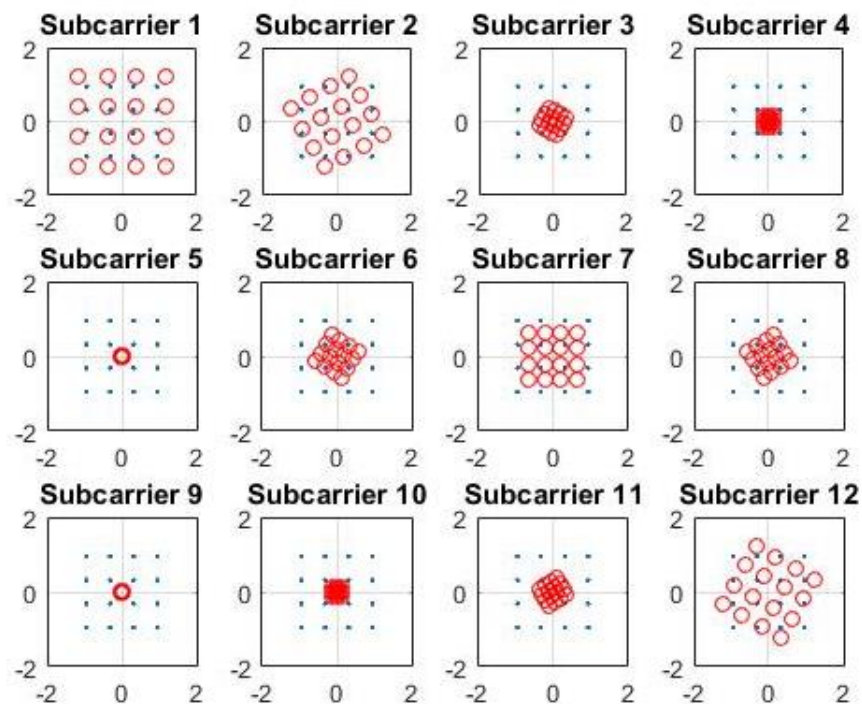


**Figure 1.1.2.2:** Mapping sub carriers to transferred modulated OFDM symbols

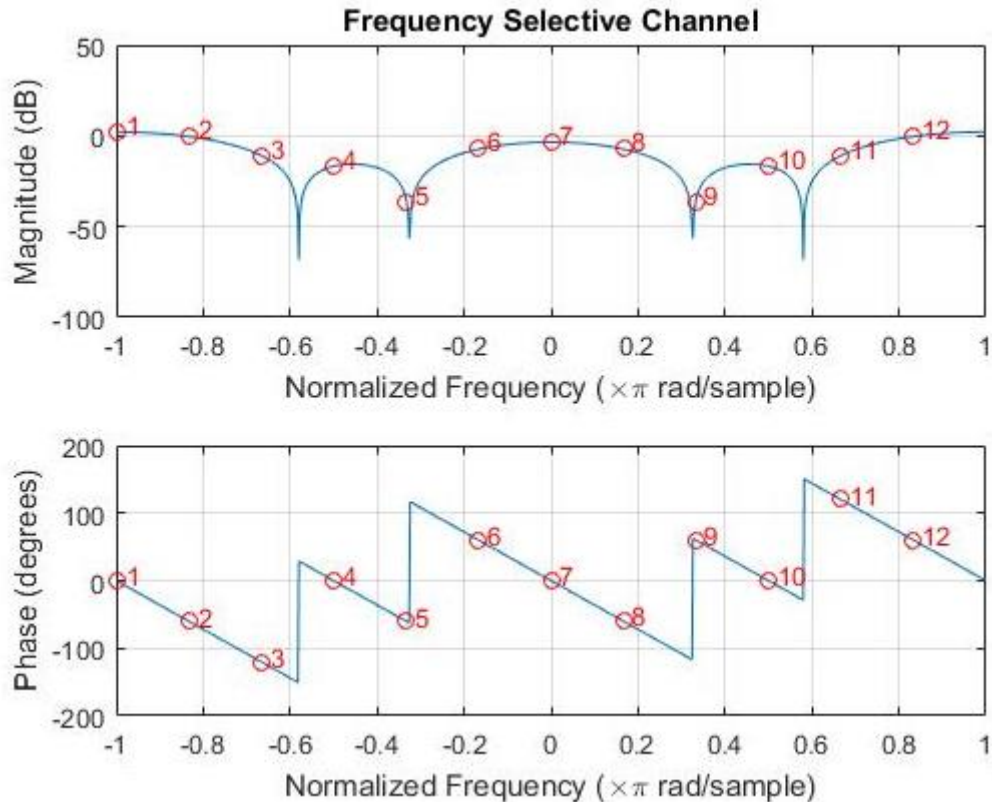


**Figure 1.1.2.3.:** Frequency and phase response

## 1.2. MOTIVATION

Before going to the discussion let's have a brief review of prior techniques.

- The main limitation of FDMA and TDMA (Frequency/Time Division Multiple Access) are the capacity (the number of users, which can be accommodated without interference).
- The CDMA (Code Division Multiple Access) technique has been developed mainly for capacity reasons.
- CDMA techniques can potentially accommodate more users than either TDMA or FDMA.
- W-CDMA is a 3G wireless standard, evolved from CDMA to support the wideband services at data rate higher than 2 Mbps.
- The wide band signal like DS-SS-CDMA (Direct Sequence CDMA) has a problem of frequency selective multipath fading.

- Frequency selective multipath fading is common in “Urban and Indoor Environment” and it is significant source of performance degradation.
- The performance degrades more if the number of users increases.
- It is observed that the narrow band signals are less sensitive to ISI and frequency selective fading.

Therefore, orthogonal multi-carrier modulation combined with CDMA has been used to solve the problem.

It is obvious that a parallel system is capable of carrying more information than a cascaded system, simply because it uses a variety of frequency bands. However, the significant advantage of OFDM is that it is robust in frequency selective channels, which results from either multipath fading or other communication interferences. In order to deal with frequency selective fading, the transmitted OFDM signals are divided into many sub-channels so that those sub-channels can be considered frequency flat approximately as the number of  $N$  sub-channels become large enough. Hence the OFDM signals will suffer less channel distortion than the conventional modulated signals.

Under OFDM modulation, the symbol duration becomes  $N$  times longer. For example, if the input data rate is 20Mbps, then, the symbol duration is 50 ns, however, in an OFDM system with 128 subcarriers, the symbol duration could become 6.4 us. If these two kinds of symbols are modulated and transmitted through a channel with a particular rms value say, rms = 60 ns, it is clear that the system with a longer symbol duration would perform better. In practice, the DVB-T2 standard suggests to use 2,048 subcarriers, or 8,192 subcarriers. In these cases, the symbol duration can be even increased by several thousand times.

FFT based OFDM system can be replaced by Fractional Fourier transform(FrFT).It is Discrete Fourier Transform (DFT) shifted by a fractional amount in frequency space (multiplying the input by a linear chirp) and evaluating at a fractional set of frequency points (e.g. considering only a small portion of the spectrum). Introduction to FrFT to OFDM systems was mainly due to less sensitivity of OFDM systems to Carrier Frequency offsets than the FFT counterparts. Further the advantages of FFT and FrFT OFDM based systems have been discussed.

### 1.3. ADVANTAGES & DISADVANTAGES OF OFDM BASED ON FFT AND FrFT

#### 1.3.1 Advantages

- High spectral efficiency.
- Efficient implementation using FFT.
- Low sensitivity to time synchronization error.
- OFDM has improved quality of narrow band interference.
- Can easily adapt to severe channel conditions without complex equalization.
- Robust against ISI and multipath Fading channel.
- Forward error correction is employed to accurate for sub-carrier that super form deep fades.
- Use of FrFT more Robust against ISI and multipath Fading channel as compare to FFT based- OFDM.
- FrFT -based OFDM less sensitive to CFO and STO.
- FrFT -based OFDM less sensitive to Doppler frequency spreading.

#### 1.3.2 Disadvantages

- Sensitive to frequency synchronization problem.
- Sensitivity to CFO at the receiver.
- Sensitivity to STO at the receiver.
- High High Peak-to-Average Power Ratio (PAPR), requiring linear transmitter circuitry, which suffers from poor power efficiency.
- FrFT -based OFDM increase the computational complexity.

### 1.4. APPLICATION

After the IFFT/FFT technique was introduced, the implementation of OFDM became more convenient. Generally speaking, the OFDM applications may be divided into two categories-wired and wireless technologies. In wired systems such as Asymmetric Digital Subscriber Line (ADSL) and high speed DSL, OFDM modulation may also be referred as Discrete Multitone Modulation (DMT). In addition, wireless OFDM applications may be shown in numerous standards such as:

- IEEE 802.11a/g, IEEE 802.16a [10].

- Asymmetric Digital Subscriber Line (ADSL) services [10].
- Digital Audio Broadcasting (DAB) [10].
- Digital Terrestrial Television Broadcasting: DVB-T in Europe, ISDB in Japan
- 4G, IEEE 802.11n, IEEE 802.16, and IEEE 802.20 [10].
- Generalized Frequency Division Multiplexing (GFDM) in 5th Generation Non-Orthogonal Waveforms (5GNOW) based on GFDM [47].
- Aspects of timing and frequency synchronization for LTE-A system.

OFDM was also applied for the development of Digital Video Broadcasting (DVB) in Europe, which was widely used in Europe and Australia. In the DVB standards, the number of subcarriers can be more than 8,000, and the data rate could go up as high as 15Mbps. At present, many people still work to modify the IEEE 802.16 standard, which may result in an even higher data rate up to 100Mbps.

## 1.5. ORGANIZATION OF THESIS

In Chapter 2 performance comparison of various channel estimation techniques in OFDM systems is considered, with figure of merits presented in form of Bit Error Rate (BER) and the implementation complexity. Also an attempt is made to simulate OFDM systems using Artificial Neural Networks (ANN) with focus on Peak to Average Power ratio (PAPR) reduction. Following this implementation of channel estimation using ANN, a comparison is made between this technique among a few conventional channel estimation techniques.

Chapter 3 contains three sections: first discusses about the third generation partnership project (3GPP) specifications and frame structure for Long Term Evolution (LTE). After that, an attempt is made to design the physical layer transceiver section of the LTE in Matlab, incorporating channel estimation techniques. This is followed by introduction to the non-orthogonal multicarrier waveforms used in the 5G, due to issues discussed later

Chapter 4 presents a historical development of OFDM system along with literature survey on performance analysis of FFT-based OFDM system, A discussion of the system model in presence of CFO and Channel estimation error with mathematical formulation of transmitter, channel and receiver. The exact closed form bit error rate (BER) and symbol error rate (SER) expressions for FFT-based OFDM systems with CFO and Channel Estimation Error are analysed. BER performances of BPSK, QPSK, 16-QAM are compared

for Rayleigh fading channel. Numerical results are given to verify the accuracy of the derivations. The chapter is concluded by giving some final remarks

Chapter 5 contains the conclusions for the work and proposes future scope of the thesis and recommendations to extend it to other multi carrier modulation schemes.

\*\*\*\*\*

# CHAPTER-II

---

## CHANNEL ESTIMATION IN OFDM SYSTEMS

Topics:

**2.1.** Literature Survey on techniques for Channel Estimation

**2.2.** System Model

**2.3.** Channel Estimation Techniques

**2.3.1.** Block Type Pilot Channel Estimation

**2.3.1.1** LS Estimator

**2.3.1.2** MMSE Estimator

**2.3.1.3** Modified MMSE Estimator

**2.3.1.4** Estimation with Decision Feedback

**2.3.2.** Comb- Type Pilot channel Estimation

**2.3.2.1** LS Estimator with 1 D Interpolation

**2.3.2.2** Linear Interpolation(LI)

**2.3.2.3. Second Order Interpolation (SOI)**

**2.3.2.4. Low Pass Interpolation(LPI)**

**2.3.2.5. Spline Cubic Interpolation(SCI)**

**2.3.2.6. Time Domain Interpolation (TDI)**

**2.4. Linking Artificial Neural Networks to OFDM systems**

**2.4.1. System Model and PAPR Formulation**

**2.4.2. Artificial Neural Networks**

**2.4.2.1. Choice of efficient training algorithm**

**2.4.2.2. Practical Implementation**

**2.4.2.3. Complexity Analysis**

**2.5. Artificial Neural Network Channel estimation based on Levenberg-Marquardt for OFDM Systems**

**2.5.1 Application of ANN as Channel Estimators**

**2.6. Simulated Results**

---

In this chapter, a performance comparison of various channel estimation techniques in OFDM Systems is considered, with figure of merits presented in form of Bit Error Rate (BER) and of complexity in terms of implementation. Also an attempt is made to simulate OFDM systems using Artificial Neural Networks (ANN) with focus on Peak to Average Power ratio (PAPR) reduction and extension to WLAN and WiMAX standards. Following this implementation of channel estimation using ANN is considered and its performance is compared with that of a few conventional channel estimation techniques.

## 2.1. LITERATURE SURVEY ON TECHNIQUES FOR CHANNEL ESTIMATION

OFDM systems (as, for instance, the DAB standard [24]) modulate the subcarriers differentially [25]. The information symbols may be encoded differentially from one OFDM symbol to the next within one subcarrier, or differentially between adjacent subcarriers within one OFDM symbol. Even in a fading channel environment, such a modulation does not need the tracking of the subcarrier attenuations (tracking of the carrier frequencies has still to be done). The performance sacrifice associated with this modulation scheme compared to coherent modulation schemes is often motivated by its simple receiver structure and its avoidance of pilot symbols. However, if the subcarriers are coherently modulated, as in the DVB standard [26], estimation of the channel's attenuations of each subcarrier is necessary. These estimates are used in the channel equalizer, which, in an OFDM receiver, may consist of one complex multiplication for each subcarrier in an OFDM symbol.

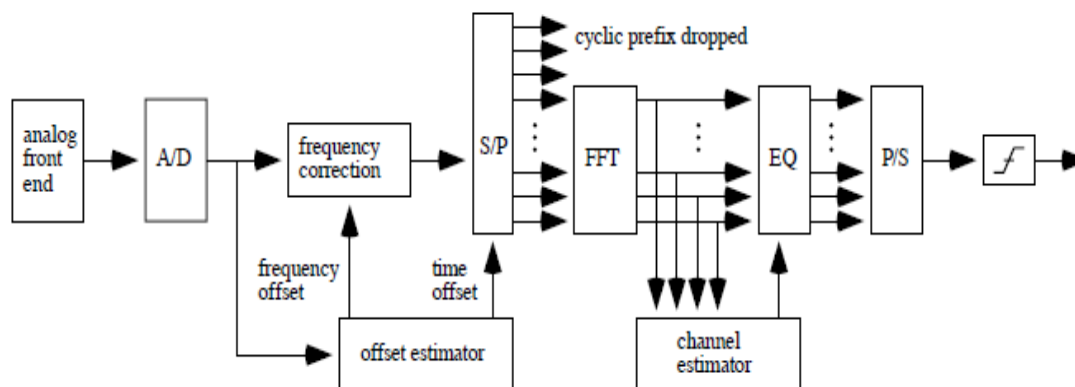


Figure 2.1.1.: Time/frequency offset correction and channel estimation/equalization in an OFDM receiver.

Figure 2.1.1, shows the receiver structure for a coherent OFDM receiver. An OFDM signal has an approximately Gaussian amplitude distribution when the number of subcarriers is large. Therefore, very high peaks in the transmitted signal can occur. This property is often measured via the signal's peak-to-average power ratio, which for the OFDM signal is high. To be able to transmit and receive these peaks without clipping, the A/D and D/A (Digital to Analog converter) need to be designed with high demands on range and precision. If the dynamic ranges of the A/D and D/A are increased, the resolution also needs to be increased in order to maintain the same quantization noise level. Therefore, an OFDM signal may require expensive A/Ds and D/As compared to many other modulation formats, and for some applications suitable A/Ds and D/As may not be available at all. Techniques to reduce PAPR have been discussed in later sections.

Orthogonal frequency division multiplexing (OFDM) is a promising technology for broadband wireless communication systems due to its low complexity equalization capability in frequency selective fading channel and its adaptability/scalability to the channel condition. By definition, OFDM expects the subcarriers to be orthogonal. But, the factors such as carrier frequency mismatching, time variations due to Doppler shift or phase noise usually eliminate the orthogonality of the subcarriers. This gives rise to ICI which degrades the performance of OFDM systems significantly [27].

Channel estimation in OFDM is usually performed with the aid of pilot symbols. Since each subcarrier is flat fading, techniques from single carrier flat fading systems are directly applicable to OFDM. For such systems *pilot-symbol assisted modulation* (PSAM) on flat fading channels [28] involves the sparse insertion of known pilot symbols in a stream of data symbols. The attenuation of the pilot symbols is measured and the attenuations of the data symbols in between these pilot symbols are typically estimated/interpolated using time correlation properties of the fading channel. The concept of PSAM in OFDM systems also allows the use of the frequency correlation properties of the channel. The time-frequency grid in Figure 2.1.2, illustrates three ways of inserting pilot symbols among data symbols. The first pilot pattern inserts entirely known OFDM symbols in the OFDM signal. The second modulates pilot symbols on a particular set of subcarriers. The third pattern uses scattered pilot symbols, as in the DVB standard.

Most documented channel estimation concepts consist of two steps, one or both of which use the correlation of the channel. First, the attenuations at the pilot positions are measured and possibly smoothed using the channel correlation. These measurements then serve to estimate (interpolate) the complex-valued attenuations of the data symbols in the second step. This second step uses the channel correlation properties either with interpolation filters or with a decision-directed scheme. Depending on the pilot pattern (see Figure 2.1.2) the estimation strategies diverge here.

Hoeher [29], for instance, proposed a scattered pilot pattern. The interpolation in the presented scheme uses the channel measurements with two Wiener FIR Filters. The First FIR interpolates and smoothens the channel attenuations in frequency while the second Wiener Filter interpolates and smoothens the channel attenuations in time. This scheme exploits the channel correlation properties in the design of the interpolating Wiener FIR Filters. In general, the correlation properties and the SNR needed to design the estimator are not known. Therefore, Hoeher [29] proposes to design the estimator for fixed, assumed values of the channel correlations and SNR. Recent publications by Edfors *et al.* [30] and Li *et al.* [31], focus on the First pilot pattern of Figure below, where completely known OFDM symbols are sparsely inserted in the stream of OFDM symbols. The channel attenuations in between these OFDM symbols are then either interpolated using the channel time correlation or the estimator is applied on consecutive OFDM symbols in a decision-directed scheme [32].

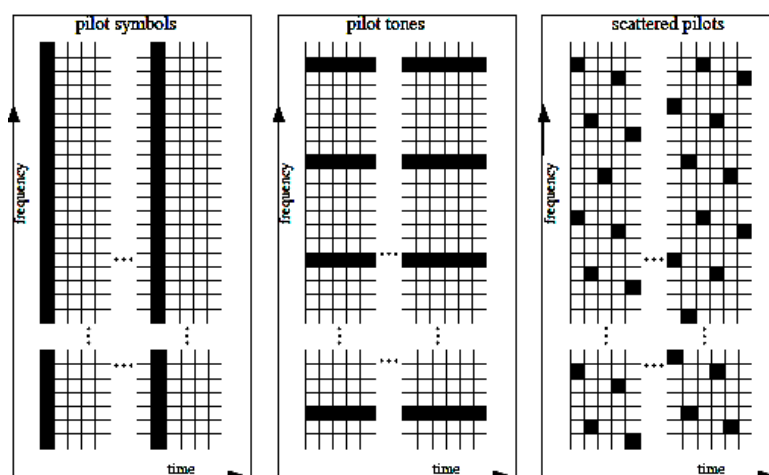


**Figure 2.1.2:** Time-frequency grid for an OFDM system with three pilot patterns: entirely known OFDM symbols Block type(left), pilot subcarriers- Comb Type (middle) and scattered pilots (right).

## 2.2. SYSTEM MODEL

The basic idea underlying OFDM systems is the division of the available frequency spectrum into several subcarriers. To obtain a high spectral efficiency, the frequency responses of the subcarriers are overlapping and orthogonal, hence the name OFDM. This orthogonality can be completely maintained with a small price in a loss in SNR, even though the signal passes through a time dispersive fading channel, by introducing a cyclic prefix (CP). Figure below depicts the block diagram of the baseband OFDM system.

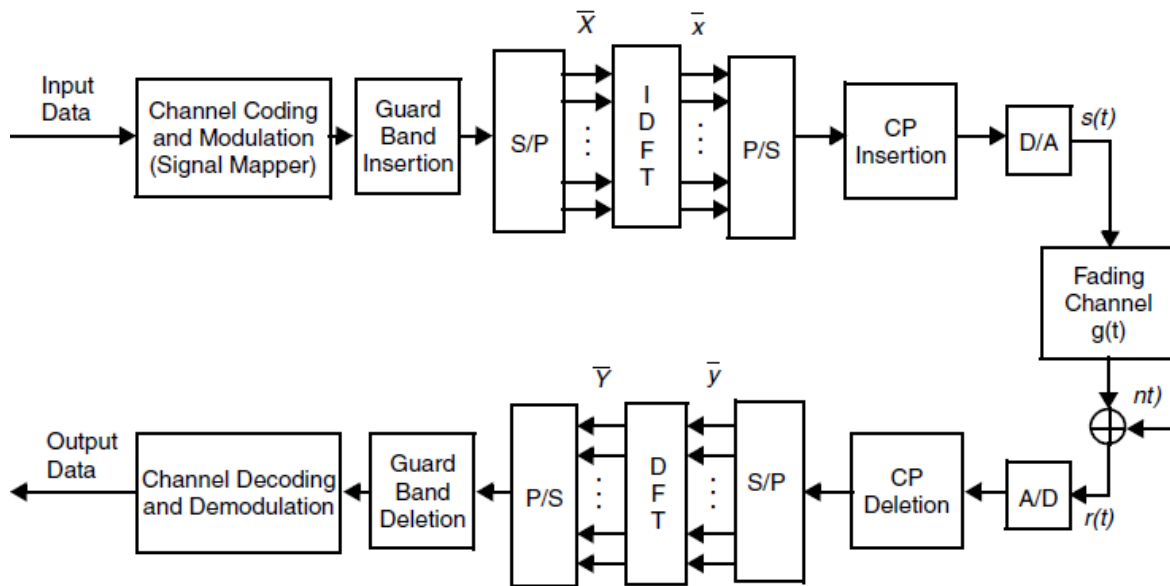


**Figure 2.2.1:** Digital implementation of Baseband OFDM system

The binary information is first grouped, coded, and mapped according to the modulation in a “signal mapper.” After the guard band is inserted, an  $N$ -point inverse discrete-time Fourier transform (IDFT $_N$ ) block transforms the data sequence into time domain (note that  $N$  is typically 256 or larger). Following the IDFT block, a cyclic extension of time length  $T_G$ , chosen to be larger than the expected delay spread, is inserted to avoid intersymbol and intercarrier interferences. The D/A converter contains low-pass filters with bandwidth  $1/T_s$ , where  $T_s$  is the sampling interval. The channel is modeled as an impulse response  $g(t)$  followed by the complex additive white Gaussian noise (AWGN)  $n(t)$ , where  $\alpha_m$  is a complex values and  $0 \leq \tau_m T_s \leq T_G$ .

$$g(t) = \sum_{m=1}^M \alpha_m \delta(t - \tau_m T_s) \tag{2.2.1}$$

At the receiver, after passing through the analog-to-digital converter (A/D) and removing the CP, the DFT<sub>N</sub> is used to transform the data back to frequency domain. Lastly, the binary information data is obtained back after the demodulation and channel decoding.

Let  $\bar{\mathbf{X}} = [\mathbf{X}_k]^T$  and  $\bar{\mathbf{Y}} = [\mathbf{Y}_k]^T$  ( $k = 0, \dots, N-1$ ) denote the input data of IDFT block at the transmitter and the output data of DFT block at the receiver, respectively. Let  $\bar{\mathbf{g}} = [\mathbf{g}_n]^T$  and  $\bar{\mathbf{n}} = [\mathbf{n}_n]^T$  ( $n = 0, \dots, N-1$ ) denote the sampled channel response and AWGN, respectively. Define the input matrix  $\underline{\mathbf{X}} = \text{diag}(\bar{\mathbf{X}})$  and the DFT matrix,

$$\underline{\mathbf{F}} = \begin{bmatrix} \mathbf{W}_N^{00} & \dots & \mathbf{W}_N^{0(N-1)} \\ \vdots & \ddots & \vdots \\ \mathbf{W}_N^{(N-1)0} & \dots & \mathbf{W}_N^{(N-1)(N-1)} \end{bmatrix} \quad (2.2.2)$$

where  $\mathbf{W}_N^{i,k} = \left(\frac{1}{\sqrt{N}}\right)^{-j2\pi(ik/N)}$ . Also define  $\bar{\mathbf{H}} = \text{DFT}_N(\bar{\mathbf{g}}) = \underline{\mathbf{F}} \bar{\mathbf{g}}$  and  $\bar{\mathbf{N}} = \underline{\mathbf{F}} \bar{\mathbf{n}}$ , under the assumptions that the interferences are completely eliminate, the output of the IDFT block will be

$$\bar{\mathbf{Y}} = \text{DFT}_N(\text{IDFT}_N(\bar{\mathbf{X}}) \otimes \bar{\mathbf{g}} + \bar{\mathbf{n}}) = \underline{\mathbf{X}} \underline{\mathbf{F}} \bar{\mathbf{g}} + \bar{\mathbf{N}} = \underline{\mathbf{X}} \bar{\mathbf{H}} + \bar{\mathbf{N}} \quad (2.2.3)$$

This equation demonstrated that an OFDM system is equivalent to a transmission of data over a set of parallel channels. As a result, the fading channel of the OFDM system can be viewed as a 2D lattice in a time-frequency plane, which is sampled at pilot positions and the channel characteristics between pilots are estimated by interpolation. The art in designing channel estimators is to solve this problem with a good trade-off between complexity and performance.

### 2.3. CHANNEL ESTIMATION TECHNIQUES

The two basic 1D channel estimations in OFDM systems are illustrated in **Figure above**. The first one, block-type pilot channel estimation, is developed under the assumption of slow fading channel, and it is performed by inserting pilot tones into all subcarriers of OFDM symbols within a specific period. The second one, comb-type pilot channel estimation, is introduced to satisfy the need for equalizing when the channel changes even from one OFDM block to the subsequent one. It is thus performed by inserting pilot tones into certain subcarriers of each OFDM symbol, where the interpolation is needed to estimate the conditions of data subcarriers. The strategies of these two basic types are analyzed in the next sections

### 2.3.1 BLOCK-TYPE PILOT CHANNEL ESTIMATION

In block – type pilot based channel estimation, OFDM channel estimation symbols are transmitted periodically and all subcarriers are used as pilots. The task here is to estimate the channel conditions (specified by  $\bar{H}$  or  $\bar{g}$ ) given the pilot signals (specified by matrix  $\underline{X}$  or vector  $\bar{X}$ ) and received signals (specified by  $\bar{Y}$ ), with or without using certain knowledge of the channel statistics. The receiver uses the estimated channel conditions to decode the received data inside the block until the next pilot symbol arrives. The estimation can be based on least square (LS), minimum mean- square error (MMSE), and modified MMSE.

#### 2.3.1.1 LS ESTIMATOR

The LS estimator minimizes the parameter  $(\bar{Y} - \underline{X}\bar{H})^H (\bar{Y} - \underline{X}\bar{H})$ , where  $(.)$  means the conjugate transpose operation. It is shown that the LS estimator of  $\bar{H}$  is given by [2].

$$\hat{H}_{LS} = \underline{X}^{-1}\bar{Y} = \left[ \left( \frac{X_k}{Y_k} \right) \right]^T \quad (k = 0, \dots, N - 1) \quad (2.3.1.1)$$

Without using any knowledge of the statistics of the channels. The LS estimators are calculated with very low complexity, but suffer from a high mean-square error.

#### 2.3.1.2 MMSE ESTIMATOR

The MMSE estimator employs the second order statistics of the channel conditions to minimize the mean square error. Denote by  $\underline{R}_{gg}$ ,  $\underline{R}_{HH}$  and  $\underline{R}_{YY}$  the auto covariance matrix of  $\bar{g}$ ,  $\bar{H}$  and  $\bar{Y}$ . Also denote by  $\sigma_N^2$  the noise variance. Assume the channel vector  $\bar{g}$  and the noise  $\bar{N}$  are uncorrelated, it is derived that

$$\begin{aligned} \underline{R}_{HH} &= E \{ \bar{H} \bar{H}^H \} = E \{ (\underline{F}\bar{g})(\underline{F}\bar{g})^H \} = \underline{F} \underline{R}_{gg} \underline{F}^H \\ \underline{R}_{gY} &= E \{ \bar{g} \bar{Y}^H \} = E \{ \bar{g} (\underline{X} \underline{F} \bar{g} + \bar{N})^H \} = \underline{R}_{gg} \underline{F}^H \underline{X}^H \\ \underline{R}_{YY} &= E \{ \bar{Y} \bar{Y}^H \} = \underline{X} \underline{F} \underline{R}_{gg} \underline{F}^H \underline{X}^H + \sigma_N^2 \underline{I}_N \end{aligned} \quad (2.3.1.2)$$

Assume  $\underline{R}_{gg}$  and  $\sigma_N^2$  are known at the receiver in advance, the MMSE estimator of  $\bar{g}$  is given by  $\hat{g}_{MMSE} = \underline{R}_{gY} \underline{R}_{YY}^{-1} \bar{Y}^H$  [2-5]. If  $\bar{g}$  is not Gaussian,  $\hat{g}_{MMSE}$  is not necessarily a minimum mean- square estimator, but it is still the best linear estimator in the mean- square sense.

$$\begin{aligned} \hat{H}_{MMSE} &= \underline{F} \hat{g}_{MMSE} = \underline{F} \left[ (\underline{F}^H \underline{X}^H)^{-1} \underline{R}_{gg}^{-1} \sigma_N^2 + \underline{X} \underline{F} \right]^{-1} \bar{Y} \\ &= \underline{F} \underline{R}_{gg} \left[ (\underline{F}^H \underline{X}^H \underline{X} \underline{F})^{-1} \sigma_N^2 + \underline{R}_{gg} \right]^{-1} \underline{F}^{-1} \hat{H}_{LS} \\ &= \underline{R}_{HH} \left[ \underline{R}_{HH} + \sigma_N^2 (\underline{X}^H \underline{X})^{-1} \right]^{-1} \hat{H}_{LS} \end{aligned} \quad (2.3.1.3)$$

The MMSE estimator yields much better performance than LS estimators, especially under the low SNR scenarios. A major drawback of the MMSE estimator is its high computational complexity, especially if matrix inversions are needed each time the data in  $\underline{X}$  changes.

### 2.3.1.3 MODIFIED MMSE ESTIMATOR

Modified MMSE estimators are studied widely to reduce complexity [2-4]. Among them, an optimal low rank MMSE (OLR-MMSE) estimator is described here, with the following simplification techniques.

- 1 The first simplification of MMSE estimator is to replace the term  $(\underline{X} \underline{X}^H)^{-1}$  with its expectation  $E\{(\underline{X} \underline{X}^H)^{-1}\}$ . Assuming the same signal constellation on all tones and equal probability on all constellation points, we have

$$E\{(\underline{X} \underline{X}^H)^{-1}\} = E\left\{\left|\frac{1}{X_k}\right|^2\right\} \underline{I}$$

- Defining the average SNR as  $\overline{SNR} = E\{|X_k|^2\}/\sigma_N^2$  and the term  $\beta = E\{|X_k|^2\}/E\left\{\left|\frac{1}{X_k}\right|^2\right\}$ . The term  $\sigma_N^2 (\underline{X} \underline{X}^H)^{-1}$  is then approximate by  $(\beta/\overline{SNR}) \underline{I}$ , where  $\beta$  is a constant depending only on the signal constellation. For example, for 16-QAM transmission,  $\beta = 17/9$ .

- 2 Most of the energy in  $\bar{g}$  is contained in, or near, the first  $(L + 1)$  taps where

$L = \lceil T_G/T_S \rceil N$ , here  $N$  is DFT size. Therefore only the taps with significant energy,

that is, the upper left corner of the auto covariance matrix  $\underline{R}_{gg}$ .

- 3 The third simplification uses the singular value decomposition (SVD). The SVD of  $\underline{R}_{HH}$  is  $\underline{R}_{HH} = \underline{U} \underline{\Lambda} \underline{U}^H$ , where  $\underline{U}$  is a unitary matrix containing the singular vectors and  $\underline{\Lambda}$  is a diagonal matrix containing the singular values  $\lambda_0 \geq \lambda_1 \geq \dots \geq \lambda_{N-1}$  on its diagonal.

Combining all simplification techniques, the OLR- MMSE estimator is explained as follows,. The system first determines the number of ranks required by the estimator, denoted by  $p$  which should be no smaller than  $(L + 1)$ . Then, given the signal constellation, the noise variance and the channel auto covariance matrix  $\underline{R}_{HH}$ , the receiver pre calculates  $\beta$ ,  $\overline{SNR}$ , the unitary matrix  $\underline{U}$  and the singular values  $\lambda_k$ . It thus obtains the  $(N \times N)$  diagonal matrix  $\underline{\Delta}_p$  with entries

$$\delta_k = \begin{cases} \left[ \frac{\lambda_k}{\lambda_k + \frac{\beta}{\overline{SNR}}} \right] & k = 0, 1, \dots, p - 1 \\ 0 & k = p, \dots, N - 1 \end{cases} \quad (2.3.1.3)$$

The OLR-MMSE estimator with rank  $p$  is given by  $\hat{H}_{OLR-MMSE} = \underline{U} \underline{\Delta}_p \underline{U}^H \hat{H}_{LS}$ . OLR-MMSE estimator can be interpreted as first projecting the LS estimates onto a subspace and then performing the estimation. Because the subspace has small dimension and still describes the channel well, the complexity of OLR-MMSE estimator is much lower than MMSE estimator with a good performance. However, the low-rank estimators introduce an irreducible error floor due to part of the channel that does not belong to the subspace.

#### 2.3.1.4. ESTIMATION WITH DECISION FEEDBACK

In block- type pilot based channels, the estimators are usually calculated once per block and used until the next pilot symbol arrives. The channel estimation with decision feedback is depicted to check for performance improvement, where the estimators inside the block are updated using the pilots and obtains  $\hat{H} = \{\hat{H}_k\}(k = 0, \dots, N - 1)$ , which is based on LS, MMSE or modifiedMMSE. Inside the block, for each coming symbol and for its each

subcarrier, the estimated transmitted signal is found by the previous  $\hat{H}_k$  according to the formula  $\hat{X}_k = \frac{Y_k}{\hat{H}_k \cdot \{\hat{X}_k\}}$  is mapped to the binary data through the demodulation according to the signal demapper as  $\{\hat{X}_k\}$ . The estimated channel  $\hat{H}_k$  is updated by  $\hat{H}_k = Y_k / \hat{X}_k$  and is used in the next symbol.

### 2.3.2. Comb- Type Pilot Channel Estimation

In comb-type pilot based channel estimation, as depicted in figure above, for each transmitted symbol,  $N_p$  pilot signals are uniformly inserted into  $\hat{X}$  with  $S$  subcarriers apart from each other, where  $S = \frac{N}{N_p}$ . The receiver knows the pilot locations  $\bar{P} = [P_k]^T$  ( $k = 0, \dots, N_p - 1$ ), the pilot values  $\bar{X}^p = [X_k^p]^T$  ( $k = 0, \dots, N_p - 1$ ) and the received signal  $\bar{Y}$ . The LS estimated to the channel conditions at the pilot subcarriers ( $\bar{H}^p$ ) are calculated by

$$\hat{H}_{LS}^p = \left[ \frac{Y(P_0)}{X_0^p}, \frac{Y(P_1)}{X_1^p}, \dots, \frac{Y(P_{N_p-1})}{X_{N_p-1}^p} \right]^T \quad (2.3.2)$$

The task here is to estimate the channel conditions at the data subcarriers (specified by  $\bar{H}$  with length  $N$ ), given the LS estimates at pilot subcarriers  $\hat{H}_{LS}^p$ , received signals  $\bar{Y}$ , and certain additional knowledge of channel statistics. One of the solutions include LS estimator with 1 D interpolation.

#### 2.3.2.1 LS Estimator with 1 D Interpolation

1D interpolation is used to estimate the channel at the data subcarriers, where the vector  $\hat{H}_{LS}^p$  with length  $N_p$  is interpolated to the vector  $\hat{H}$  with length  $N$ , without using additional knowledge of the channel statistics.

#### 2.3.2.2. Linear Interpolation (LI)

The LI method performs better than the piecewise-constant interpolation, where the channel estimation at the data subcarrier between two pilot  $\hat{H}_{LS}^p(k)$  and  $\hat{H}_{LS}^p(k + 1)$  is given by:

$$\hat{H}(kS + t) = \hat{H}_{LS}^p(k) + \left( \hat{H}_{LS}^p(k+1) - \hat{H}_{LS}^p(k) \right) \left( \frac{t}{S} \right) \quad (0 \leq t \leq S)$$

(2.3.2.2)

### 2.3.2.3 Second-Order Interpolation (SOI)

The SOI method performs better than the LI method, where the channel estimation at the data subcarrier is obtained by weighted linear combination of three adjacent pilot estimates.

### 2.3.2.4 Low Pass Interpolation (LPI)

The LPI method is performed by inserting zeros into the original  $\hat{H}_{LS}^p$  sequence and then applying a low-pass finite length impulse response (FIR) filter, which allows the original data to pass through unchanged. This method also interpolates such that the mean square error between the interpolated points and their ideal values is minimized.

### 2.3.2.5 Spline Cubic Interpolation (SCI)

The SCI method produces a smooth and continuous polynomial fitted to given data points.

### 2.3.2.6 Time Domain Interpolation (TDI)

The TDI method is a high resolution interpolation based on zero-padding and DFT/IDFT. It converts  $\hat{H}_{LS}^p$  to time domain by IDFT and then interpolate the time domain sequence to N points with simple piecewise-constant method [5]. Finally, the DFT converts the interpolated time domain sequence back to the frequency domain.

In [5], the performance among these estimation techniques usually ranges from the best to worst as follows: LPI, SCI, TDI, SOI and LI. Also, LPI and SCI yield almost the same best performance in the low and middle SNR scenarios, while LPI outperforms SCI at high SNR scenario. In terms of the complexity, TDI, LPI and SCI have roughly the same computational burden, while SOI and LI have less complexity. As a result, LPI and SCI are usually recommended because they yield the best trade off between performance and complexity.

## 2.4. LINKING ARTIFICIAL NEURAL NETWORKS TO OFDM SYSTEMS

OFDM is becoming widely used technique in broadcast wireless communication due to its capability of high rate data transmission with efficient bandwidth and rugged immunity to the

frequency selection fading channels. Multicarrier communication systems are competing well with single carrier systems, but suffer from a serious drawback that is high peak-to-average power ratio (PAPR).

To reduce PAPR various alternative solutions have been proposed in the literature [33-35], but each has its own pros and cons. Clipping being the simplest technique for reducing the PAPR; however it is a nonlinear process and causes both in band and out of band distortion. The Out of band (OOB) distortions can be alleviated through filtering but results in significant peak re-growth. Moreover repetition of clipping and filtering process [36] may lead to degradation in bit error rate (BER) performance. The distortion less methods of PAPR reduction are based on either by introducing redundancy like selective mapping (SLM), partial transmit sequence (PTS) and selective scrambling [37] or by a joint block coding and modulation schemes with Golay and Reed –Muller codes [38-40].

The PTS and SLM methods are the most attractive and significant probabilistic techniques due to their good performance in terms of PAPR reduction. The main drawback of these techniques is the requirement to send side information at receiver to recover original data. If the side information may be corrupted, the original data cannot be recovered correctly. Therefore, some extra protection bits have to be employed for the protective transmission of side information to guarantee reasonable BER performance, resulting in decrease in spectrum efficiency.

The block coding techniques [41], can only be applied to M-ary Phase shift keying (MPSK) modulation and become infeasible for larger values of  $N$  due to computations needed. Though, few methods [42-43] also use pilot tones and unused subcarrier to reduce the PAPR without increasing BER but result in a slight broadening of the original spectrum.

Soft Computing based schemes are also being successfully applied to reduce PAPR in OFDM system due to their inherent qualities like adaptive in nature, no requirement of physical behaviour of model and importantly the less complexity [44-46].

Here one of the soft computing based scheme namely Neural Network based switching of null subcarrier and data subcarrier technique is adapted to reduce the PAPR of the multicarrier system, the described scheme allows no side information and low on complexity.

### 2.4.1 SYSTEM MODEL AND PAPR FORMULATION

Following the same system model of OFDM system as above, with a block of  $N$  orthogonal symbols  $\{X = X_k, k = 0, 1, \dots, N - 1\}$  is formed with each symbol modulating one of a set of subcarriers  $f_k, k = 0, 1, \dots, N - 1$ , where,  $N$  is the number of subcarriers of OFDM system. For discrete-time OFDM, the  $L$  times oversampled IFFT output expressed as [47]

$$x[n] = \frac{1}{\sqrt{N}} \sum_{k=0}^{N-1} X_k e^{j2\pi nk/LN}, 0 \leq n \leq LN - 1 \quad (2.4.1)$$

The PAPR computed from  $L$ -times oversamples time domain OFDM signal samples can be defined as [47]

$$PAPR\{x[n]\} = \frac{\max_{0 \leq n \leq LN-1} [|x[n]|^2]}{E[|x[n]|^2]} \quad (2.4.2)$$

Many multicarrier standards possess null carriers inherently which are also known as virtual or unmodulated subcarriers. These are unused carriers where no energy is transmitted. In the scheme one or more null replaced with pre identified data sub carriers in order to offer the least PAPR [48]. The null data subcarriers are switched with the data subcarriers, this switching action modify the input to IFFT operator in multicarrier system transmitter, and thus the IFFT operator's output and its PAPR. Number of switching possibilities which can be evaluated as

$$S_{switch} = \frac{(N - N_{null})!}{N_{sw}! (N - N_{null} - N_{sw})!} \quad (2.4.3)$$

where  $N, N_{null}$  and  $N_{sw}$  are total number of subcarriers, null subcarriers and switched null subcarriers, respectively. The number of switching possibilities increases manifold with the number of subcarriers in multicarrier standards. To reduce the computational complexity, a neural network with Levenberg-Marquardt training scheme is used to achieve a fair amount

of complexity reduction without sacrificing the BER performance of the system. This scheme requires no channel side information due to the fact that the permutation of the switched data subcarriers remain unchanged after the switching. Unlike other PAPR reduction techniques, the constellation remains unchanged at each data sub- carriers during the process.

#### 2.4.2 ARTIFICIAL NEURAL NETWORK

Artificial neural networks (ANNs) are one of the popular branches of artificial intelligence. They have very simple neuron-like processing elements (called nodes or artificial neurons) connected to each other by weighting. The weights on each connection can be dynamically adjusted until the desired output is generated for a given input. An artificial neuron model consists of a linear combination followed by an activation function. Different types of activation functions can be utilized for the network; however, the common ones, which are sufficient for most applications, are the sigmoidal and hyperbolic tangent functions.

The general structure of an( Multi-Layer Perceptron Neural Network) MLPNN is given in Figure 2.4.2.1 and consists of three layers: an input layer, with a number of neurons equal to the number of variables of the problem, an output layer, where the Perceptron response is made available, with a number of neurons equal to the desired number of quantities computed from the inputs, and an intermediate or hidden layer. While an MLPNN consisting of only the input and the output layers provide satisfaction for linear problems, additional intermediate layers are required in order to approximate nonlinear problems. For example, all problems which can be solved by a perceptron can be solved with only a hidden layer, but it is sometimes more efficient to use two (or more) hidden layers.

Once the system with neural network has been trained off-line, using Training algorithms, it behaves like a generated system model which performs integer multiplication and addition to obtain the desired signal when the input signal is presented.

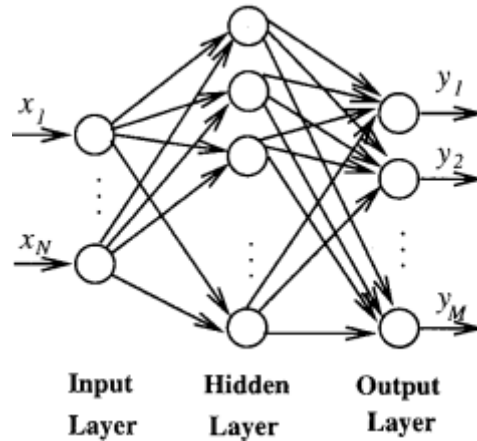


**Figure 2.4.2.1:** A feedforward neural network. Each circle represents a neuron which sums the inputs and passes the sum through an activation function. Each arc represents multiplication by a scalar weight.

### 2.4.2.1 CHOICE OF EFFICIENT TRAINING ALGORITHM

The steepest descent algorithm is a first-order algorithm. It uses the first order derivative of the total error function to find the minima in error space. When there is a great difference in magnitude between the largest and smallest eigenvalues, the steepest descent algorithm will converge slowly. The performance can be improved if the search directions are adjusted to conjugate, instead of being orthogonal. If conjugate directions are used for the function, the function can be exactly minimized in least number of iterations.

Another algorithm namely, Newton's method, has a property called quadratic termination, which means that it minimizes a quadratic function exactly in a finite number of iterations. However it requires calculation and storage of the second derivatives, which becomes a problem when number of parameters is large. In such a situation, methods that require only first derivatives but still have quadratic termination are preferred. Gauss-Newton over standard Newton's methods that the former does not require the calculation of second derivatives (Hessian matrix) of the total error function, by introducing Jacobian matrix  $J$ , However, the Gauss-Newton algorithm still faces the same convergent problem like the Newton algorithm for complex error space optimization. The update rule of Gauss-Newton is

$$w_{k+1} = w_k - (J_k^T J_k)^{-1} J_k e_k ,$$

(2.4.2.1)

where  $w_{k+1}$  and  $w_k$  are updated and old weight vectors respectively,  $e_k$  are error vector of the network. There is a problem if the matrix  $J_k^T J_k$  is not invertible. In order to make sure that the approximated Hessian matrix  $J_k^T J_k$  is invertible, Levenberg-Marquardt algorithm introduces another approximation to Hessian matrix as

$$H = J^T J + \mu I, \quad (2.4.2.2)$$

where  $J$  and  $I$  are Jacobian and Identity matrix respectively and  $\mu$  is combination coefficient ( $\mu > 0$ ). Combining above equations, the update rule of Levenberg-Marquardt algorithm can be given as

$$w_{k+1} = w_k - (J_k^T J_k + \mu I)^{-1} J_k e_k \quad (2.4.2.3)$$

The Levenberg-Marquardt algorithm blends the steepest descent method and the Gauss-Newton algorithm and therefore it inherits advantage of faster convergence of Gauss-Newton algorithm and stability of the steepest descent method. Therefore, Levenberg-Marquardt algorithm is one of the best choice as a learning method to train a feed-forward neural network.

#### 2.4.2.2. PRACTICAL IMPLEMENTATION

The Levenberg-Marquardt is selected to train the multilayer perceptron neural network. The neural network is trained using the data patterns with low PAPR obtained from the null subcarrier switching scheme [18]. To reduce complexity, the time domain original signals are first decomposed into real and imaginary parts as shown in Figure 2.4.2.2.1.

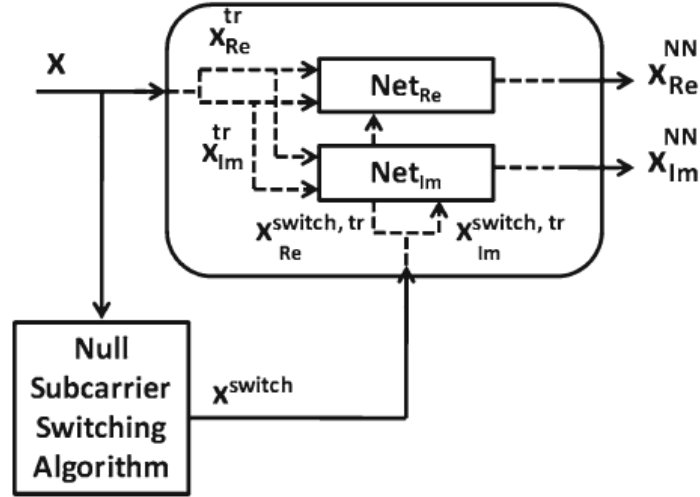


Figure 2.4.2.2.1: Block Diagram of training process for ANN based method

The steps involved in training procedure are summarized below:

1. Use original time domain data  $\mathbf{X}$  as an input to the null subcarrier switching algorithm to obtain  $\mathbf{X}^{switch}$  i.e. a signal with reduced PAPR.
2. Split  $\mathbf{X}$  and  $\mathbf{X}^{switch}$  into two sets, namely the training set  $\mathbf{X}^{tr}, \mathbf{X}^{switch, tr}$  and the test set  $\mathbf{X}^{ts}, \mathbf{X}^{switch, ts}$  in 70% and 30% of original count respectively.
3. Decompose into real and imaginary parts of the original data  $\mathbf{X}^{tr} (\mathbf{X}_{Re}^{tr}, \mathbf{X}_{Im}^{tr})$  and null subcarrier switching algorithm output  $\mathbf{X}^{switch, tr} (\mathbf{X}_{Re}^{switch, tr}, \mathbf{X}_{Im}^{switch, tr})$ .
4. Obtain  $\mathbf{X}_{Re}$  and  $\mathbf{X}_{Im}$  through training the two separate networks  $\mathbf{Net}_{Re}$  and  $\mathbf{Net}_{Im}$  presenting pairs  $[(\mathbf{X}_{Re}^{tr}, \mathbf{X}_{Im}^{tr}), \mathbf{X}_{Re}^{switch, tr}]$  and  $[(\mathbf{X}_{Re}^{tr}, \mathbf{X}_{Im}^{tr}), \mathbf{X}_{Im}^{switch, tr}]$  to the networks serially.
5. Test with the values of  $\mathbf{X}^{ts}$  (test set) to validate the networks  $\mathbf{Net}_{Re}$  and  $\mathbf{Net}_{Im}$ .

### 2.4.2.3. COMPLEXITY ANALYSIS

The designed Neural Network shown in Figure 2.4.2.2.1 is simple with 2:2:1 architecture (input nodes: hidden nodes: output nodes). The complexity of the described algorithm in term of number of integer multiplications per OFDM symbol is  $12 \times N$ , while the number of integer addition and activation function (transig) is  $10 \times N$  and  $4 \times N$  respectively. In Table 2.1, a complexity comparison of OFDM (with switching) and OFDM (NN method with switching) schemes is summarized. Typically, integer additions are half complex than complex additions, whereas, integer multiplications are four times simpler than complex

multiplications. Thus the described NN method is much less complex than OFDM (with switching) scheme, since it does not need several (I)DFT operations.

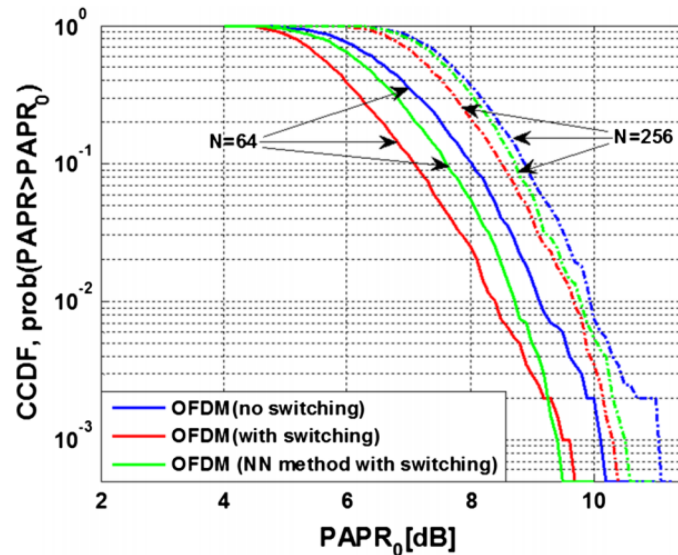


**Figure 2.4.2.3.1:** Comparison of PAPR's CCDF with number of subcarriers  $N = 64$  (Wireless LAN standard) and  $N = 256$  (WiMAX standard)

The complementary cumulative distribution function (CCDF) plots of different schemes are shown in Figure 2.4.2.3.1, it can be observed that in both the OFDM standards (i.e. Wireless LAN and WiMAX) the proposed scheme outperform the original OFDM(no switching) method but appears less efficient to OFDM (with switching) method. This is due to error approximation involved in all neural network learning based methods. From Fig. , it is observed that the value of PAPR of proposed method ( $\approx 9.3$  dB for wireless LAN, and  $\approx 10.63$  dB for WiMAX) is approximately 1 dB lower than OFDM (no switching) scheme ( $\approx 10.25$  dB for wireless LAN, and  $\approx 11.42$  dB for WiMAX). It is also shown in Figure, that CCDF plots of OFDM (NN method with switching) scheme specially with 64 subcarriers appear better than both the schemes at higher end of PAPR values.

Method	OFDM (with switching)			OFDM (NN method with switching)		
	Complexity relation	802.11a	802.16e	Complexity relation	802.11a	802.16e
I(DFT)	$1 \times S$	1,326	19,900	–	–	–
Complex multiplication	$(\frac{N}{2} \times \log_2 N) \times S$	254592	$2.03e^7$	–	–	–
Complex addition	$2 \times (\frac{N}{2} \times \log_2 N) \times S$	509184	$4.07e^7$	–	–	–
Integer multiplication	–	–	–	$12 \times N$	768	3072
Integer addition	–	–	–	$10 \times N$	640	2560
Check operation	$1 \times S$	1326	19900	–	–	–
Activation function	–	–	–	$4 \times N$	256	1024

N (number of subcarriers in OFDM standard) and S (number of switching possibilities)

Table:2.1 Complexity analysis for OFDM(with switching) and OFDM(without switching)

## 2.5 Artificial Neural Network Channel Estimation Based on Levenberg-Marquardt for OFDM Systems

There have been proposed several techniques for channel estimation in OFDM system as displayed in previous sections. Among these techniques, both pilot-based channel estimation and blind channel estimation techniques are most popular. When bandwidth is limited, the pilot-based channel estimation is not appropriate since inserting pilot signals into OFDM symbol causes waste of bandwidth. Pilot-based estimation techniques can be based on least-squares (LS), minimum mean-square error (MMSE) and linear minimum mean-square error (LMMSE) estimators. LS estimators have low complexity, but they suffer from many artifacts such as a high mean-square error (MSE), especially if the system operates with low signal-to-noise ratios (SNR). On the other hand, MMSE estimators, based on time-domain channel statistics, are high-complexity estimators. They have satisfactory performance for sample-spaced channel environments, but they have limited performance for non-sample spaced channels and high SNR's. Finally, LMMSE estimators have good performance for both sample-spaced and non-sample-spaced channels. Particularly, a low-complexity frequency-domain LMMSE estimator had been studied by Tolochko and Faulkner [49]. However, its performance can be further improved based on real time knowledge of the time-domain channel parameters, especially in the cases; OFDM training symbols used require

interpolation at the receiver end, the system operates in the changing channel environments and system has high SNR's.

In blind techniques, no training sequence is required. It uses certain underlying mathematical properties of the data being sent. This technique has a drawback of being extremely computationally intensive. This is the disadvantage of the blind techniques. Because of no training sequence required, it is appropriate for applications where bandwidth is scarce. This estimation technique can be based on recursive least square (RLS) or LMS .

ANN's can perform complex mapping between its input and output space and are capable of forming complex decision regions with nonlinear decision boundaries. Further, because of nonlinear characteristics of the ANN's, these networks of different architecture have found successful application in channel estimation problem [50-51]. One of the earliest applications of the ANN in digital communication channel equalization is reported by Siu et al. [51]. ANN is proposed as a channel estimator for QAM and QPSK constellation. In [52], a three-layer ANN was used to predict channel for MIMO systems. A unique scheme was proposed using pilot-symbol-aided OFDM systems by Sun and Yuan [53]. Differences between this scheme and [53] are that here no need of any pilot-symbol-aid and we also use Levenberg-Marquardt (LM) training algorithm to increase the convergence rate instead of the least mean error (LSE).

Here, an artificial neural network (ANN) based channel estimation technique as an alternative to pilot based channel estimation technique for OFDM systems over Rayleigh fading channels has been described. In this technique, there are no pilot symbols which added to OFDM. Therefore, this technique is more bandwidth efficient compared to pilot based channel estimation techniques. Moreover, this technique is making full use of the learning property of neural network. By using this feature, there is no need of any matrix computation and the technique is less complex than the pilot based techniques.

2.5.1 APPLICATION OF ANN AS CHANNEL ESTIMATOR

Neural networks contain neurons with nonlinear activation functions in the input layer and the hidden layer and neurons with linear activation functions in the output layer. ANN has Multi-Layer Perceptron (MLP) structure, which uses forward propagation neural network. Various training algorithms exist for MLP. To increase the convergence rate, Levenberg-Marquardt (LM) algorithm was used in our work. MLPNN consisting of one input layer, two hidden layers and one output layer was used to predict channel response.

Block diagram of the proposed ANN based technique is shown in Fig. 2.5.1.1. The signal  $x_i$  is OFDM signal which is affected by channel impact. Before demodulation, a channel estimation technique should be applied to the signal. At the beginning of the estimation process, this complex signal is split into two parts: real and imaginary. These parts are normalized between  $-1$  and  $+1$  before training. As shown in Figure, each part is trained and estimated at different neural network. Real part of signal is trained and estimated at NNR and imaginary part of signal is trained and estimated at NNI. After training and estimation, these components are merged again and demodulated. The estimated output of the system is given as

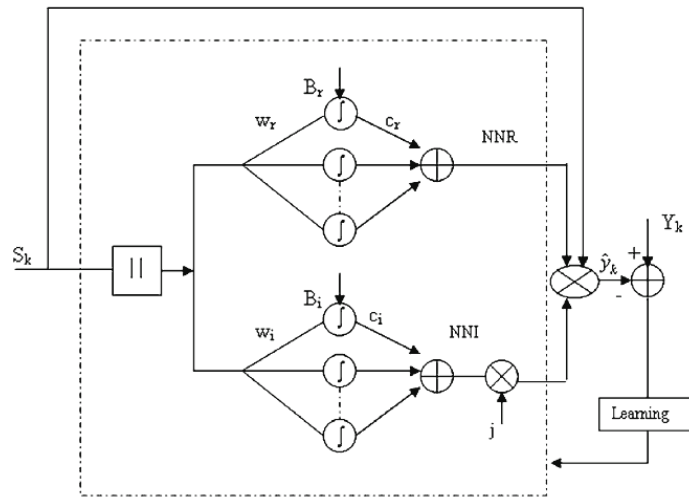


Figure2.5.1.1: Artificial Neural Network Structure

$$\hat{y}_k = NNR(R[X_k]) + jNNI(Im[X_k])$$

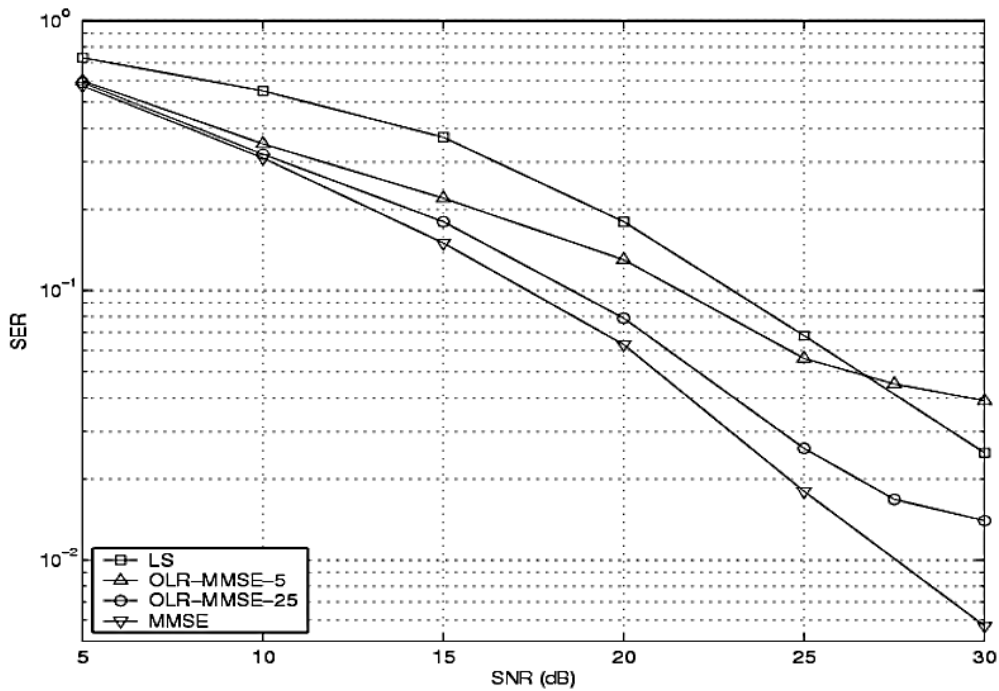
$$\text{Here, } NNR(R[X_k]) = \sum_{n=1}^m c_{rn} f(w_{rn} R[X_k] + b_{rn})$$

$$NNI(Im[X_k]) = \sum_{n=1}^m c_{in} f(w_{in} R[X_k] + b_{in}) \quad (2.5.1)$$

The activation function  $f(\cdot)$  is hyperbolic tangent sigmoid  $\{w_{rn}, c_{rn}, b_{rn}\}$  and  $\{w_{in}, c_{in}, b_{in}\}$  are weights of subnetwork NNR and NNI respectively. In order to minimize the error, Levenberg-Marquardt algorithm is used.

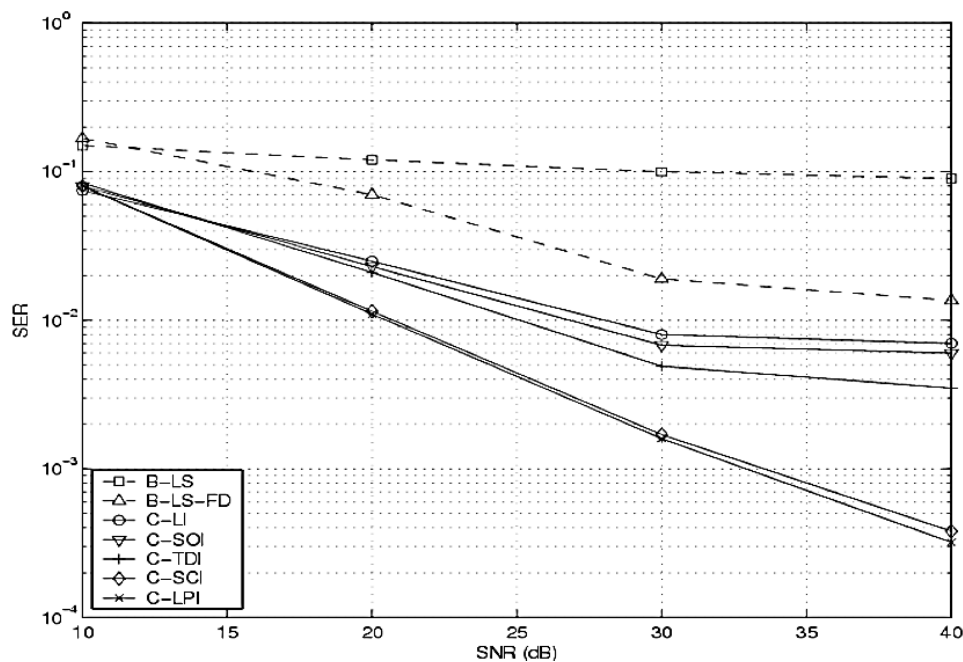
## 2.6 SIMULATIONS RESULTS AND DISCUSSIONS

In Figure 2.6.1, the symbol error rate (SER) versus the average SNR is plotted for the proposed block-type pilot channel estimation schemes over a slow fading channel with a bandwidth of 500 kHz, 16QAM modulation, DFT size  $N = 64$ , and a cyclic prefix  $L = 4$ . In this figure, the legends LS, MMSE, OLR-MMSE-5, and OLR-MMSE-25 present the estimators based on LS, MMSE, OLR-MMSE with rank  $p = 5$  and OLR-MMSE with rank  $p = 25$ , respectively, without the decision feedback. The MMSE estimator yields the best performance, and LS yields the worst. Also, for the OLR-MMSE estimator, a SER floor is shown due to loss of channel information by reducing the rank of the channel correlation matrix.



**Figure 2.6.1:** SER Performance versus SNR for Block-Type Pilot Channel Estimation Based on LS, MMSE, and OLR-MMSE algorithms[]

Figure 2.6.2, compares the SER performance of the estimation schemes with block-type pilot arrangement and comb-type pilot arrangement over a fast fading channel with Doppler frequency 70 Hz. The parameters are 17.5 kHz bandwidth, 16QAM modulation, DFT size  $N = 1024$ , the number of pilot subcarriers per symbol  $N_p = 128$ , and a cyclic prefix  $L = 256$ . In the figure, the legends B-LS, B-LS-FD represent the block-pilot channel estimation based on LS algorithm, with and without decision feedback, respectively; and the legends C-LI, C-SOI, C-TDI, C-SCI and C-LPI represent the comb-type pilot estimation based on LS algorithm, with the linear interpolation, the second order interpolation, the time domain interpolation, the spline cubic interpolation and the low-pass interpolation, respectively. The results show that the comb-type estimation schemes outperform block-type schemes, which is because the channel changes so fast that there are even changes for adjacent OFDM symbols. It is also shown that the performance among the comb-type estimation techniques usually ranges from the best to the worst as follows: low-pass, spline cubic, time-domain, second order, and linear.



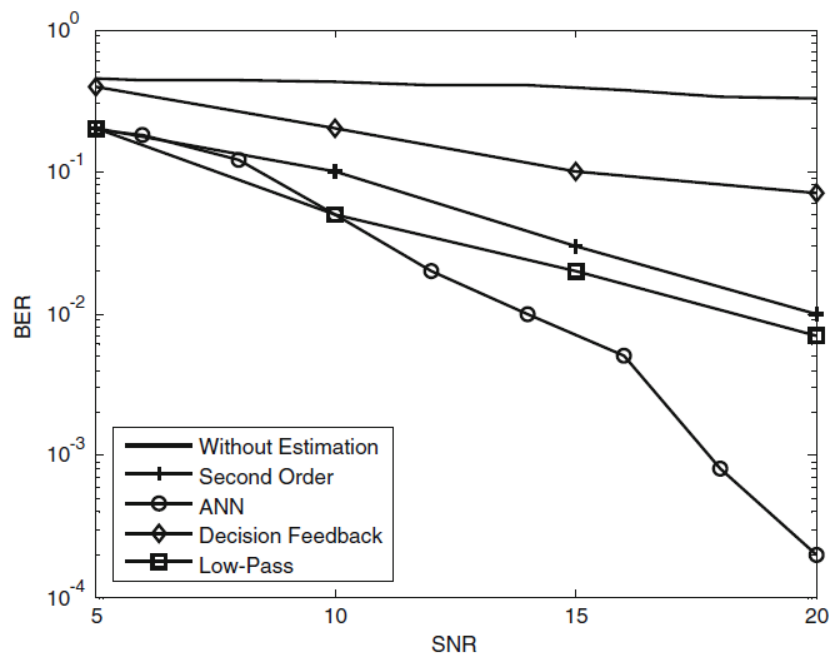
**Figure 2.6.2:** SER Performance versus SNR for the Channel Estimators Based On LS with Block-Type and Comb-Type Pilot Arrangements[]

Figure 2.6.3, ANN based channel estimator is designed using MATLAB. Rayleigh Frequency selective fading caused by multipath could lead to carriers used, being heavily attenuated due to destructive interference at the receiver. This can result in the carriers being lost in the noise. To increase OFDM system performance under frequency selective channels, we

propose an ANN based channel estimation technique. We compare the performance of this technique by applying 16QAM and BPSK as modulation schemes over multipath channel modeled to Rayleigh fading channels.

For figure of merits, bit-error rate (BER) has been used. Simulations have been realized and optimizations have been realized by MATLAB. The BER results of the study have been figured out by MATLAB. In Fig. , a comparison of pilot based channel estimation technique proposed before as low-pass, second order and decision feedback and the proposed ANN based technique has been simulated.

For simulation studies randomly generated QPSK modulated OFDM symbols have been carried out in Matlab (R2015a) environment with Machine learning and statistical toolbox. The training part of neural network is done with 70% of symbols and rest 30% symbols are selected for testing. The maximum number of iterations was fixed to be 1000. In this study, parameters of the IEEE 802.11a (Wireless LAN) and IEEE 802.16e (WiMAX) standards are chosen. For switching, two 'innermost' null subcarriers (indexed as  $\pm 27$  in IEEE 802.11a standard with  $N_{sw} = 2$ ) are used one at either side of the data subcarrier band with  $N - N_{null} = 52$ . Similarly, two 'innermost' null subcarriers (indexed as  $\pm 101$  in IEEE 802.16e standard with  $N_{sw} = 2$ ) are used for switching one at either side of data subcarrier band with  $N - N_{null} = 200$ .



**Figure 2.6.3:** 16QAM Modulation with Rayleigh fading- Comparison of conventional channel estimates techniques with those implemented with Artificial Neural Network

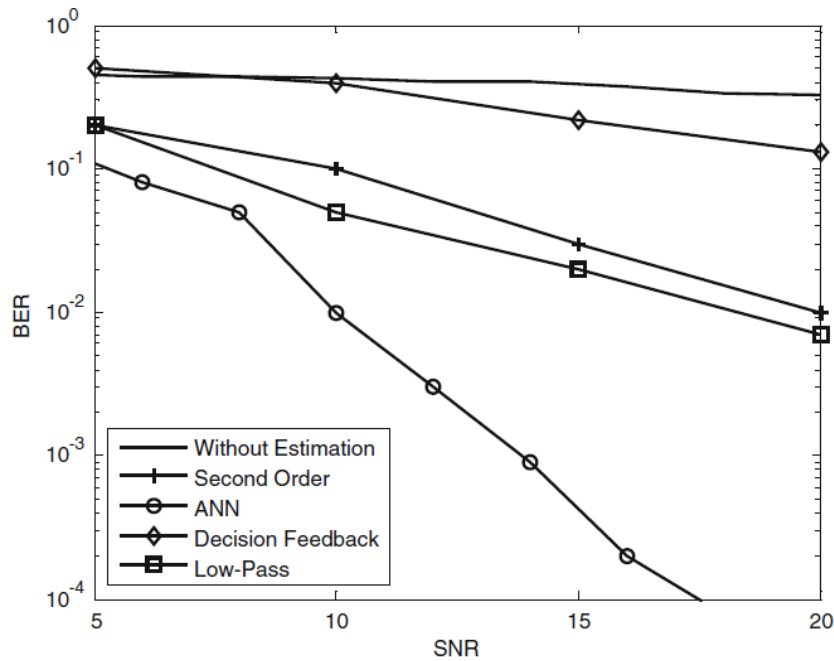


Figure 2.6.4: BPSK Modulation with Rayleigh fading -Comparison of conventional channel estimates techniques with those implemented with Artificial Neural Network

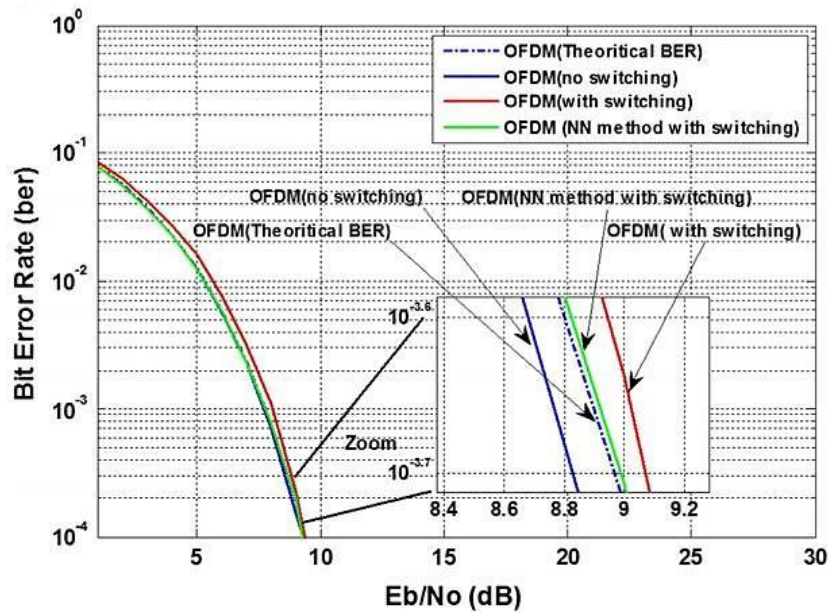


Figure 2.6.5: Comparison of BER performance for Wireless LAN standard

In Figure 2.6.5 and Figure 2.6.6, the BER performance of both the OFDM standards (i.e. Wireless LAN and WiMAX) with different schemes are shown and compared respectively. In these figures, all the schemes (OFDM (no switch), OFDM (with switching) and OFDM

(NN method with switching) have been evaluated in the presence of Additive White Gaussian Noise (AWGN). It can be observed that the proposed NN method outperforms the OFDM (with switching) scheme and remains at par with OFDM (no switching).

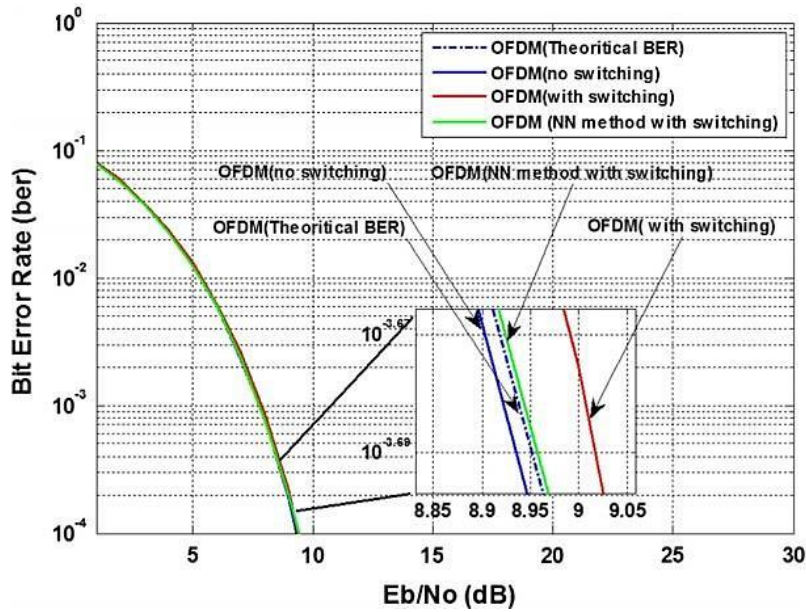


Figure2.6.6: Comparison of BER performance for WiMAX standard

This clearly shows that the proposed method improves the BER performance noticeably with huge reduction in computational complexity in comparison to OFDM (with switching) method. Therefore described method inherently possess all the drawbacks of the original scheme. Although the proposed method removes the need of CSI, but at low SNR situation, its BER performance is not good enough. Because the low SNR induces incorrect “un-switching” at the receiver which may further deteriorates the BER performance.

\*\*\*\*\*

# CHAPTER-III

---

## CHANNEL ESTIMATION IN LTE DOWNLINK

Topics:

**3.1.** Introduction to 3GPP Specifications

**3.2.** Design of Physical Layer LTE Downlink

**3.2.1.** Frame Structure

**3.2.1.1.** Physical Signals

**3.2.1.2.** Reference Signals

**3.2.1.3.** Synchronization Signals

**3.2.1.3.1.** Primary Synchronization Signals(PSS)

**3.2.1.3.2.** Secondary Synchronization Signals(SSS)

**3.2.2.** OFDM Modulation

**3.2.3.** Multipath fading propagation conditions

**3.2.4.** OFDM Demodulation

### **3.2.5. Channel Estimation for Downlink 3GPP-LTE systems**

#### **3.2.5.1 Pilot Signal Estimation**

#### **3.2.5.2 Interpolation**

##### **3.2.5.2.1. Linear Interpolation**

##### **3.2.5.2.2. DFT based Interpolation**

#### **3.2.5.3 Noise Estimation**

### **3.3. Simulated Results and Discussion**

### **3.4. Development in Multicarrier systems**

---

This chapter contains three sections: first discusses about the third generation partnership project (3GPP) specifications and frame structure for Long Term Evolution(LTE). After that, an attempt is made to design the physical layer transceiver section of the LTE in Matlab, incorporating channel estimation techniques. This is followed by introduction to the non-orthogonal multicarrier waveforms used in the 5G, due to issues discussed later.

### 3.1. INTRODUCTION TO 3GPP SPECIFICATIONS

LTE or the E-UTRAN (Evolved Universal Terrestrial Access Network), introduced in 3GPP Release 8, is the access part of the Evolved Packet System(EPS). The main requirements for the new access network are high spectral efficiency, high peak data rates, short round trip time as well as flexibility in frequency and bandwidth. The specifications for LTE are produced by the Third Generation Partnership Project, in the same way as the specifications for UMTS and GSM. They are organized into *releases* [54], each of which contains a stable and clearly defined set of features. The use of releases allows equipment manufacturers to build devices using some or all of the features of earlier releases, while 3GPP continues to add new features to the system in a later release. Within each release, the specifications progress through a number of different versions. New functionality can be added to successive versions until the date when the release is frozen, after which the only changes involve refinement of the technical details, corrections and clarifications. 3GPP continues to expand the LTE platform to new services, while improving its efficiency to meet the increasing mobile broadband demand. Ever since introduction of LTE in Release 8, there have been significant improvements in the following releases. For instance Release 9 introduced complete integration of femtocell concept evolved multimedia broadcast and multicast service (eMBMS), positioning support (LCS) and also added new spectrum bands (e.g., 800 MHz and 1500 MHz) for LTE operation. In Release 10 main new functionalities introduced in LTE-Advanced are Carrier Aggregation (CA), enhanced use of multi-antenna techniques and support for Relay Nodes (RN).

LTE was required to deliver a peak data rate of 100 Mbps in the downlink and 50 Mbps in the uplink. This requirement was exceeded in the eventual system, which delivers peak data rates of 300 Mbps and 75 Mbps respectively. For comparison, the peak data rate of

## CHANNEL ESTIMATION IN LTE DOWNLINK

WCDMA, in Release 6 of the 3GPP specifications, is 14Mbps in the downlink and 5.7Mbps in the uplink. It cannot be stressed too strongly, however, that these peak data rates can only be reached in idealized conditions, and are wholly unachievable in any realistic scenario. A better measure is the *spectral efficiency*, which expresses the typical capacity of one cell per unit bandwidth. LTE was required to support a spectral efficiency three to four times greater than that of Release 6 WCDMA in the downlink and two to three times greater in the uplink. Latency is another important issue, particularly for time-critical applications such as voice and interactive games.

### 3.2. DESIGN OF PHYSICAL LAYER LTE DOWNLINK

#### 3.2.1. Frame Structure

Starting from “3GPP Releases 8” specification, we are developing the physical layer downlink model of Long-Term Evolution (LTE) downlink at 20MHz by following the frame structure of Frequency Division Duplex shown in Figure 2.1. The detail frame structure of the FDD is given Figure 2.1. It only shows the structure of radio frame.

Description of radio frame given below:

- 1) Time duration of radio frame is 10 ms.
- 2) The number of samples in radio frame (10 ms) is 307200 (307.200 K) samples. This means that the number of samples per second is  $307200 \times 100 = 30.72$  M samples/sec.
- 3) Number of sub frame in radio frame is 10.
- 4) Number of slots in one sub frame is 2. This means that we have 20 slots within radio frame.

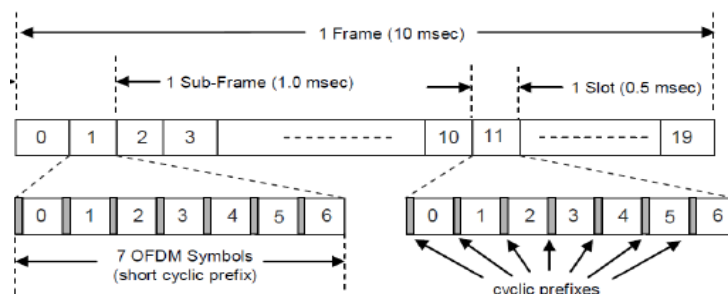


**Figure3.2.1.1.** Frame structure of LTE in FFD mode

In the 1<sup>st</sup> slot of the radio frame there are 7 OFDM symbols. A detailed description of the slot is shown in Figure 2.2 If you magnify a sub frame to show the exact timing and samples, it can be illustrated as below. The length shown in this illustration does not vary with the

## CHANNEL ESTIMATION IN LTE DOWNLINK

Sampling Rate, but the number of samples in each symbol and CP varies with the sampling rate. The number of samples shown in this illustration is based on the case of 30.72 MHz sampling rate.

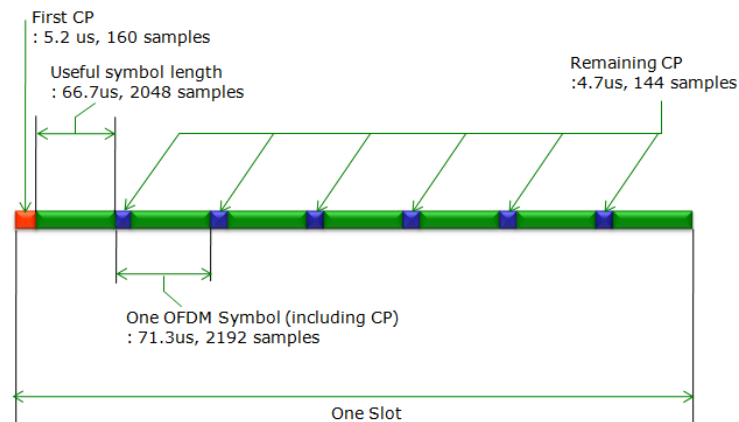


**Figure 3.2.1.2.** 1<sup>st</sup> slot of LTE radio frame

### 3.2.1.1. Physical Signals

The final information streams are the physical signals, which support the lowest-level operation of the physical layer. These are listed in Table 6.6. In the uplink, the mobile transmits the *demodulation reference signal* (DRS) at the same time as the PUSCH and PUCCH, as a phase reference for use in channel estimation. It can also transmit the *sounding reference signal* (SRS) at times configured by the base station, as a power reference in support of frequency-dependent scheduling. The downlink usually combines these two roles in the form of the *cell specific reference signal* (RS). *UE specific reference signals* are less important, and are sent to mobiles that are using beamforming in support of channel estimation. The specifications introduce other downlink reference signals as part of Releases 9 and 10. The base station also transmits two other physical signals, which help the mobile acquire the base station after it first switches on. These are known as the *primary synchronization signal* (PSS) and the *secondary synchronization signal* (SSS).

Signal	Release	Name	Use	Direction
DRS	R8	Demodulation reference signal	Channel estimation	UL
SRS	R8	Sounding reference signal	Scheduling	
PSS	R8	Primary synchronization signal	Acquisition	DL
SSS	R8	Secondary synchronization signal	Acquisition	
RS	R8	Cell specific reference signal	Channel estimation and scheduling	DL
	R8	UE specific reference signal	Channel estimation	
	R8/R9	MBMS reference signal	Channel estimation	
	R9	Positioning reference signal	Location services	
	R10	CSI reference signal	Scheduling	

**Table 3.1** :Physical Signals in both Uplink(UL) and Downlink(DL)

## CHANNEL ESTIMATION IN LTE DOWNLINK

Five types of downlink reference signals as defined in Table. Release 8 uses two types of downlink reference signal, but the cell-specific reference signals are the most important, which are defined below and later mapped on to the resource grid for one sub frame.

### 3.2.1.2. Reference Signals

We are considering the cell specific reference signal shall be transmitted in all downlink sub frames. Cell-specific reference signals are transmitted on one or several of antenna ports 0 to 3. For the mean time we are considering only the signal antenna ports. The cell-specific reference signal is a kind of gold sequence known as pseudo random sequence. Reference signal is generated by combining the two gold Sequences. Generation of two golden sequence represented as  $x1(n)$  and  $x2(n)$  and correlation of  $x1(n)$  and  $x2(n)$  results into the gold sequences shown in Figure 2.3, used as a cell- specific reference

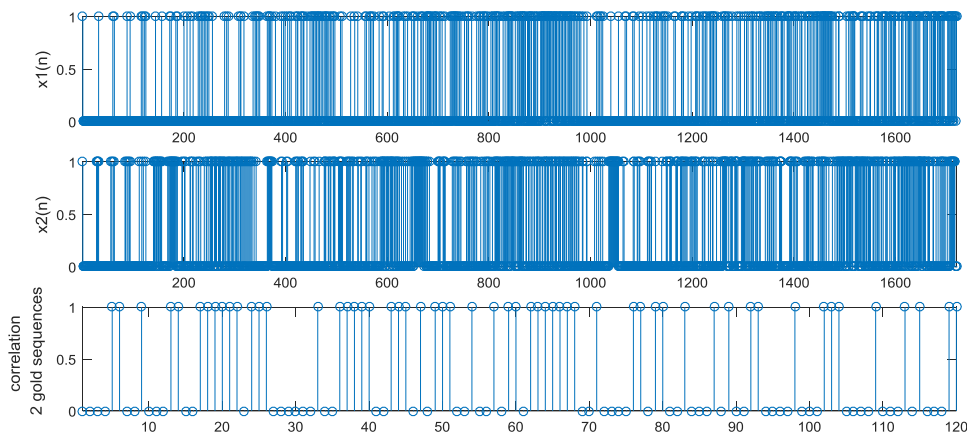


Fig. 3.2.1.2.1 Cell-specific reference signals

### 3.2.1.3 Synchronization Signals

The physical cell identity is a number between 0 and 503, which is transmitted on the synchronization signals, it determines the exact set of resource elements that are used for the cell-specific reference signals. Two types of synchronization signals are used, Primary Synchronization Signals(PSS) and Secondary Synchronization Signals(SSS).

#### 3.2.1.3.1 Primary Synchronization Signals(PSS)

Primary synchronization signal (PSS) is a specific physical layer signal that is used for frame synchronization with the following characteristics:

- Mapped to 72 sub-carriers (6 resource blocks), centred on the DC sub-carrier.
- PSS equation generation using the Zadoff-Chu Sequence.

## CHANNEL ESTIMATION IN LTE DOWNLINK

- Used for Downlink Frame Synchronization
- Used for determining the physical Cell ID

The sequence  $d(n)$  used for the primary synchronization signal is generated from a frequency-domain Zadoff-Chu sequence according to

$$d(n) = \begin{cases} e^{-j\pi u n(n+1)/63} & n=0,1,\dots,30 \\ e^{-j\pi u (n+1)(n+2)/63} & n=31,\dots,61 \end{cases} \quad (3.2.1.3.1)$$

where  $u$  is the root sequence index (root:25,29 and 34) of Zadoff-Chu. These sequences exhibit the useful property that cyclically shifted versions of themselves are orthogonal to one another. After generation of PSS sequence we need to perform the correlation between the different roots such as 25, 29 and 34. The results of correlation are shown in Figure 2.4

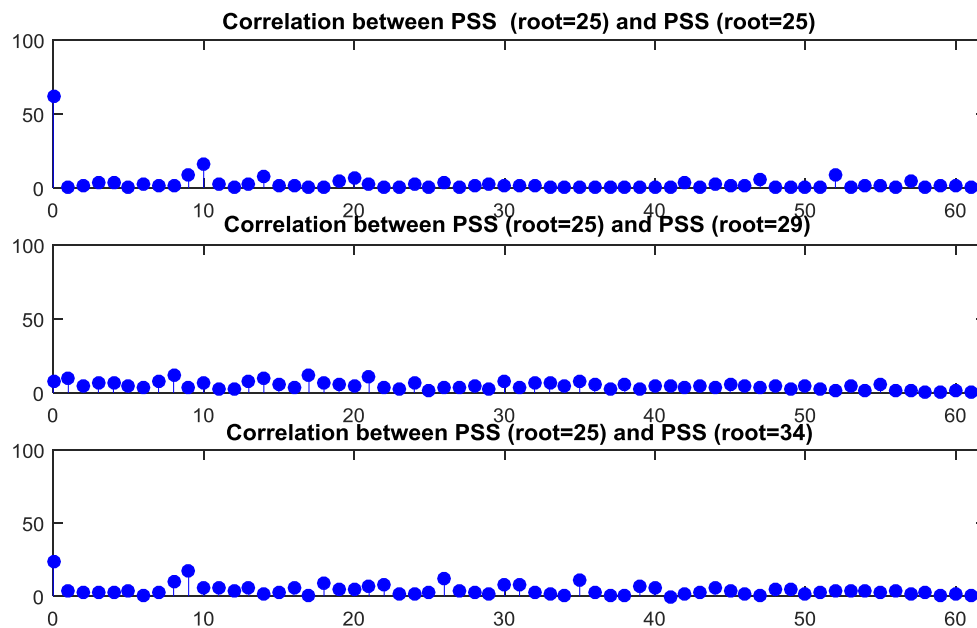


Fig. 3.2.1.3.1.1. Correlation between the different roots

### 3.2.1.3.2 Secondary Synchronization Signals(SSS)

Secondary synchronization signal (SSS) is a specific physical layer signal also used for frame synchronization and for finding the group ID with the following characteristics:

- Mapped to 72 sub-carriers (6 resource blocks), centered around the DC sub-carrier.
  - The sequence of SSS in sub-frame 0 and the one in subframe 5 are different from each other

## CHANNEL ESTIMATION IN LTE DOWNLINK

- Made up of 62 Scrambling Sequence (based on m-sequence)
  - The value in odd indexed resource element and the one in even indexed resource elements is generated by different equation

The sequence  $d(0), \dots, d(61)$  used for the second synchronization signal is an interleaved concatenation of two length-31 binary sequences. The concatenated sequence is scrambled with a scrambling sequence given by the PSS.

The combination of two length-31 sequences defining the secondary synchronization signal differs between subframe 0 and subframe 5 according to

$$d(2n) = \begin{cases} s_0^{m_0}(n)c_0(n) & \text{in subframe 0} \\ s_1^{m_1}(n)c_0(n) & \text{in subframe 5} \end{cases}$$

$$d(2n+1) = \begin{cases} s_1^{m_1}(n)c_1(n)z_1^{m_0}(n) & \text{in subframe 0} \\ s_0^{m_0}(n)c_1(n)z_1^{m_1}(n) & \text{in subframe 5} \end{cases}$$
(3.2.1.3.2)

where  $0 \leq n \leq 30$ . The indices  $m_0$  and  $m_1$  are derived from the physical-layer cell identity and two sequences  $s_0^{m_0}(n)$  and  $s_1^{m_1}(n)$  are defined as two different cyclic shifts of the m-sequence

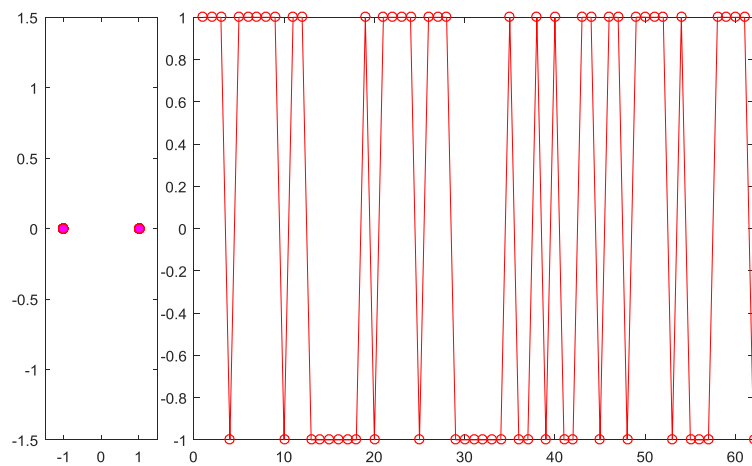


**Figure 3.2.1.3.2.** SSS signal of 62 symbols

From the Figure 3.2.1.3.2 we can see that left plot for the constellation diagram and the right plot for SSS made by a kind of scrambling sequence (based on m-sequence). After the generation of PSS, SSS sequences and cell-specific reference signal then we mapped these sequence along with the data in resource grid.

### 3.2.2 OFDM Modulation

Operations performed in OFDM Modulation is DC subcarrier insertion, inverse fast Fourier transform (IFFT) calculation, cyclic prefix insertion, and optional raised cosine windowing and overlapping of adjacent OFDM symbols of the complex symbols in the resource array, grid. grid is a 3-D array containing the resource elements (REs) for a number of sub frames across all configured antenna ports. It could also be multiple concatenated matrices to give multiple sub frames, using concatenation across the columns or second dimension. The antenna planes in grid are each OFDM modulated to yield the columns of the output waveform. grid can span multiple sub frames. Windowing and overlapping are applied between all adjacent OFDM symbols, including the last of one sub frame and the first of the next. Therefore, a different result is obtained than if OFDM Modulation is called on individual sub frames and then those time-domain waveforms are concatenated. In that case, the resulting waveform has discontinuities at the start or end of each sub frame. It is recommended that all sub frames for OFDM modulation first be concatenated before calling OFDM Modulation on the resulting multi-sub frame array. However, individual sub frames can be OFDM modulated and the resulting multi-sub frame time-domain waveform created by manual overlapping.

### 3.2.3. Multipath fading propagation Conditions

Multipath Fading channel model specifies the following 3 delay profiles:

- 1 Extended Pedestrian A model (EPA)
- 2 Extended Vehicular A model (EVA)
- 3 Extended typical urban model (ETU)

A set of 3 channel models are implemented to simulate the multipath fading propagation conditions. The multipath fading is modelled as a tapped-delay line with a number of taps at fixed positions on a sampling grid. The gain associated with each tap is characterized by a distribution and the maximum Doppler frequency that is determined from the mobile speed. For each tap, the method of filtered noise is used to generate channel coefficients with the specified distribution and spectral power density.

## CHANNEL ESTIMATION IN LTE DOWNLINK

<b>Extended Pedestrian A (EPA)</b>				
Path #	Doppler (Hz)	Fading Type	Delay (ns)	Relative Loss (dB)
1	5	Rayleigh	0	0
2	5	Rayleigh	30	1.0
3	5	Rayleigh	70	2.0
4	5	Rayleigh	90	3.0
5	5	Rayleigh	110	8.0
6	5	Rayleigh	190	17.2
7	5	Rayleigh	410	20.8

<b>Extended Vehicular A (EVA)</b>				
Path #	Doppler (Hz)	Fading Type	Delay (ns)	Relative Loss (dB)
1	70	Rayleigh	0	0.0
2	70	Rayleigh	30	1.5
3	70	Rayleigh	150	1.4
4	70	Rayleigh	310	13.6
5	70	Rayleigh	370	0.6
6	70	Rayleigh	710	9.1
7	70	Rayleigh	1090	7.0
8	70	Rayleigh	1730	12.0
9	70	Rayleigh	2510	16.9

<b>Extended Typical Urban (ETU)</b>				
Path #	Doppler (Hz)	Fading Type	Delay (ns)	Relative Loss (dB)
1	300	Rayleigh	0	1.0
2	300	Rayleigh	50	1.0
3	300	Rayleigh	120	1.0
4	300	Rayleigh	200	0.0
5	300	Rayleigh	230	0.0
6	300	Rayleigh	500	0.0
7	300	Rayleigh	1600	3.0
8	300	Rayleigh	2300	5.0
9	300	Rayleigh	5000	7.0

**Table 3.2:** EPA, EPA, ETU propagation fading model description

### 3.2.4. OFDM Demodulation

The demodulation performs one FFT operation per received OFDM symbol to recover the received subcarrier values. These values are then used to construct each column of the output resource array, grid. The FFT is positioned partway through the cyclic prefix to allow for a certain degree of channel delay spread while avoiding the overlap between adjacent OFDM symbols. The particular position of the FFT chosen here avoids the OFDM symbol overlapping used in OFDM Modulation. Since the FFT is performed away from the original zero-phase point on the transmitted subcarriers, a phase correction is applied to each subcarrier after the FFT. Then, the received subcarriers are extracted from the FFT bins, skipping unused frequency bins at either end of the spectrum and the central DC frequency bin. These extracted subcarriers form the columns of the output grid. The sampling rate of the time-domain waveform, waveform, must be the same as used in OFDM Modulation for the specified number of resource blocks, NDLRB. Waveform must also be time-aligned such that the first sample is the first sample of the cyclic prefix of the first OFDM symbol in a sub frame. This alignment can be achieved by using Downlink Frame Offset.

### 3.2.5. Channel Estimation For Downlink 3GPP-LTE Systems

LTE assigns each antenna port a unique set of locations within a sub frame to which map reference signals, means no other antenna transmits data at these locations in time and frequency. This allows channel estimation for multi –antenna configurations to be performed. Channel estimation algorithm extracts the reference signals for a transmit/ receive antenna from the received grid .Least square estimates of the channel frequency response at the pilot symbols are calculated, Least square estimates are then averaged to reduce any unwanted noise from the pilot symbols. Virtual pilot symbols are created to aid the interpolation process near the edge of the sub frame where no pilot are located, as shown in the figure .Two types of averaging can be performed, time averaging and frequency averaging. Time averaging is performed across each subcarrier that contains a pilot symbol, resulting in a column vector containing an average amplitude and phase for each subcarrier that is carrying a reference signal. Averaging the channel estimates at pilot symbol locations is a simple yet powerful tool, but the window size must be carefully chosen. Using a large window size on a fast fading channel could result in averaging out not only noise, but also channel

## CHANNEL ESTIMATION IN LTE DOWNLINK

characteristics. As depicted in figure the case of  $(1 \times 15)$  window (time averaging),  $(13 \times 1)$  window (frequency averaging) and  $(9 \times 9)$  window (time and frequency averaging). Performing too much averaging on a system with a small amount of noise can have an adverse effect on the quality of the channel estimates. Therefore, using a large averaging window for a fast changing channel could cause the estimate of the channel to appear flat, resulting in a poor estimate of the channel and affecting the quality of the equalization.

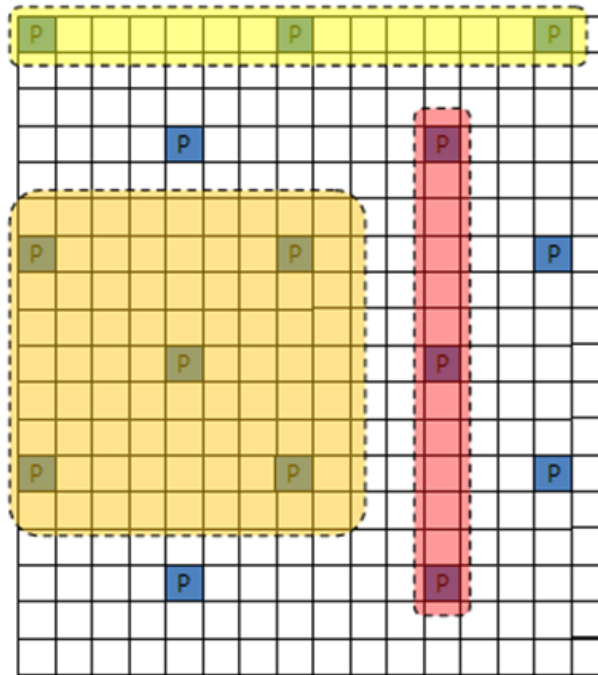


**Figure 3.2.5.1.:** Averaging Channel estimates at pilot symbol locations

The pilot signals are first extracted from the received signals, and the channel transfer function is estimated from the received pilot signals and known pilot signals. In many instances, the edges of the resource grid do not contain any pilot symbols. This effect is shown in the resource grid in the following figure.

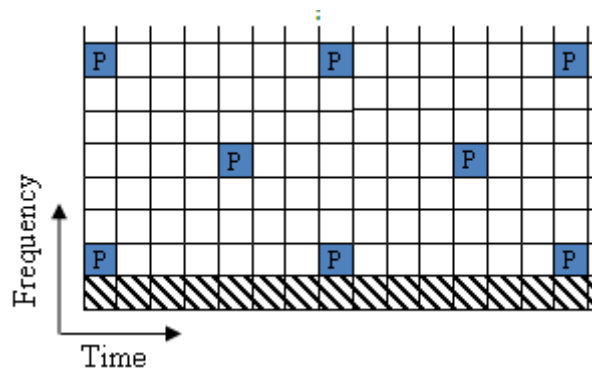


**Figure 3.2.5.1.2:** Scenario for virtual Pilots Subsystem. P-Pilot, dashed array- Resource elements (RE) which cannot be determined by interpolation

## CHANNEL ESTIMATION IN LTE DOWNLINK

As displayed in the figure above, the channel estimates at the edges cannot be interpolated from the pilot symbols. To overcome this problem, virtual pilot symbols are created. Virtual pilot symbols on all edges are placed on the received grid to allow cubic interpolation. Virtual pilots are created as depicted in figure below.

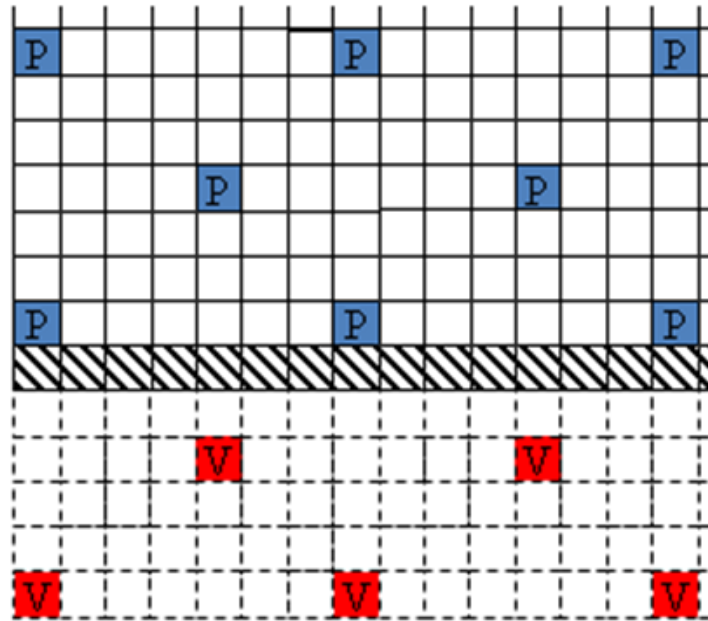


**Figure 3.2.5.1.3:** Virtual Pilot Placement

In this system, the resource grid is extended, with virtual pilot symbols created in locations which follow the original reference signal pattern. The presence of virtual pilot symbols allows the channel estimate at the resource element, which previously could not be calculated by interpolation, to be calculated by interpolation using original and virtual pilot symbols. For calculating virtual Pilot symbol values:

1. The closest 10 ordinary pilots in terms of Euclidean distance in time and frequency are selected. The searches are optimized to consider 10 of these pilots, rather than checking all possible pilots. Based on the possible configurations of the cell Reference Signal, using 10 pilots provides sufficient time and frequency diversity in the pilots for the virtual pilot calculation.
2. Using this set of the 10 pilots, the closest three pilot symbols are selected. These three symbols must occupy at least two unique subcarriers and two unique OFDM symbols.
3. Using this set of three pilots, two vectors are created. One vector between the closest and furthest pilot symbols, and one vector between the second closest and furthest pilot symbols.

## CHANNEL ESTIMATION IN LTE DOWNLINK

4. The cross-product of these two vectors is calculated to create a plane on which the three points reside.
5. The plane is extended to the position of the virtual pilot to calculate the value based on one of the actual pilot values.

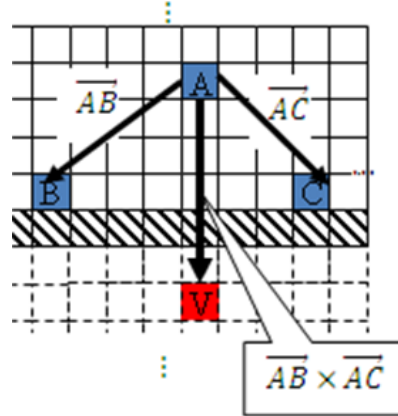


**Figure 3.2.5.1.4.:** Calculating Virtual Pilot Symbol values

Then, the channel responses of subcarriers that carry data are interpolated by using the neighboring pilot channel responses. Further, the pilot signals estimation and channel interpolation algorithms are discussed.

### 3.2.5.1. PILOT SIGNAL ESTIMATION

In following we assume amplitudes of the complex pilot signal  $X_p(m)$ ,  $m = 0, \dots, N_p - 1$ , are normalized to be unity for simplicity. Let  $\mathbf{h}_p = [H_p(0) H_p(1) \dots H_p(N_p - 1)]^T$ , be the channel response of pilot subcarriers and  $\mathbf{y}_p = [Y_p(0) Y_p(1) \dots Y_p(N_p - 1)]^T$ , be the received pilot signals vector, which can be rewritten as:  $\mathbf{y}_p = \mathbf{X}_p \mathbf{h}_p + \mathbf{w}_p$ , where

$$\mathbf{X}_p = \begin{bmatrix} X_p(0) & & 0 \\ & \ddots & \\ 0 & & X_p(N_p - 1) \end{bmatrix} \quad (3.2.5.1.1)$$

And  $\mathbf{w}_p$  is the vector of Gaussian noise in pilot subcarriers. The estimate of pilot signals based on least squares (LS) criteria is given by :

$$\begin{aligned} \hat{\mathbf{h}}_{p,LS} &= [H_{p,LS}(0) H_{p,LS}(1) \dots H_{p,LS}(N_p - 1)]^T = \mathbf{X}_p^{-1} \mathbf{y}_p \\ &= \begin{bmatrix} \frac{Y_p(0)}{X_p(0)} & \frac{Y_p(1)}{X_p(1)} & \dots & \frac{Y_p(N_p - 1)}{X_p(N_p - 1)} \end{bmatrix}^T, \end{aligned} \quad (3.2.5.1.2)$$

## CHANNEL ESTIMATION IN LTE DOWNLINK

The LS estimate of  $\hat{\mathbf{h}}_{p,LS}$  is susceptible to Gaussian noise. The Linear minimum mean square error (LMMSE) estimator only uses the frequency correlation of channel. The mathematical representation for LMMSE estimator of pilot signals is as follows[4,5]

$$\begin{aligned}\hat{\mathbf{h}}_{p,LMMSE} &= [H_{p,LMMSE}(0) \dots H_{p,LMMSE}(N_p - 1)]^T \\ \hat{\mathbf{h}}_{p,LMMSE} &= \mathbf{R}_{p\hat{p}} \mathbf{R}_{p\hat{p}}^{-1} \mathbf{y}_p = \mathbf{R}_{pp} \mathbf{X}_p^H (\mathbf{X}_p \mathbf{R}_{pp} \mathbf{X}_p^H + \sigma^2 \mathbf{I})^{-1} \mathbf{y}_p \\ &= \mathbf{R}_{pp} \left( \mathbf{R}_{pp} + \frac{\mathbf{1}}{SNR} \mathbf{I} \right)^{-1} \mathbf{h}_p\end{aligned}$$

here,  $\mathbf{R}_{p\hat{p}} = E\{\mathbf{h}_p \mathbf{y}_{\hat{p}}^H\} = E\{\mathbf{h}_p (\mathbf{X}_p \mathbf{h}_p + \mathbf{w}_p)^H\} = \mathbf{R}_{pp} \mathbf{X}_p^H$ ,

$$\begin{aligned}\mathbf{R}_{\hat{p}\hat{p}} &= E\{\mathbf{y}_p \mathbf{y}_p^H\} = E\{(\mathbf{X}_p \mathbf{h}_p + \mathbf{w}_p)(\mathbf{X}_p \mathbf{h}_p + \mathbf{w}_p)^H\} \\ &= \mathbf{X}_p \mathbf{R}_{pp} \mathbf{X}_p^H + \sigma^2 \mathbf{I} \\ \mathbf{R}_{pp} &= E\{\mathbf{h}_p \mathbf{h}_p^H\}\end{aligned}$$

(3.2.5.1.3)

where  $\hat{\mathbf{h}}_p$  is the least-square estimate of  $\mathbf{h}_p$  as shown in equation above,  $\mathbf{h}_p$  is the frequency response of the pilot signal,  $\mathbf{R}_{pp}$  is the channel auto-covariance matrices,  $\sigma^2$  is the variance of  $\mathbf{w}$ . The comparison of complexity analysis in the LS and LMMSE algorithm is shown below.

Complexity	LS Estimator	LMMSE Estimator
Complex multiplication	$N_p$	$2N_p^3 + N_p^2$
Complex addition	0	$2N_p^3 + 2N_p^2$

**Table 3.3.:**Complexity of Least Squares(LS) and Least Minimum Mean Square Error(LMMSE)

### 3.2.5.2. INTERPOLATION

Once the noise has been reduced or removed from the least squares pilot symbol averages and sufficient virtual pilots have been determined, it is possible to estimate the missing values from the channel estimation grid. After the estimations of the channel frequency responses of pilot tones are obtained, the channel responses of data tones can be derived by interpolation with adjacent pilot tones. Here linear interpolation and DFT based interpolation method which due to their inherent simplicity are easy to implement.

### 3.2.5.2.1. Linear Interpolation

In linear interpolation algorithm, two successive pilot subcarriers are used to determine the channel response for data subcarriers that are located in between the pilots. For the data subcarrier  $k$ ,  $mL \leq k < (m + 1)L$ , the estimated channel response using linear interpolation method is given by :

$$\begin{aligned} \hat{H}(k) &= \hat{H}(mL + l) \\ &= \hat{H}_p(m) + \frac{l}{L} \left( \hat{H}_p(m + 1) - \hat{H}_p(m) \right) \end{aligned} \quad (3.2.5.2.1)$$

Where  $0 \leq l < L$  and  $L$  is the frequency spacing of two consecutive pilot subcarriers, where  $k \geq mL$ . Then the extrapolation method is expressed as:

$$\begin{aligned} \hat{H}(k) &= \hat{H}(mL + l) \\ &= \hat{H}_p(m) + \frac{l}{L} \left( \hat{H}_p(m) - \hat{H}_p(m - 1) \right) \end{aligned} \quad (3.2.5.2.2)$$

### 3.2.5.2.2. DFT based Interpolation

Initially, the channel frequency response at the pilot positions is known, by using equations above. The transformed version in time domain employing the IDFT

$$\hat{g}_s = IDFT(\hat{\mathbf{h}}_p)$$

where  $\hat{\mathbf{h}}_p$  represent a samples version of an estimation of the channel's frequency responses, In time domain, zero padding is carried out in vector  $\hat{\mathbf{h}}_p$ , to obtain vector  $\hat{\mathbf{g}}$ .

$$\hat{\mathbf{g}} = [\hat{\mathbf{g}}_s \quad 0]_{1 \times N},$$

Finally, the result is transformed back to the frequency domain by DFT,

$$\hat{\mathbf{h}} = DFT(\hat{\mathbf{g}}),$$

where  $\hat{\mathbf{h}}$  is a frequency- domain  $1 \times N$  vector which contains the estimation of the channel frequency response at any of the  $N$  subcarriers. An important benefit of DFT based interpolation in terms of complexity is the low computational load of the DFT/IDFT when implemented as fast transforms. Therefore, this interpolation technique is desirable for implementation in digital receivers.

Complexity	DFT Based Interpolation	Linear Interpolation
Complex multiplication	$\frac{1}{2}[N\log(N) + K_d\log(K_d)]$	$2K$
Complex addition	$\frac{1}{2}[N\log(N) + K_d\log(K_d)]$	$K$

**Table 3.4.:** Complexity of DFT based interpolation and Linear interpolation

### 3.2.5.3. Noise Estimation

The performance of some receivers can be improved through knowledge of the noise power present on the received signal. The estimated channel response at known reference signal location is used to provide an estimate of the noise power spectral density(PSD).

The noisy least-squares estimates and the noise averaged pilot symbol estimates provide an indication of the channel noise. The least- squares estimates and the averaged estimates contain the same data, apart from additive noise. Simply taking the difference between the two estimates results in a noise level value for the least squares channel estimates at pilot symbol locations. Considering again,

$$\tilde{H}_p(k) = \frac{Y_p(k)}{X_p(k)} = H_p(k) + noise \tag{3.2.5.3.1}$$

Averaging the instantaneous channel estimates over the smoothing window, we have

$$\tilde{H}_p^{AVG}(k) = \frac{1}{|S|} \sum_{m \in S} \tilde{H}_p(m) \approx H_p(k) \tag{3.2.5.3.2}$$

where  $S$  is the set of pilots in the smoothing window and  $|S|$  is the number of pilots in  $S$ . Thus, an estimate of the noise at a particular pilot resource element can be formed using

$$\overline{noise} = \tilde{H}_p(m) - \tilde{H}_p^{AVG}(k) \tag{3.2.5.3.3}$$

It is not possible to remove all the noise using averaging. Because it is only possible to reduce the noise, only an estimate of the noise power can be made. Also in the case of a noise free system or system with high SNR, averaging could have a detrimental effect on the quality of the least squares estimates.

## CHANNEL ESTIMATION IN LTE DOWNLINK

### 3.2.6. Simulated Results

The system parameters for the LTE downlink are listed below in the Table:

Parameters	Values
Bandwidth	1.4MHz
FFT Size	128
Resource Blocks in Frequency Domain	6
Subcarriers in frequency domain	72
Normal cyclic prefix Modulation symbol rate	1.008 Msps
Extended Cyclic prefix Modulation symbol rate	0.864 Msps
Number of Transmit Antenna	1
Number of receive Antenna	1
Modulation	16-QAM
Sampling Rate(Mega samples per second)	1.92
Velocity	36km/h
Equalization	MMSE
Number of OFDM symbols per slot	7

**Table 3.5:** Parameters of LTE downlink System

When using the normal Cyclic Prefix:

- Duration of the first prefix within a slot is  $160 \times T_s$
- Duration of subsequent prefixes within a slot is  $144 \times T_s$

When using extended Cyclic Prefix the duration of the prefix is always  $512 \times T_s$ . The table listed below depicts the resource allocations for Synchronization and Reference signals used in the formulation of LT downlink Physical Layer.

	Channel Bandwidth 1.4MHz
Synchronization Resource Elements per 10ms Radio Frame	$2 \times 144 = 288$
<b>Normal Cyclic Prefix</b>	
Synchronization Resource Elements per 10ms Radio Frame	10080 <i>overhead</i> (2.9%)
Reference Signal Resource Elements per Resource Block (1 Antenna Port)	4 <i>overhead</i> $\left(\frac{4}{84} = 4.8\%\right)$
<b>Extended Cyclic Prefix</b>	
Synchronization Resource Elements per 10ms Radio Frame	8640 <i>overhead</i> (3.3%)

## CHANNEL ESTIMATION IN LTE DOWNLINK

Reference Signal Resource Elements per Resource Block (1 Antenna Port)	$4 \text{ overhead } \left( \frac{4}{72} = 5.6\% \right)$
--	---

**Table 3.6.:** Resource Allocation for Synchronization Signals and Reference signals using both normal and Extended Cyclic prefix

### Downlink Physical Channels

**PBCH-** The Physical Broadcast Channel used to broadcast the Master Information Block(MIB) using the BCH transport channel and BCCH logical channel.

**PCFICH-** Physical Control Format Indicator Channel is used at the start of each 1ms sub frame to signal the number of symbols used for PDCCH transmission.

**PHICH-** Physical Hybrid ARQ Indicator Channel is used to signal positive or negative acknowledgements for uplink data transferred on the PUSCH.

**PDSCH-** Physical Downlink shared Channel (PDSCH) is used to transfer system information, paging and other signaling messages and application data.

### Downlink Transport Channels

**BCH-**Broadcast channel transfers the Master Information Block using BCCH Logical channel.

**PCH-**Paging Channel transfers the paging message using PCCH logical channel.

**DL-SCH-**Downlink Shared Channel is used to transfer System Information Blocks(SIB) and application data.

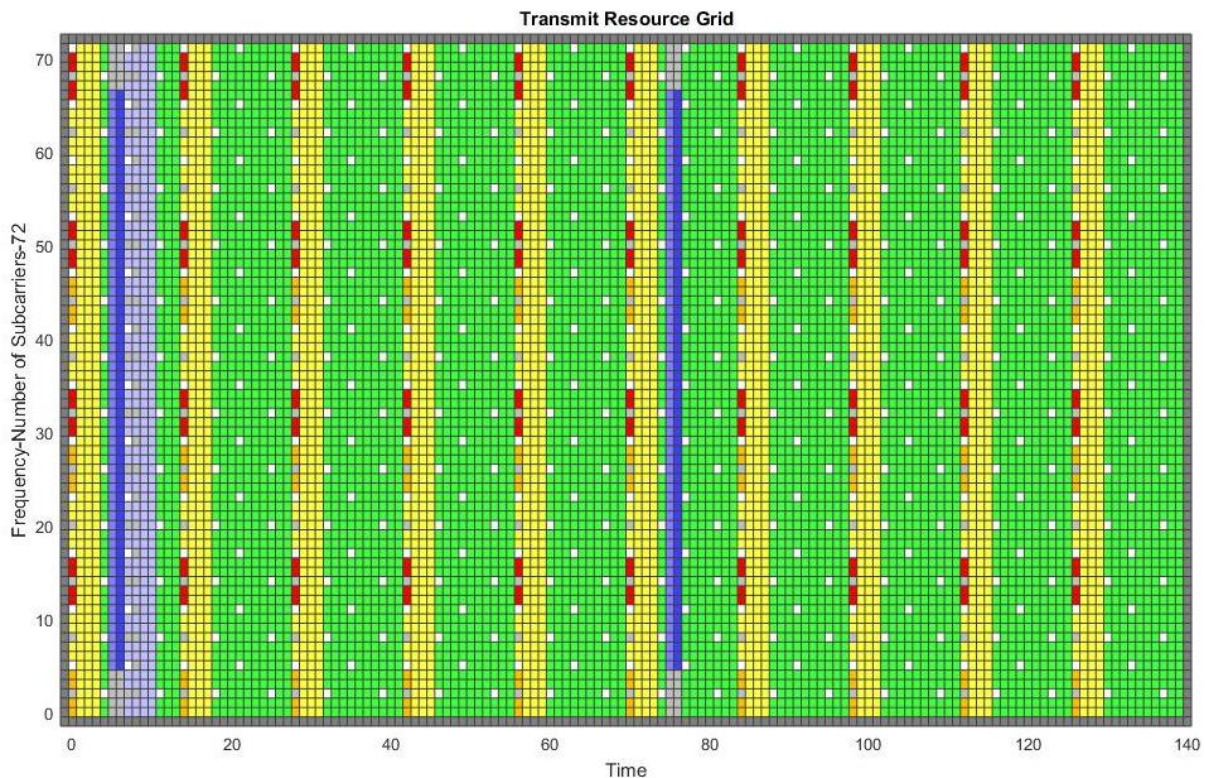


**Figure 3.2.6.1.:** Transmit Resource Grid with 72 subcarriers

## CHANNEL ESTIMATION IN LTE DOWNLINK

We can represent an LTE signal in a two dimensional map as shown in Figure 3.2.6.1. The horizontal axis is time domain and the vertical axis is frequency domain. The minimum unit on vertical axis is a sub carrier and the minimum unit on horizontal axis is symbol. For both time domain and frequency domain, there are multiple hierarchies of the units, meaning a multiple combination of a smaller unit become a larger units.

Figure 3.2.6.1 depicts the transmit resource grid for six resource blocks, with 12 subcarriers per resource block. It represents a complete LTE frame structure with the Primary and secondary synchronization signals in the beginning of first and the fifth OFDM symbol in the time domain axis. The reference signals are placed according to Zadoff Chu sequences according so there is zero correlation between two sequences. These signals are used for channel estimation. This whole grid can be allocated for one user, depending on the size of the data. For an instance an image  $366 \times 640$  will consume 12 frames for one user.

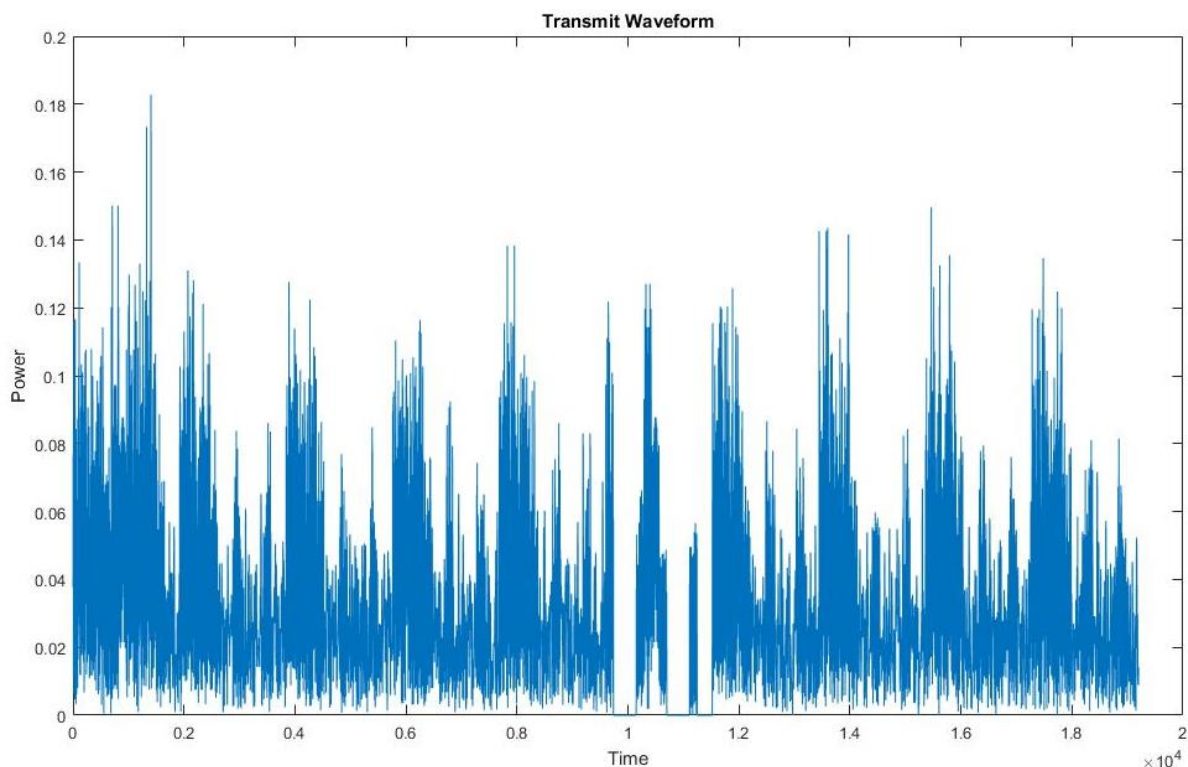


**Figure 3.2.6.2.:** Transmit waveform

## CHANNEL ESTIMATION IN LTE DOWNLINK

Figure 3.6.2 shows the Reference Measurement Channel (RMC) channel waveform at the transmitter end. This is for one sub frame and random data generation. 3GPP defines many standard-compliant reference signals (RMC, FRC and E-TM- TS 36.101). These waveforms for many purposes, including validating an RF component on a realistic LTE waveform, assessing the impact of an LTE interferer on another wireless system (or the opposite), or testing the correctness of LTE receiver on a flexible, synthesized LTE waveform.

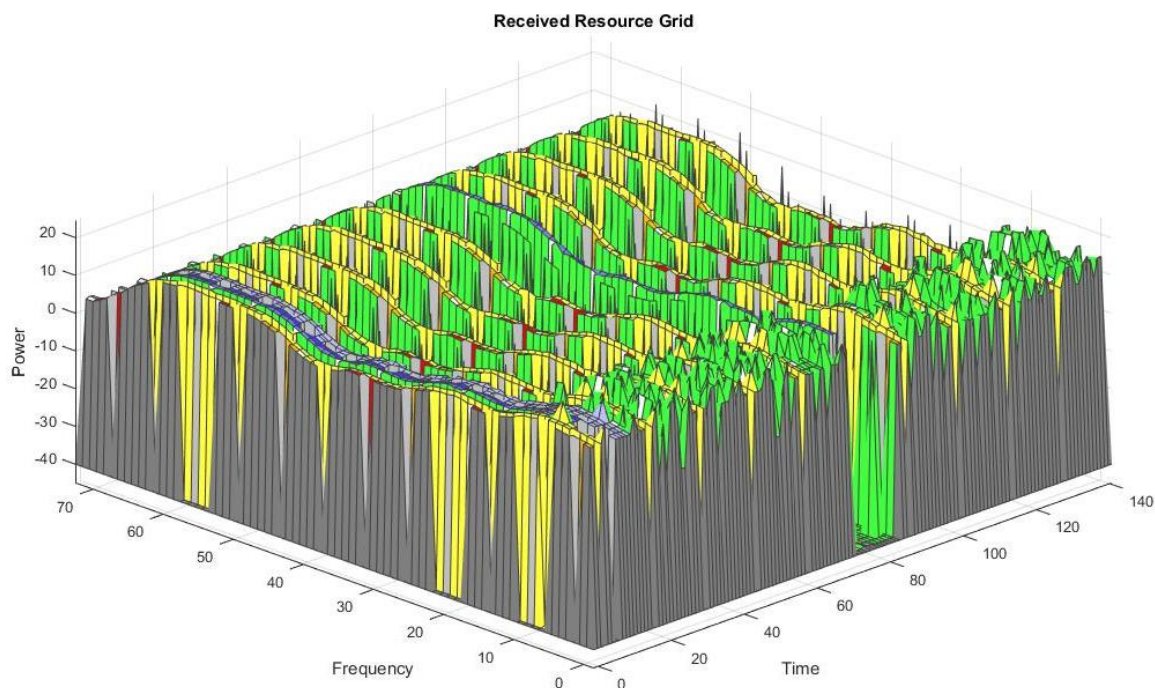


**Figure 3.2.6.3.:** Received Resource Grid passed through Extended Typical Urban model(ETU) multipath fading propagation condition

Among waveforms in LTE System standard-compliant reference measurement channels (RMCs) and fixed reference channels (FRCs), uplink and downlink. Figure 3.2.6.3 represents the equivalent grid when the transmit grid is passed through a selected propagation fading channel. In this case it is chosen to be Extended Typical Urban Model, it is one of proposed multipath fading propagation condition for LTE. These multipath fading propagation model are defined in 3GPP deliverables TS 36.101/TS 36.104.

## CHANNEL ESTIMATION IN LTE DOWNLINK

Figure 3.2.6.4 represent the received waveform in accordance with the received resource grid passed through the various propagation fading models waveforms are filtered with the delay profiles specified in the Table 3.2. These delay profiles are resampled to match the input signal sampling rate.

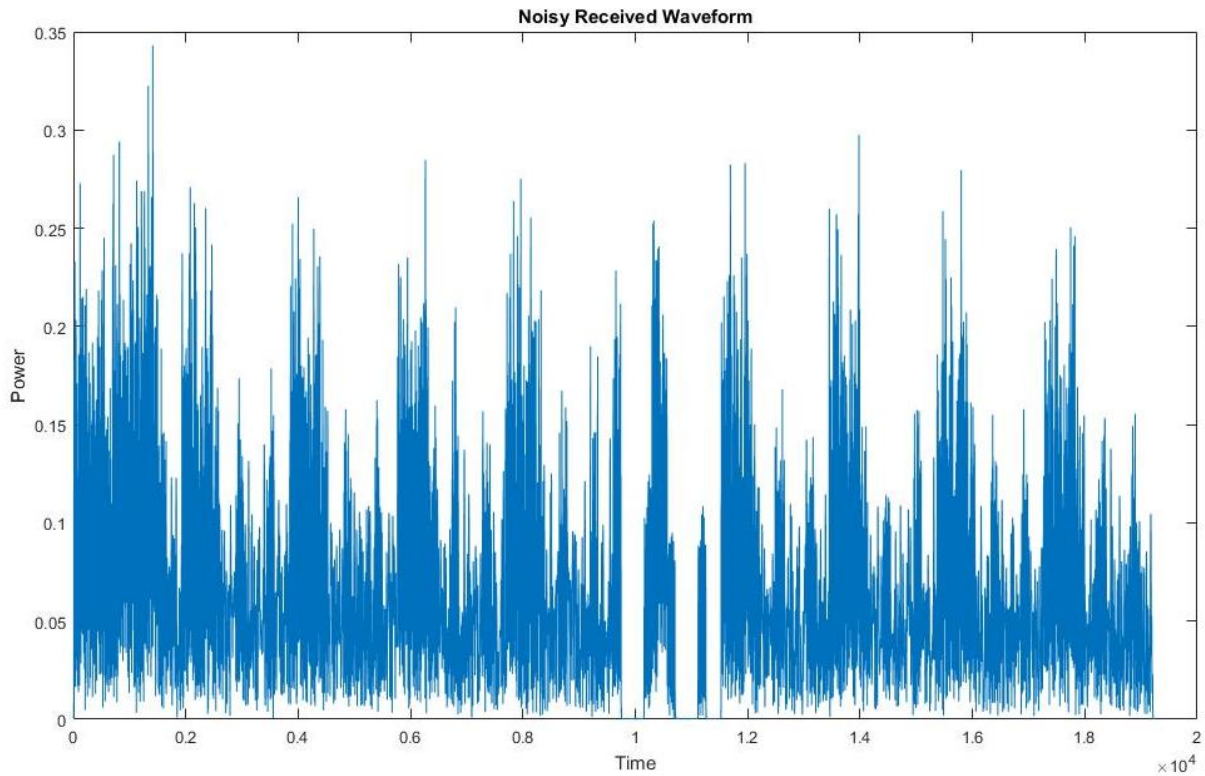


**Figure 3.2.6.4.:** Noisy Received Waveform

In the received waveform is in accordance to the assumption that the number of the receive antennas taken is one. If, we consider multiple antenna case the waveform would be distorted and normalized power had to be distributed over the number of antennas.

Also it is assumed that the correlation between the user equipment (UE) and eNodeB antenna is low. The low on correlation among the antennas is equivalent to no noise due to the orientation phase shifts introduced in the system.

The Rayleigh fading can be modeled using two different types. 'Dent' is modeled using the modified Jakes fading model described in "Jakes Fading Model Revisited", P. Dent, G. E. Bottomley and T. Croft, Electronics Letters Vol. 29 No. 13 and 'GMEDS' is modeled using the Generalized Method of Exact Doppler Spread(GMEDS). Here GMEDS model is used incorporating the moving user, responsible for the Doppler spread.

## CHANNEL ESTIMATION IN LTE DOWNLINK

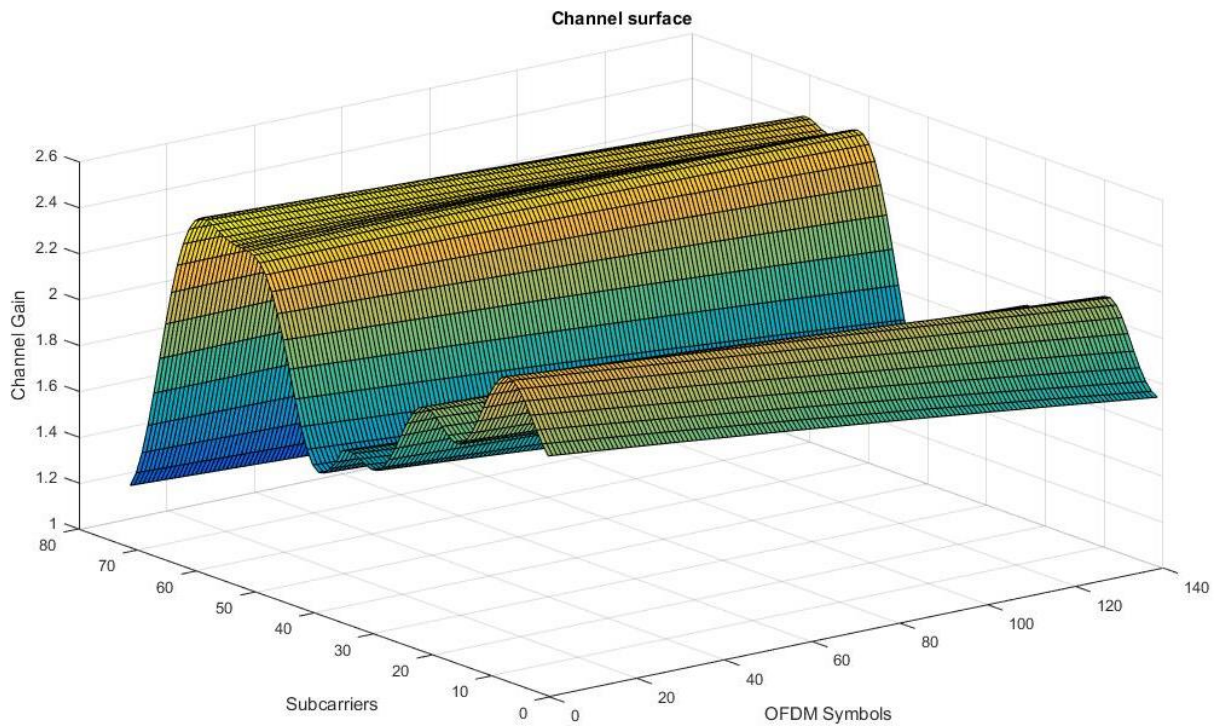


**Figure 3.2.6.5.:** Perfect Channel surface for Extended Typical Urban model(ETU) multipath fading propagation condition

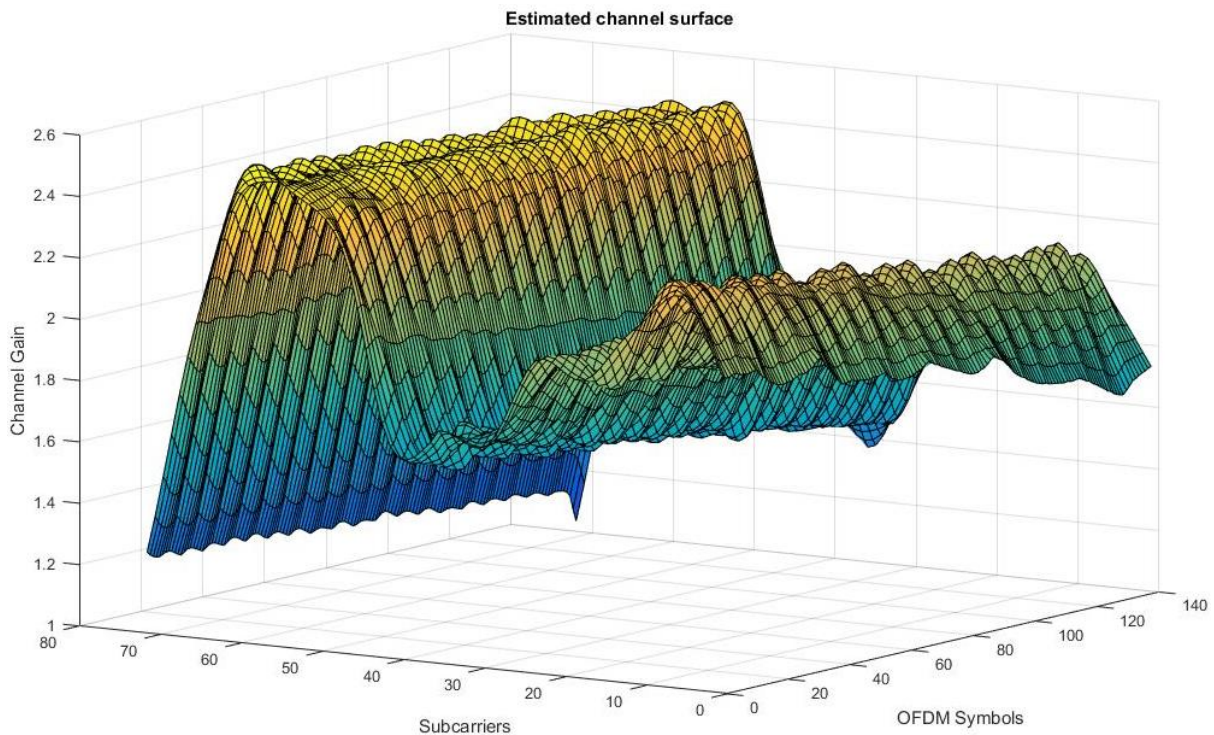


**Figure 3.2.6.6.:** Estimated Channel Surface for Extended Typical Urban model(ETU) multipath fading propagation condition, Type of Channel Estimator LMMSE.

## CHANNEL ESTIMATION IN LTE DOWNLINK

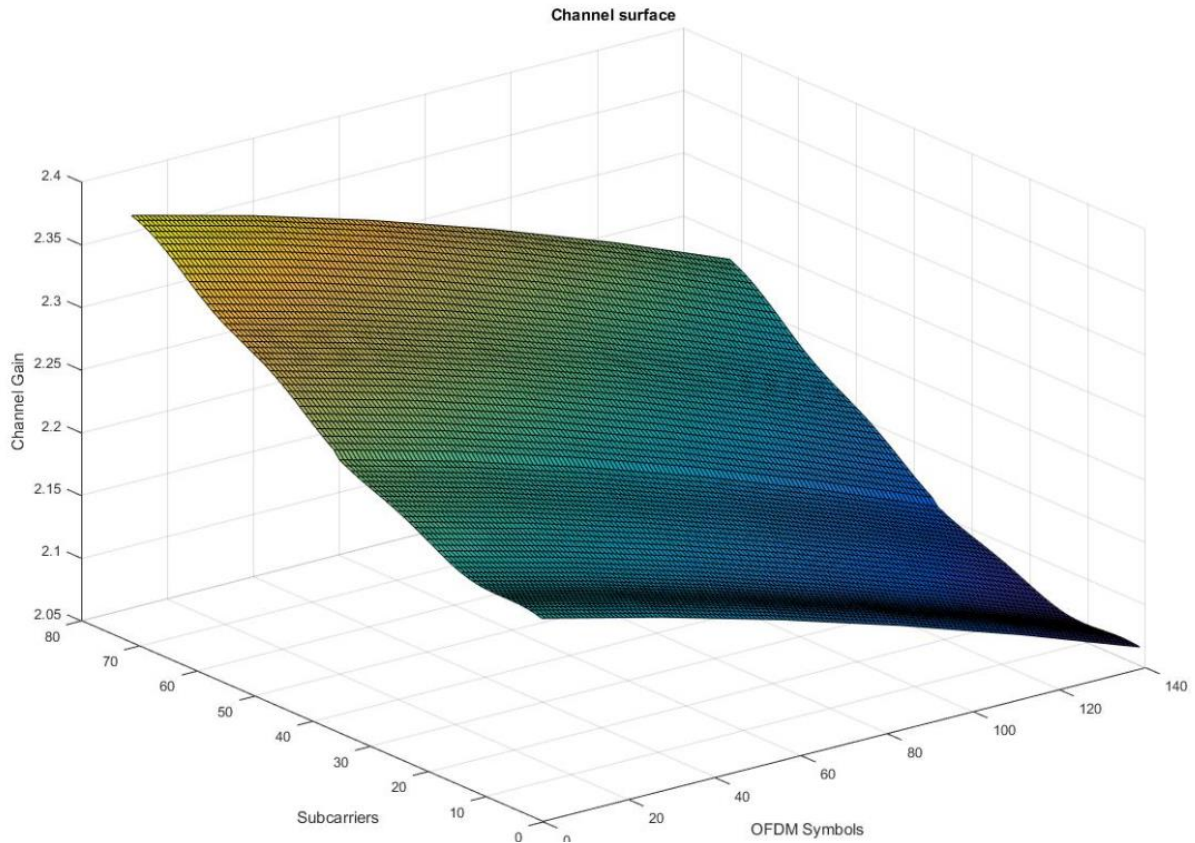


**Figure 3.2.6.7.:** Perfect Channel surface for Extended Pedestrian A model(EPA) multipath fading propagation condition

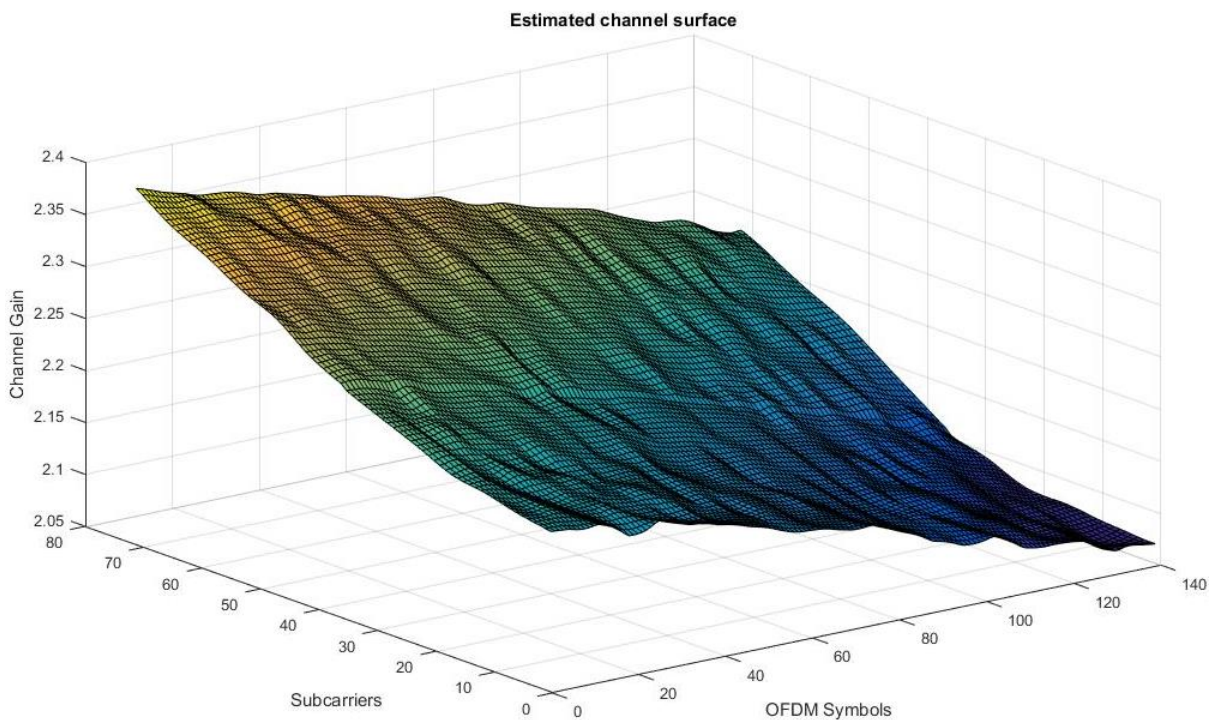


**Figure 3.2.6.8.:** Estimated Channel Surface for Extended Pedestrian A model(EPA) multipath fading propagation condition

## CHANNEL ESTIMATION IN LTE DOWNLINK

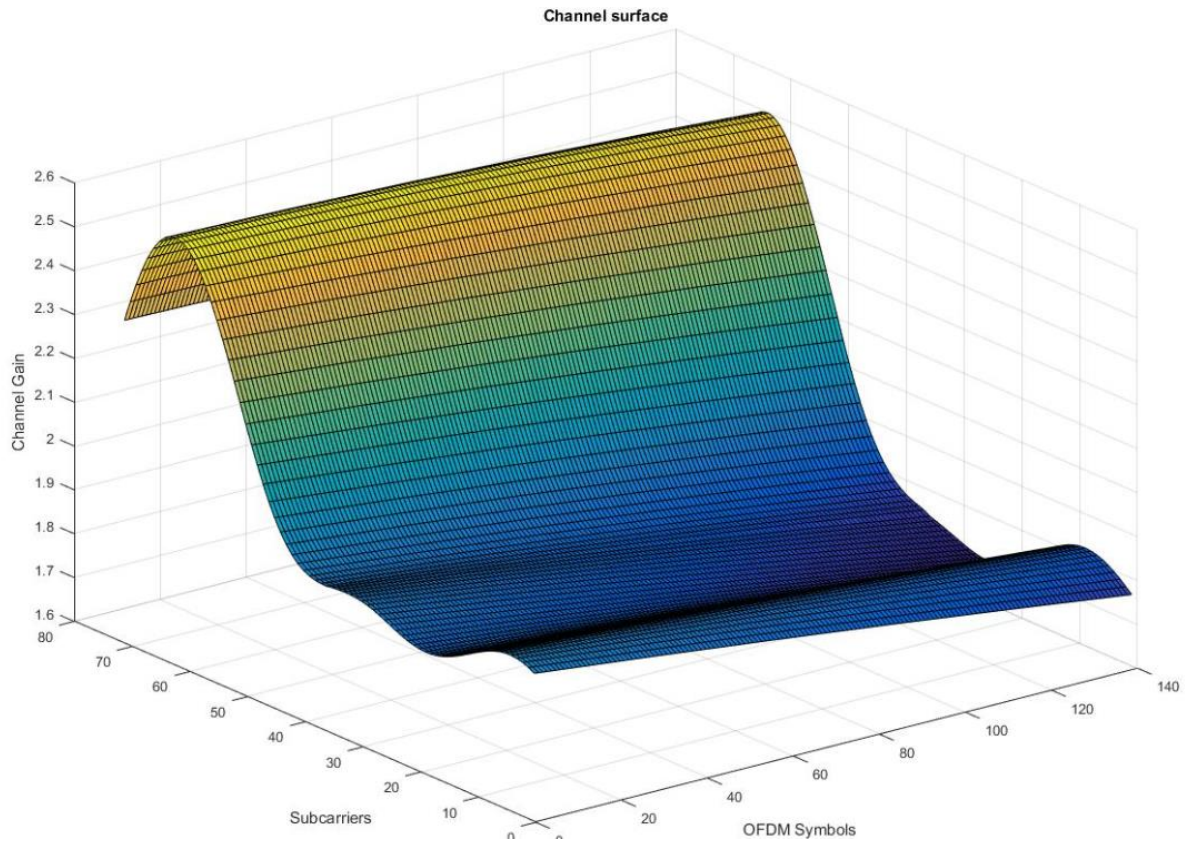


**Figure 3.2.6.9.:** Perfect Channel Surface for Extended Vehicular A model multipath fading propagation condition

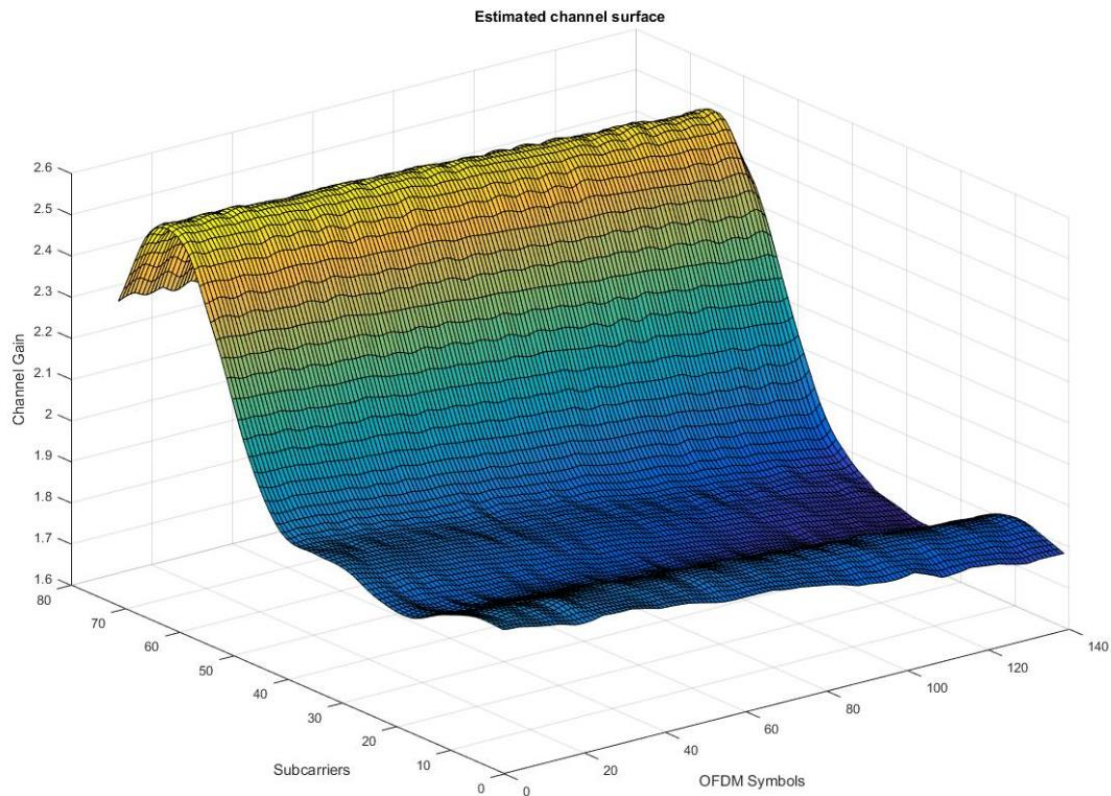


**Figure 3.2.6.10:** Estimated Channel surface for Extended Vehicular A model multipath fading propagation condition

Three types of multipath propagation model conditions have been simulated in the system which channel estimation techniques applied to each.

Figure 3.2.6.5 represents a channel gain response with respect to the subcarriers in frequency domain and OFDM symbols in Time domain. It depicts perfect channel response when passed through Extended Typical Urban model (ETU) multipath fading propagation condition.

Figure 3.2.6.6 represents a channel gain response with respect to the subcarriers in frequency domain and OFDM symbols in Time domain. It depicts estimated channel response when passed through Extended Typical Urban model (ETU) multipath fading propagation condition. For the estimation of the channel LMMSE estimator has been used. The window size for the frequency domain and time domain for the interpolation across the frequency and time domain has been taken unity. For a good estimate in case of a fast varying channel the window size for the averaging of the reference signals acting as pilot can be varied.

Figure 3.2.6.7 represents a channel gain response with respect to the subcarriers in frequency domain and OFDM symbols in Time domain. It depicts perfect channel response when passed through Extended Pedestrian A model (EPA) multipath fading propagation condition.

Figure 3.2.6.8 represents a channel gain response with respect to the subcarriers in frequency domain and OFDM symbols in Time domain. It depicts estimated channel response when passed through Extended Typical Urban model (ETU) multipath fading propagation condition. For the estimation of the channel LMMSE estimator has been used. The averaging window can be changed since the channel is not a fast varying channel. However the window for averaging across the frequency and time domain has been fixed across three models to have a comparative viewpoint over the performance.

Figure 3.2.6.9 represents a channel gain response with respect to the subcarriers in frequency domain and OFDM symbols in Time domain. It depicts perfect channel response when passed through Extended Vehicular A model (EPA) multipath fading propagation condition.

Figure 3.2.6.10 represents the channel estimation performed by using LMMSE estimator with the averaging window across time and frequency set to unity.

## CHANNEL ESTIMATION IN LTE DOWNLINK

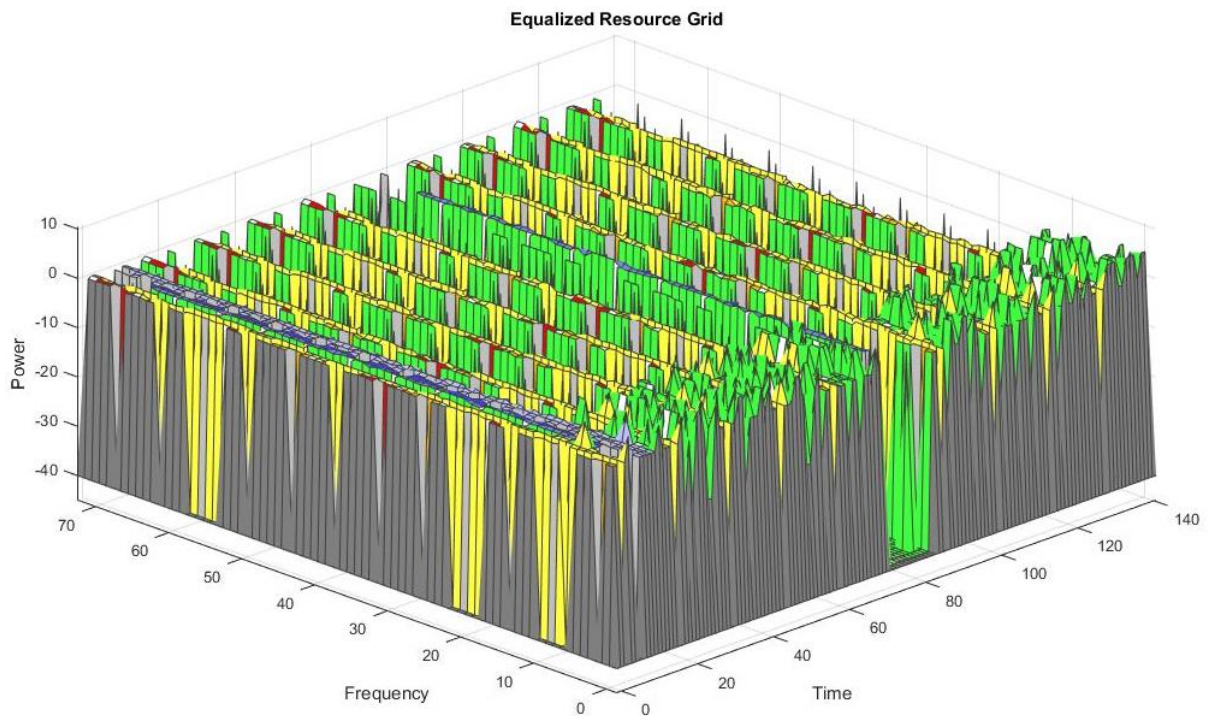


Figure 3.2.6.11.: Equalized Resource Grid, Type of Equalizer: MMSE

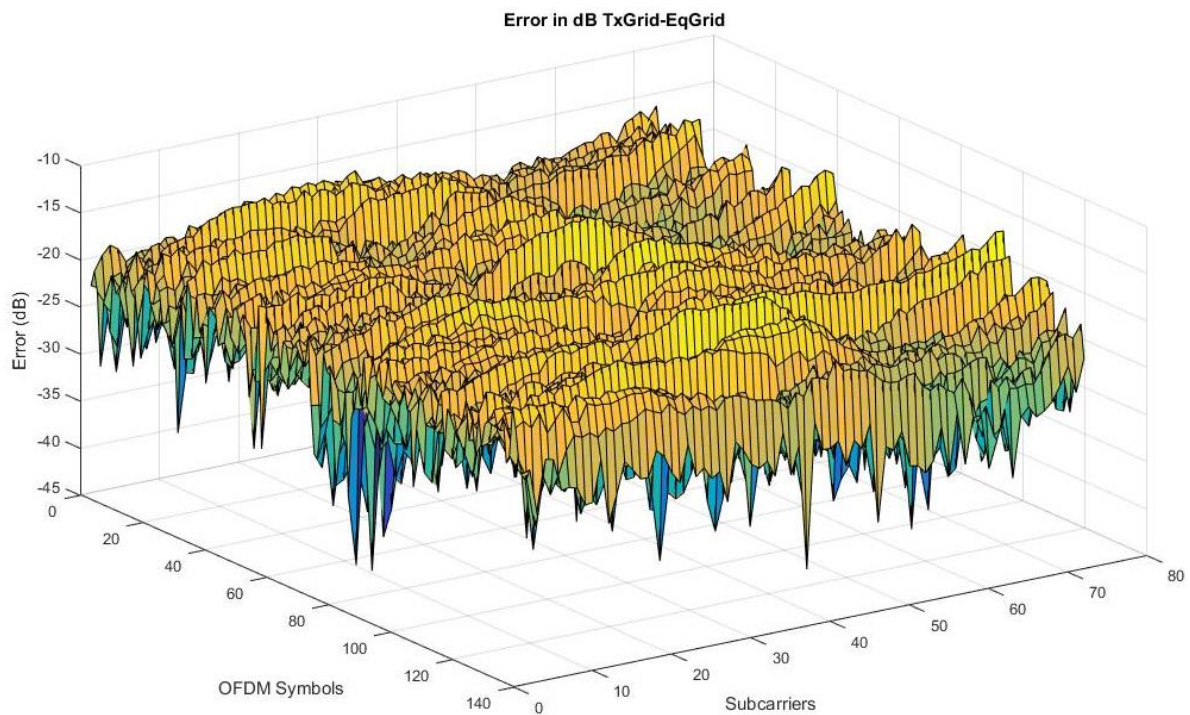


Figure 3.2.6.12.: Error In Equalization

## CHANNEL ESTIMATION IN LTE DOWNLINK

Figure 3.2.6.11 represents the equalized grid of the transceiver section. The equalizer employed here is MMSE. Figure 3.2.6.12 depicts the error in decibels in reference to the power of each resource block. The error has been calculated by the difference in the transmitted grid power for each resource element across the frequency and the time domain and that of the equalized grid at the receiver section. The result depicted for Extended typical urban propagation model condition.

### 3.3. DEVELOPMENT IN MULTICARRIER SYSTEMS

The most prominent multicarrier system OFDM is known to cause strong spectral leakage. This persists even when using pulse shaping techniques or guard carriers. In certain applications such as cognitive radios and uplink of multiuser multicarrier systems, where a subset of subcarriers is allocated to each user, OFDM may not be a desirable solution due to spectral leakage. In a cognitive radio setting where both primary (nongenerative nodes) and secondary users (cognitive nodes) transmit independently and may be based on different standards. In such a setting, the only way that one may adopt to separate the primary and secondary user signals is through a filtering mechanism. OFDM is thus a poor fit because the filters associated with its synthesized subcarrier signals (at the transmitter) and the analyzed subcarrier signals (at the receiver) have relatively large side lobes and such lobes will result in leakage of signal powers among the bands of different users. Figure 3.3.1 depicts the problem of spectral leakage and high side lobe energy occupation, with the graph of the power spectral density per unit frequency with the normalized frequency.

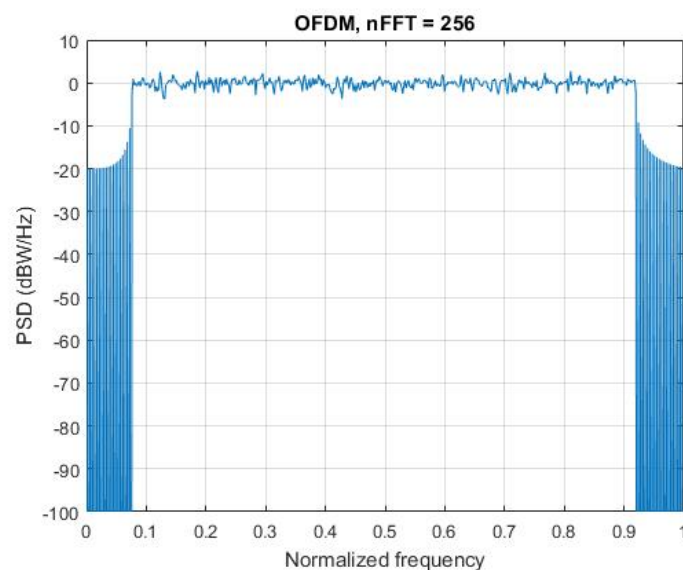


**Figure 3.3.1** Spectral Leakage in OFDM system

## CHANNEL ESTIMATION IN LTE DOWNLINK

As an example, an LTE system at 20 MHz channel bandwidth uses 100 resource blocks of 12 subcarriers each, at an individual subcarrier spacing of 15 KHz. This utilizes only 18 MHz of the allocated spectrum, leading to a 10 percent loss. Additionally, the cyclic prefix of 144 or 160 samples per OFDM symbol leads to another ~7 percent efficiency loss, for an overall 17 percent loss in possible spectral efficiency.

The above problems could be greatly reduced if the filters that synthesize/analyse the subcarrier signals had a small side lobes. Such filter banks can be designed with arbitrarily small side lobes and, therefore, are an ideal choice in multiple access as well as broadband data transmission. As simulated in Figure 3.3.2, the fairly reduced side lobes in FBMC compared to OFDM systems.

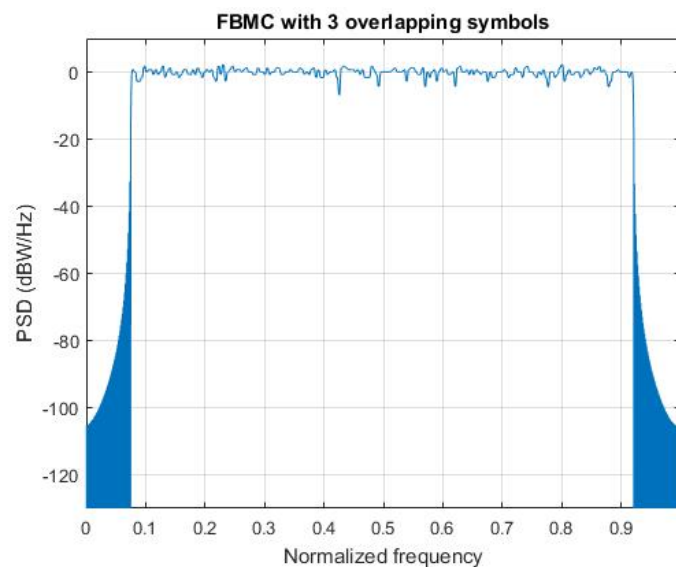


**Figure 3.3.2** Filter Bank Multicarrier Technique with reduced side lobes

Also with the now defined ITU requirements for 5G systems, applications require higher data rates, lower latency and more efficient spectrum usage. This section focuses on the new modulation technique known as Universal Filtered Multi-Carrier (UFMC) and compares it with OFDM within a generic framework.

UFMC is seen as a generalization of Filtered OFDM and FBMC (Filter Bank Multi-carrier) modulations. The entire band is filtered in filtered OFDM and individual subcarriers are filtered in FBMC, while groups of subcarriers (sub bands) are filtered in UFMC. This subcarrier grouping allows one to reduce the filter length (when compared with FBMC). Also, UFMC can still use QAM, which works with existing MIMO schemes.

## CHANNEL ESTIMATION IN LTE DOWNLINK

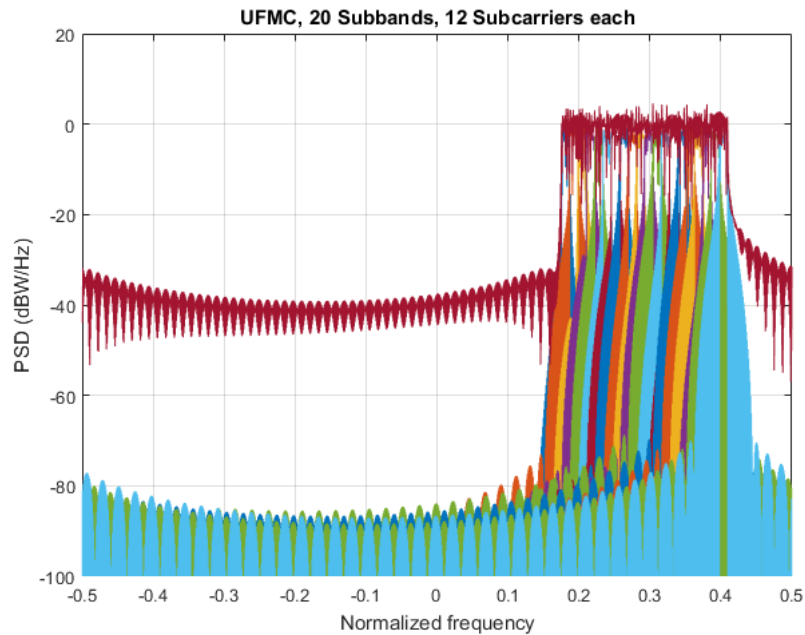


**Figure 3.3.3** Universal Filtered multicarrier technique with 20 sub bands and 12 carriers each

The full band of  $N$  subcarriers is divided into sub bands. Each sub band has a fixed number of subcarriers and not all sub bands need to be employed for a given transmission. An  $N$  point (Inverse Fast Fourier Transform) IFFT for each sub band is computed, inserting zeros for the unallocated carriers. Each sub band is filtered by a filter of length, and the responses from the different sub bands are summed. The filtering is done to reduce the out-of-band spectral emissions. Different filters per sub band can be designed, however, in this example, the same filter is used for each sub band. A Chebyshev window with parameterized side lobe attenuation is employed to filter the IFFT output per sub band. Figure 3.3.3 depicts the following simulation procedure followed for simulating UFMC technique.

# CHAPTER-IV

---

## **OFDM SYSTEM IN PRESENCE OF CHANNEL ESTIMATION ERROR & CARRIER FREQUENCY OFFSET**

Topics:

- 4.1.** Historical Development of OFDM
- 4.2.** Literature Survey on OFDM System in Presence of Channel Estimation Error and Carrier Frequency Offset.
- 4.3.** System Model
  - 4.3.1.** Transmitter Model
    - 4.3.1.1.** Cyclic Prefix or guard band insertion
  - 4.3.2** Channel Model
    - 4.3.2.1.** Frequency Selective Rayleigh Channel
  - 4.3.3.** Receiver Model
  - 4.3.4.** Effect of Channel Estimation Error

#### **4.4. BER Analysis of effects of Channel Estimation error in presence of Carrier Frequency Offset**

##### **4.4.1. BPSK Modulation**

##### **4.4.2. QPSK Modulation**

##### **4.4.3. 16-QAM Modulation**

#### **4.5. Simulation Results**

##### **4.5.1. Discussion of Simulation Results**

---

In this chapter, historical development of OFDM system along with literature survey on performance analysis of FFT-based OFDM system, and discussion of system model in presence of CFO and Channel estimation error with mathematical formulation of transmitter, channel and receiver. The exact closed form bit error rate (BER) and symbol error rate (SER) expressions for FFT-based OFDM systems with CFO and Channel Estimation Error are analysed. BER performances of BPSK, QPSK, 16-QAM are compared for Rayleigh fading channel. Numerical results are given to verify the accuracy of the derivations. The chapter is concluded by giving some final remarks.

#### 4.1. HISTORICAL DEVELOPMENT OF OFDM

Taking a brief discussion about the historical development of OFDM (milestones in history). Through this initially developed OFDM, attentions of researches moved towards the performance analysis of OFDM system. So firstly, summarizing the beginning of OFDM.

**Table-4.1:** Summary of OFDM

1965	P. A. Bello <i>et al.</i> [13]	Initial multicarrier (MCM) system KINEPLEX [13-14]
1967	M. Zimmerman <i>et al.</i> [14]	
1968	R.W. Chang <i>et al.</i> [15]	MCM employing overlapped band limited orthogonal signals.
1967	Saltzberg <i>et al.</i> [18]	MCM system employing orthogonal time staggered QAM.
1971	S.B. Weinstein <i>et al.</i> [20]	OFDM became more popular after the use of DFT to generate the orthogonal subcarriers
1980	J.S. Chow <i>et al.</i> [21]	Suggested the use of DFT based OFDM for high speed modems
1980	Hirosiki <i>et al.</i> [24]	Suggested a system for Saltsberg O-QAM OFDM system
1985	Cimini <i>et al.</i> [25]	Analytical and simulated results on the performance of OFDM modems
1988-1995	ETSI DAB standard [41]	first OFDM based standard for digital broadcasting system

## 4.2. LITERATURE SURVEY ON OFDM SYSTEM IN PRESENCE OF CHANNEL ESTIMATION ERROR AND CFO

In OFDM based systems when coherent modulation is employed at the transmitter, channel state Information(CSI) is necessary for the demodulation of the transmitted signals at the receiver. Various CSI estimators and their corresponding performance analysis have been studied and appeared in the literature. Pilot-symbol-assisted modulation(PSAM) with or without diversity have been analysed in “An analysis of pilot assisted modulation for Rayleigh fading channels” by **J.K Cavers** and “Exact error rate analysis of diversity 16QAM with channel estimation error” by **L.Cao** and **N.C Beaulieu**.

The use of PSAM in both time and frequency domains for time varying frequency selective channels have been investigated in “Two dimensional pilot symbol aided channel estimation by Weiner filtering” by P.Hoehner, S.Kaiser and “Pilot symbol aided channel estimation for OFDM in wireless systems” by Y.Li. In “Joint estimation of channel and data symbols” by Y.Song, S.Roy it is displayed that to improve the spectral efficiency pilot tones are transmitted only at the beginning of the frame and the channel estimator exploits the error correcting capability of a forward error correction decoder to reconstruct the transmitted data sequences and mitigate the effects of the channel estimator error.

When OFDM- based wireless system operate in a slowly fading multiple access environment the use of training (preamble) symbols to facilitate the channel estimation task has been specified in “Effect of channel estimation error in OFDM-based WLAN” by H.Cheon. Here he authors considered the channel estimate is not only corrupted by additive white Gaussian noise(AWGN) but also by the Intercarrier Interference(ICI) due to residual carrier frequency offset(CFO).

After the historical development of OFDM system moving towards the problem formulation on performance analysis of OFDM system. Two methods were available for the analysis of the resultant degradation in performance. Firstly, the statistical average of the ICI could be used as a performance measure. Secondly, the BER caused by CFO and STO could be approximated by assuming the ICI to be Gaussian. So that I have taken the performance analysis of OFDM system in presence of CFO and STO in terms of BER. The performance analysis in different channel environments (flat fading, frequency selective fading, etc.) with CFO has been done by different authors in [55-56]. Furthermore, the effect of CFO and STO

combined was considered in [57]. Before moving towards the problem formulation, I would like to discuss the brief summary of performance analysis of FFT -based OFDM system given by many authors.

“Probability of Error Calculation of OFDM Systems with Frequency Offset” by **K. Sathananthan** and **C. Tellambura** [58], 2001. In [58], a precise numerical techniques is given for calculating the effect of the CFO on the BER in an OFDM system. The subcarriers are modulated with binary phase shift keying (BPSK) and the analysis workout as using a series due to Beaulieu. For QPSK and 16-QAM cases, they used an infinite series expression for the error function in order to express the average probability of error in terms of the two-dimensional characteristic function of the ICI. The results are derived for the average probability of error in case of BPSK, QPSK and 16-QAM modulation techniques. In same work a Gaussian approximation is proposed for the approximate SNR degradation.

In 2002, “Effect of Channel Estimation Error in OFDM –Based WLAN” was proposed. In this letter, the performance degradation due to the channel estimation error in the OFDM based wireless LAN (WLAN), the average effective SNR and average bit error probabilities (BEPs) were analytically derived in Rayleigh fading channel.

Later, in 2005 a “BER of OFDM Systems Impaired by Carrier Frequency Offset in Multipath Fading Channels” was given by **Luca Rugini** and **Paolo Banelli** [59]. This paper contains an analytical approach to evaluate the error probability of OFDM system subject to CFO in frequency selective channel, characterized by Rayleigh and Rician fading. By properly exploiting the Gaussian approximation of the ICI, it is shown that BER for an uncoded OFDM system with quadrature amplitude modulation (QAM) can be expressed by the sum of a few integrals, whose number depends on the constellation size, each integral can be evaluated numerically. In Rayleigh fading, by using a series expansion that involves generalized hyper geometric functions, each integral can be evaluated. This letter has basically proposed the result for QAM technique by assuming different channel environments Rayleigh fading and Rician fading.

Further in 2007 a “Effects of Receiver Windowing on OFDM Performance in the Presence of Carrier Frequency Offset” discussed by **Norman C. Beaulieu** and **Peng Tan** [60] was published. The paper has a derived expression of an exact BER expression for an OFDM system with windowing reception, and it is found that performance of OFDM in terms of BER is improved using window family.

In 2009 a paper on “an Exact Error Probability Analysis of OFDM Systems with Frequency Offset” was given by **Prathapasinghe Dharmawansa, Nandana Rajatheva, and Hlaing Minn** [61]. The paper also comprises all the work related to performance evaluation, done till then. Characteristic functions and Beaulieu series have been used to derive exact BER expressions in the presence of ICI. They have followed the procedure presented in **Sathananthan and Tellambura** and **Rugini and Banelli** [59] with different mathematical insight to derive the exact closed form BER/SER expressions for OFDM with ICI over AWGN, frequency selective and flat fading channel. They have not considered the Gaussian approximation of the ICI, instead they have shown that the probability density function of ICI is a mixture of Gaussian densities with properly selected parameters. In 2010 a letter was published on Closed Form BER Expressions for BPSK OFDM Systems with Frequency Offset by **R. Uma Mahesh** and **A. K. Chaturvedi** [62]. This letter addresses the performance degradation caused by the presence of CFO in OFDM systems. In this paper they have modified the result given in [61]. The results in [61] was analysed for lower values of CFO and there was a difference between analytical and simulated results for higher values of CFO. In this paper the modification is done for higher values of CFO for flat and frequency selective Rayleigh fading channels.

Very few literatures studied on the combined effects of STO and CFO in OFDM system for BER evaluation. Some recent work shows about BER performance considering both CFO and STO are [63]. Due to high sensitivity of OFDM systems to synchronization errors, they treated the ICI introduced by residual frequency and timing offsets. By Following with the result of [64], **R. Uma Mahesh** and **A. K. Chaturvedi** derived BER expression with frequency and fractional timing offsets over AWGN and flat Rayleigh fading channels [64]. This approach is convenient to analyse BER, but it's the computational complexity grows exponentially. Furthermore, In [63] by exploiting CHF and Beaulieu series, evaluated BER expressions of BPSK impaired by residual frequency and timing offsets over frequency selective Rayleigh fading channel. **A. Hamza, et al.** [65] gave the first time Closed Form SER Expressions for QPSK OFDM Systems CFO in Rayleigh Fading Channel. This thesis considers the two dimensional PDF and CHF for deriving the SER expression.

**Table 4.2:** Summary of performance Analysis of FFT -based OFDM system with CFO .

1990	Cases <i>et al.</i> [27]	Gave analytical and experimental results of OFDM system
1991-1993	Hara <i>et al.</i> [29-31]	Rayleigh frequency selective fading channel Bit Error Rate Performance for Multicarrier Modulation Radio Transmission
1995	T. Pollet <i>et al.</i> [55]	BER sensitivity of OFDM to carrier frequency offset & wiener phase noise
2001	K. Sathananthan <i>et al.</i> [58]	Calculated the probability of Error of OFDM Systems with Frequency Offset [35]
2002	Hyunsoo Cheon	Effect of Channel estimation Error in OFDM
2005	Luca Rugini, <i>et at.</i> [59]	Analytical approach to evaluate the error probability of OFDM systems in presence of CFO for frequency selective channels
2009	P. Dharmawansa <i>et al.</i> [61]	Gave an exact error probability analysis of OFDM systems with frequency offset
2010	A. Chaturvedi <i>et al.</i> [62]	Given closed form BER expressions for BPSK OFDM systems with frequency offset
2012	R. Mahesh <i>et al.</i> [64]	BER analysis of BPSK OFDM systems with CFO and STO in AWGN and Flat fading
2012	Y. Wang, <i>et al.</i> [57]	BER analysis of BPSK OFDM systems with CFO and STO over frequency selective fading channels
2014	A. Hamza, <i>et al.</i> [65]	Closed Form SER Expressions for QPSK OFDM Systems CFO in Rayleigh Fading Channel

### 4.3. SYSTEM MODEL

The basic principle of OFDM is to split a high data rate stream into a number of lower data rate streams and then to transmit these streams in parallel using several orthogonal sub-carriers. By using this parallel transmission, the symbol duration increases and the relative amount of dispersion in time caused by multipath delay spread decreases. If  $1/T$  is the symbol rate of the input data to be transmitted then the symbol interval in the OFDM system is increased to  $NT$ . For reducing the inter-symbol interference, a guard band is inserted between successive OFDM symbols. The block diagram representation of Fast Fourier Transform (FFT) based- OFDM system with  $N$  subcarrier is shown in Figure-2.3.1. It consists of a

transmitter segment, then channel part followed by the receiver segment. The description about each segment is included below.

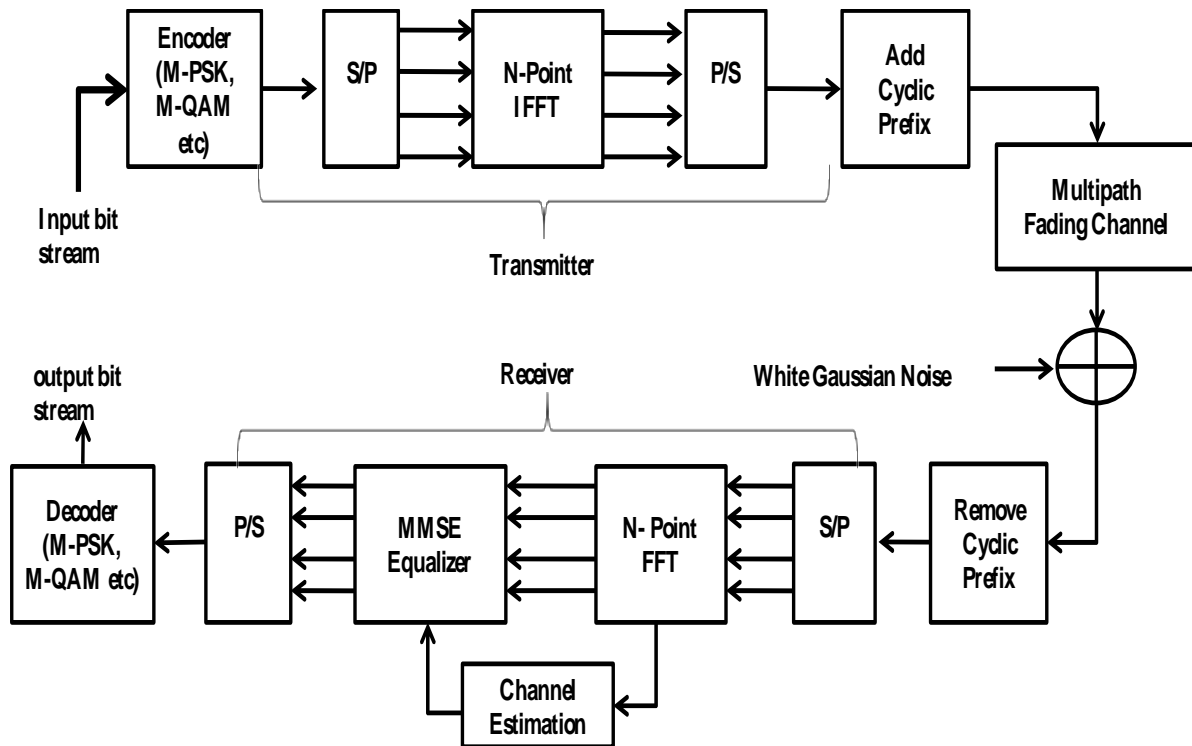


Figure-4.3.1. OFDM System Model

### 4.3.1. Transmitter Model

The input data stream bits are encoded into continuous signals by the encoder, which is first block of the transmitter. Data encoding can be done by using any of the digital modulation techniques viz. M-QAM, M-PSK, or M-FSK. After that  $N$  such symbols are transferred by the serial-to-parallel converter. These complex parallel data symbols  $\{X(k), \text{for } k = 1, 2, \dots, N\}$  are fed into the IFFT block. After taking  $N$  point IFFT, the last  $g$  samples are appended at the front (the cyclic prefix addition) to form  $x(m)$ . These complex parallel data symbols are then modulated by a group of orthogonal sub-carriers, which satisfy the following condition of orthogonality-

$$\frac{1}{T_u} \int_0^{T_u} e^{j2\pi f_k t} e^{j2\pi f_m t} dt = \begin{cases} 1, & k = m \\ 0, & k \neq m \end{cases}$$

(4.3.1.1)

where  $f_k = k/T_u$ , for  $k = 0, 1, 2 \dots, N - 1$  and  $1/T_u$  is the minimum sub-carrier spacing required. The baseband OFDM signal transmitted during  $i^{th}$  block can be written as –

$$x(i, t) = \frac{1}{\sqrt{N}} \sum_{k=0}^{N-1} X(i, k) e^{j2\pi f_k t}, \quad 0 \leq t \leq T \quad (4.3.1.2)$$

where  $T_u$  is the useful duration of one OFDM symbol,  $f_k (= k/T_u)$  is the sub-carrier frequency of the  $k^{th}$  sub-carrier  $X(i, k)$  is the complex data symbol of  $i^{th}$  block modulated on  $k^{th}$  sub-carrier and  $N$  is the total number of sub-carriers. It is assumed that the complex data symbols are un-correlated.

$$E[ X(i, k)X^*(i, k) ] = \begin{cases} 1, & k = m \\ 0, & k \neq m \end{cases} \quad (4.3.1.3)$$

where  $x^*(.)$  represents the complex conjugate of  $x(.)$ . The discrete form of the baseband OFDM signal  $x(i, t)$  in (2.3.1.2) can be expressed as-

$$x(i, m) = \frac{1}{\sqrt{N}} \sum_{l=0}^{N-1} X(i, k) e^{j\frac{2\pi m l}{N}}, \quad m = 0, 1, 2 \dots \dots \dots, N - 1 \quad (4.3.1.4)$$

It is clearly visible from (2.3.1.2.4) that the transmitted signal is the IFFT of the complex input data symbols  $X(i, k)$  and hence it can be easily and efficiently generated using inverse fast Fourier transform (IFFT) as shown in Fig-2.3.1 Similarly, the FFT can be used at the receiver side for demodulation.

#### 4.3.1.1 Cyclic Prefix or Guard Band Insertion

A guard band interval is usually inserted between successive OFDM symbols to avoid the ISI caused by the delay spread of multipath channel. If a guard band interval is inserted without any signal transmission then the ISI can be eliminated almost completely. But a sudden change in waveform contains higher spectral components, resulting into ICI. Therefore the guard interval insertion technique with cyclic prefix is generally used to avoid ICI. In this method, the OFDM symbol is cyclically extended in the guard time. Due to cyclic

prefix (CP) insertion, the transmitted signal is extended to  $T_s = T_g + T$  and can be expressed as-

$$s(i, t) = \sum_{m=-N_{cp}}^{N-1} x(i, m)g_t(t - mT) \quad (4.3.1.1.1)$$

where  $g_t(\cdot)$  representing the raised cosine filter for the pulse shaping at the transmitter side,  $T$  is the sampling period and  $N_{cp}$  is the length of guard interval or cyclic prefix (CP) plays an important role in the performance of OFDM system. If the length of the guard interval (CP) is set shorter than the maximum delay of a multipath channel, the tail part of an OFDM symbol affects the head part of the next symbol, resulting in the ISI. On the other hand a long CP increases the overhead of the system.

Here it is assumed the cyclic prefix of length  $N_g$  is inserted at the beginning of each OFDM symbol and is removed in the demodulation process. Furthermore, the length of the cyclic prefix is longer than the maximum delay spread of the multipath fading channel and the ISI can be completely eliminated.

### 4.3.2. Channel Model

#### 4.3.2.1 Frequency selective Rayleigh Channel

Now the effects of multipath fading channel  $h(\tau, t)$  (channel impulse response) have been considered here with the  $n^{th}$  sample of OFDM symbol. The  $L$ -path tap-delay line model with frequency selective fading channel has been taken as in [38].

The impulse response  $h(\tau, t)$  can be expressed as-

$$h(\tau, t) = \sum_{l=0}^{L-1} h(l, t)\delta(t - \tau_l) \quad (4.3.2.1)$$

where  $h(l, t)$  and  $\tau_l$  are the complex amplitude (or tap coefficient) and propagation delay of the  $l^{th}$  path, respectively and  $\delta(t)$  is the Dirac function. The tap coefficients  $\{h(l, t), \text{ for } l = 0, 1, 2, \dots, L-1\}$  are modeled as zero mean complex Gaussian random variables having variances  $\{\sigma_l^2\}$  with  $\sigma_0^2 + \sigma_1^2 + \dots + \sigma_{L-1}^2 = 1$ . If substitute  $L = 1$  then  $h(\tau, t)$  become the flat fading channel.

Here we take a tapped delay model of the channel impulse response through which the OFDM signal passes

$$h(t) = \sum_{l=0}^{L-1} h_l \delta(t - lT/N) \quad (4.3.2.2)$$

where  $L < N_g$  is the number of multipaths, the path gains  $h_l$  are independently circularly symmetric complex Gaussian random variables with mean 0 and variance  $\sigma_l^2$ ,  $T$  is the effective OFDM symbol period. For simplicity we use the notation  $h_l = CN(0, \sigma_l^2)$

The corresponding frequency response at the subcarrier  $i$  is

$$H_i = \int_{-\infty}^{\infty} h(t) e^{-j2\pi i t / T} dt = \sum_{l=0}^{L-1} h_l e^{-j2\pi i l / N} \quad (4.3.2.3)$$

The channel frequency response  $H_i$  is also a complex Gaussian random variable with mean 0 and variance  $\sum_{l=0}^{L-1} \sigma_l^2$ .

At the beginning of a frame, the initial CFO estimate may not be accurate due to the presence of noise and the limited resource dedicated to the CFO estimation. Short preambles in WLAN can be used to obtain the coarse CFO estimate whose accuracy can be improved by succeeding fine CFO estimation based on long preambles. The normalized CFO affecting the training symbols for channel estimation is denoted by  $\epsilon = f_{\Delta} T$  where  $f_{\Delta}$  is the CFO in Hertz.

### 4.3.3. Receiver Model

After considering the effect of multipath fading channel  $h(\tau, t)$ , the  $i^{th}$  received signal  $r(i, t)$  can be expressed as-

$$r(i, t) = \sum_{l=0}^{L-1} h(l, t) s(i, t - \tau_l T) + w(t) \quad (4.3.3.1)$$

where  $w(t)$  represents the Additive White Gaussian Noise at the receiver with two sided power spectral density of  $\frac{N_o}{2}$ , where  $N_o$  is the noise power. If the length of CP is more than the maximum delay spread of multipath channel and if the STO and CFO are correctly estimated and compensated the received is impaired only by the channel. However, because of presence of estimation errors, time varying Doppler shift and oscillators drift, there exists residual timing and frequency offsets. Therefore, after removing the cyclic prefix, the received discrete time signal before the DFT block can be represented as-

$$r(i, n) = e^{\frac{j2\pi \Delta \varepsilon n}{N}} \sum_{l=0}^{L-1} h(l, t) \sum_{m=0}^{N-1} x(i, m) g(n - m - \tau_l - \Delta \theta) + w(n) \quad (4.3.3.2)$$

where  $\Delta \varepsilon = \Delta f T$  is the carrier frequency offset  $\Delta f$  normalized to sub-carrier spacing  $\frac{1}{T}$ ,  $\Delta \theta$  represent residual normalized timing offsets and  $g(\cdot)$  denotes the raised cosine impulse response which satisfies the Nyquist condition, and  $w(n)$  is the zero-mean complex AWGN with variance  $N_0$ . By taking the DFT of the received signal and substituting (2.3.3.2) we the received signal is given to the FFT block.

The output of FFT can be expressed as-

$$Y(l) = \frac{1}{\sqrt{N}} \sum_{n=0}^{N-1} r(i, n) e^{-\frac{j2\pi ln}{N}} \quad (4.3.3.3)$$

After the substituting the value of  $r(i, n)$  from the equation (2.3.3.2) in to the equation (2.3.3.3)-

$$Y(l) = \frac{1}{\sqrt{N}} \sum_{n=0}^{N-1} \left\{ e^{\frac{j2\pi \Delta \varepsilon n}{N}} \sum_{l=0}^{L-1} h(l, t) \sum_{m=0}^{N-1} x(i, m) g(n - m - \tau_l - \Delta \theta) + w(t) \right\} e^{-\frac{j2\pi ln}{N}} \quad (4.3.3.4)$$

what is the effect on the  $l^{th}$  sub-carrier of a symbol transmitted on the  $k^{th}$  sub-carrier. If  $k = l$ , then signal will be orthogonal and desired signal will be received. If  $k \neq l$ , then signal will be non-orthogonal and interference signal will be generated. The received signal can be rewritten as-

$$Y(l) = X(k)H(k)S(l) + \sum_{\substack{l=0, \\ l \neq k}}^{N-1} X(l)H(l)S(l - k + 1) + w(l) \quad (4.3.3.5)$$

where  $w(n)$  is the AWGN component in time domain,  $H(k)$  denotes the frequency response of the multipath fading channel at the  $k^{th}$  sub-channel is defined as-

$$H(k) = \sum_{l=0}^{L-1} h(l, t) e^{-\frac{j2\pi k \tau_l}{N}}$$

Then the  $m^{th}$  received training symbol after performing the fast fourier transform (FFT) is

$$Y_i(m) = e^{j\theta(m)} [\alpha H_i X_i^p + I_i] + W_i(m), i = 0, \dots, N - 1$$

(4.3.3.6)

Where the block dependent phase shift term  $\theta(m)$  also known as the phase offset, where

$\theta(m) = \frac{2\pi[m(N+N_g)+N_g]\epsilon}{N} + \frac{\pi\epsilon(N-1)}{N}$ , the symbol  $\alpha = \frac{\sin(\pi\epsilon)}{N\sin(\pi\epsilon/N)}$ , ICI due to frequency offset

$$I_i = \sum_{k=0, k \neq i}^{N-1} H_k X_k^p \frac{\sin(\pi\epsilon) e^{-j\pi(k-i)/N}}{N \sin[\pi(k-i+\epsilon)/N]}$$

(4.3.3.7)

and  $W_i(m)$  are independently, identically, distributed (I.I.D). Normalized ICI for small  $\epsilon$  and sufficiently large set of subcarriers can be approximated as:

$$\sigma_{ICI}^2 \approx 2(\pi\epsilon)^2 \sum_{m=1}^{\infty} \left(\frac{1}{m\pi}\right)^2 = \frac{(\pi\epsilon)^2}{3}$$

(4.3.3.8)

It is commonly assumed that the block dependent phase shift term  $\theta(m)$  can be perfectly compensated at the receiver by using preambles or continuous pilot tones so that the decision region of the modulation symbol is independent of the OFDM symbol index  $m$ .

#### 4.3.4. Effect of Channel Estimation Error

The channel information is estimated by dividing the demodulated pilot pattern with the known symbol  $P_i$ . In this case the estimated channel response can be

$$\hat{H}_i^\epsilon = H_i^\epsilon + (I_i^p + W_i^p)/P_i$$

(4.3.4.1)

Here we can describe a parameter  $\eta_i$  denotes the channel estimation error of the  $i^{th}$  subcarrier,  $\eta_i = (I_i^p + W_i^p)/P_i$ , and  $I_i^p$  and  $W_i^p$  are the ICI and the additive noise in demodulating the received preamble. Assuming that the channel response is stationary during one packet duration and the transmitted symbols are mutually uncorrelated, the instantaneous effective SNR of the  $i^{th}$  subcarrier is obtained as

$$\gamma_{eff}(i) = \frac{|\hat{H}_i^\epsilon|^2 \sigma_X^2}{|\eta_i|^2 \sigma_X^2 + \sigma_I^2 + \sigma_W^2} = \frac{|H_i^\epsilon + \eta_i|^2 \bar{\gamma}}{|\eta_i|^2 \bar{\gamma} + \sigma_{ICI}^2 \bar{\gamma} + 1}$$

(4.3.4.2)

Where  $\bar{\gamma}$  is the average SNR when there is no ICI, i.e.,  $\bar{\gamma} = \frac{\sigma_X^2}{\sigma_W^2}$ , where  $\sigma_X^2$  is the variance of the transmitted symbol  $X_i$ . The instantaneous SNR can be written as

$$\gamma_{eff}(i) = \frac{|\hat{H}_i^\epsilon|^2 + |\eta_i|^2 + 2\Re\{H_i^\epsilon \eta_i^*\}}{|\eta_i|^2 + \sigma_{ICI}^2 + 1/\bar{\gamma}} \quad (4.3.4.3)$$

Where  $\Re\{x\}$  is a real part of a complex value  $x$ . Since  $H_i^\epsilon$  and  $\eta_i$  are uncorrelated, the average effective SNR can be obtained as

$$\bar{\gamma}_{eff} = \left[ \frac{\sin^2(\pi\epsilon)}{N^2 \sin^2(\pi\epsilon/N)} - \sigma_{ICI}^2 - 1/\bar{\gamma} \right] I(\sigma_{ICI}^2 + 1/\bar{\gamma}, \sigma_\eta^2) + 1 \quad (4.3.4.4)$$

Where  $\sigma_\eta^2$  is the variance of  $\eta_i$ , and the definition of the definite exponential integral  $I(x, y)$ ,

$$I(x, y) = \begin{cases} \frac{1}{x} & y = 0 \\ e^{xy} \Gamma\left(0, \frac{x}{y}\right) & y > 0 \end{cases}, \text{ where } \Gamma(a, b) \text{ is the incomplete gamma}$$

function. The equation (2.3.3.7) describes the ICI coefficient at the receiver. If non-orthogonal ( $k \neq l$ ), the received signal (2.3.3.5) contains three terms: first term is desired signal, second term is ICI signal and third term is noise signal. By substituting  $H(k) = 1$  the output of FFT-based OFDM system in fading channel will be similar to the output in AWGN channel [44] Interference term occurs only if non-orthogonal sub-carrier term ( $k \neq l$ ) will be present.

#### 4.4. BER ANALYSIS OF EFFECTS OF CHANNEL ESTIMATION ERROR IN PRESENCE OF CARRIER FREQUENCY OFFSET

Following the system model as in the previous Sec., Here frequency selective Rayleigh fading channel is fixed during one transmitted frame and the channel estimation is facilitated by the preamble(training) symbols embedded in the beginning of the data frame. The first P OFDM symbols (M being the number of OFDM symbols in one frame). For each OFDM training symbol, the modulation is restricted to be BPSK and transmitted modulation symbols at each subcarrier, denoted by  $X_k^p \in \{-\sqrt{E_b}, \sqrt{E_b}\}$ , where superscript  $p$  denotes the transmitted symbol is preamble (superscript  $d$  denotes the data transmitted) and are the same for the OFDM symbol index  $m$  from 1 to P. The training symbol patterns  $X_k^p$  for  $k = 0, 1, \dots, N - 1$  are known at both the transmitter and the receiver ends.

#### 4.4.1. BPSK Modulation

For BPSK modulation, the FFT outputs of the OFDM data symbol are as defined

$$Y_i = H_i X_i^d + W_i, \quad i = 0, 1, \dots, N-1$$

where  $X_i^d \in \{-\sqrt{E_b}, \sqrt{E_b}\}$  is the BPSK symbol transmitted on the  $i^{\text{th}}$  subcarrier and we assume the probabilities are half for either being transmitted. For the  $i^{\text{th}}$  subcarrier the decision statistics for the BPSK modulated OFDM signal with the imperfect Channel State Information(CSI) is  $\Re[Y_i \hat{H}_i^*]$  and the corresponding BER is (\* denotes complex conjugation)

$$P_b(i) = P(\Re[Y_i \hat{H}_i^*] < 0 | X_i^d = \sqrt{E_b}) \quad (4.4.1.1)$$

where  $\hat{H}_i = \alpha H_i + \hat{I}_i + \hat{W}_i$ ,  $i = 0, 1, \dots, N-1$ , here  $\hat{I}_i = I_i / X_i^p$ ,  $\hat{W}_i = \frac{1}{P} \sum_{m=1}^P \frac{W_i(m) e^{-j\theta(m)}}{X_i^p}$

Conditioned on the transmitted symbol  $X_i^d$ , the received signal  $Y_i$  and channel estimate  $\hat{H}_i$  are both zero mean complex Gaussian random variables. For further calculations on the BER, following Lemma is considered:

*Lemma 1:* Let X and Y be zero mean, correlated complex valued Gaussian random variables and  $D_1 = \Re[XY^*]$ ,  $D_2 = \Im[XY^*]$ .  $\Re(x)$ ,  $\Im(x)$  denote the real and the imaginary part of  $x$ , respectively. Then

$$P(D_1 < 0) = \frac{1}{2} \left[ 1 - \frac{\Re[\mu_{XY}]}{\sqrt{\mu_{XX}\mu_{YY} - (\Im[\mu_{XY}])^2}} \right]$$

$$P(D_2 < 0) = \frac{1}{2} \left[ 1 - \frac{\Im[\mu_{XY}]}{\sqrt{\mu_{XX}\mu_{YY} - (\Re[\mu_{XY}])^2}} \right] \quad (4.4.1.2)$$

where  $\mu_{XY} = \mathbb{E}[XY^*]$ ,  $\mu_{XX} = \mathbb{E}[XX^*]$ ,  $\mu_{YY} = \mathbb{E}[YY^*]$  and  $\mathbb{E}[\cdot]$  Denotes the probabilistic expectation.

Now to obtain  $P_b(i)$ , we first compute  $\mu_{Y_i \hat{H}_i | X_i^d}$ ,  $\mu_{Y_i Y_i | X_i^d}$  and  $\mu_{\hat{H}_i \hat{H}_i | X_i^d}$  as follows

$$\mu_{Y_i \hat{H}_i | X_i^d} = \mathbb{E}[Y_i \hat{H}_i^* | X_i^d] = \mathbb{E}[(H_i X_i^d + W_i)(\alpha H_i^* + \hat{I}_i^* + \hat{W}^*) | X_i^d] = \alpha X_i^d + \mathbb{E}[H_i \hat{I}_i^*] X_i^d$$

$$\hat{I}_i = \sum_{k=0, k \neq i}^{N-1} H_k \frac{X_k^p \sin(\pi \epsilon) e^{-j\pi(k-i)/N}}{X_i^p N \sin[\pi(k-i+\epsilon)/N]} \quad \text{and} \quad \mathbb{E}[H_i \hat{I}_i^*] = \sum_{k=0, k \neq i}^{N-1} \mathbb{E}[H_i H_k^*] \frac{X_k^p \sin(\pi \epsilon) e^{-j\pi(k-i)/N}}{X_i^p N \sin[\pi(k-i+\epsilon)/N]} \quad (4.4.1.3)$$

We must compute  $\mathbb{E}[H_i H_k^*]$  for  $k \neq i$ , Since  $H_i = \sum_{l=0}^{L-1} h_l e^{-j2\pi i l / N}$ , the expectation  $\mathbb{E}[H_i H_k^*]$

$$\rho_{i,k} = \mathbb{E}[H_i H_k^*] = \begin{cases} 1 & , i = k \\ \sum_{l=0}^{L-1} \sigma_l^2 e^{j2\pi(k-i)l/N} & , i \neq k \end{cases}$$

Next  $\mu_{Y_i Y_i | X_i^d}$  is computed and is given by  $\mathbb{E}[Y_i Y_i^* | X_i^d] = |X_i^d|^2 + N_0$ , Finally  $\mu_{\hat{H}_i \hat{H}_i | X_i^d}$  is

$$\mathbb{E}[\hat{H}_i \hat{H}_i^* | X_i^d] = \mathbb{E}[(\alpha H_i + \hat{I}_i + \hat{W}_i)(\alpha H_i^* + \hat{I}_i^* + \hat{W}_i^*)] = \alpha^2 + \frac{\mathbb{E}[|I_i|^2]}{|X_i^d|^2} + \frac{N_0}{PE_b} + 2\Re(\alpha \mathbb{E}[H_i \hat{I}_i^*])$$

The expectation  $\mathbb{E}[|I_i|^2]$  in above equation is

$$\sum_{k_1=0, k_1 \neq i}^{N-1} \sum_{k_2=0, k_2 \neq i}^{N-1} \frac{\rho_{k_1 k_2} X_{k_1}^p X_{k_2}^p [\sin(\pi\epsilon)]^2 e^{-j\pi(k_1-k_2)/N}}{N^2 \phi(k_1, i) \phi(k_2, i)} \quad (4.4.1.4)$$

where  $\phi(k, i) = \sin[\pi(k - i + \epsilon)/N]$ .

For subcarrier  $i$ , the BER of the BPSK modulated OFDM signal with imperfect channel estimate can be evaluated by Lemma 1 as

$$P_b^{BPSK}(i) = P(\Re[Y_i \hat{H}_i^*] < 0 | X_i^d = \sqrt{E_b}) = \frac{1}{2} \left( 1 - \frac{\Re[\mu_{Y_i \hat{H}_i | X_i^d}]}{\sqrt{\mu_{Y_i Y_i | X_i^d} \mu_{\hat{H}_i \hat{H}_i | X_i^d} - (\Im[\mu_{Y_i \hat{H}_i | X_i^d}])^2}} \right) \quad (4.4.1.5)$$

From above expression it is known that the subcarrier BER  $P_b^{BPSK}(i)$  is not only a function of subcarrier index  $i$  but also a function of the training symbols  $X_k^p$  due to the effect of CFO. This dependency is moreover is through the ICI term  $I_i$  which is a direct consequence of CFO. If the channel estimation is performed under perfect CFO estimation ( $\epsilon = 0$ ), then  $\alpha = 1$ , and  $\mu_{Y_i \hat{H}_i | X_i^d} = X_i^d = \sqrt{E_b}$ ,  $\mu_{Y_i Y_i | X_i^d} = |X_i^d|^2 + N_0 = E_b + N_0$  and  $\mu_{\hat{H}_i \hat{H}_i | X_i^d} = 1 + \frac{N_0}{PE_b}$ . In this case, the subcarrier BER  $P_b^{BPSK}(i)$  is the same for all  $i = 0, 1, \dots, N - 1$  and average BER over all sub carriers is simplified as

$$P_b^{BPSK} = \frac{1}{N} \sum_{i=0}^{N-1} P_b^{BPSK}(i) = \frac{1}{2} \left( 1 - \frac{1}{\sqrt{\left(1 + \frac{N_0}{E_b}\right) \left(1 + \frac{N_0}{PE_b}\right)}} \right) \quad (4.4.1.6)$$

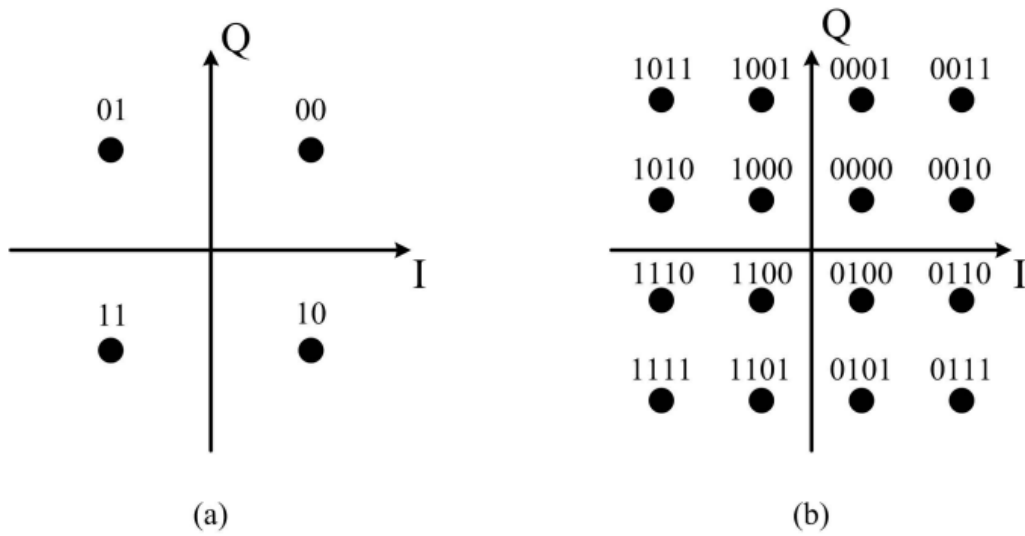


**Figure 4.4.1.:** (a) QPSK constellation with Grey coding, (b) 16-QAM constellation with grey coding

#### 4.4.2. QPSK Modulation

The constellation of QPSK is denoted by:

$$X_i^d = \left\{ \frac{[(2i-1) + (2q-1)j]\sqrt{E_s}}{\sqrt{2}}; i, q \in \{0,1\} \right\} \quad (4.4.2.1)$$

where  $j = \sqrt{-1}$  and  $E_s$  is the symbol energy. Two information bits are mapped into a QPSK constellation symbol by the Gray Encoding shown in Fig. 4.4.1 (a).

To generate the decision variable for the QPSK symbol  $X_i^d$  of subcarrier  $i$ , the constellation of the demodulated signal  $Y_i$  is scaled and rotated by the corresponding channel estimate  $\hat{H}_i$ . For each QPSK symbol, we only need to derive the BER of the Most significant bit (MSB) since the least significant bit (LSB) has the same BER as the MSB.

To compute the BER of the MSB of the QPSK constellation symbol, we consider two QPSK constellation symbols  $\frac{(1+j)\sqrt{E_s}}{\sqrt{2}}$  and  $\frac{(-1+j)\sqrt{E_s}}{\sqrt{2}}$  were sent at the transmitter end since they have different BERs due to imperfect CSI. This is different from the perfect CSI case where usually only one constellation symbol is considered to be sent due to the symmetry of the constellation and decision boundary. From Fig. 4.4.1(a) it is evident that the decision boundary for the MSB

of the QPSK symbol is the real axis and the BER of the MSB of the subcarrier  $i$  is

$$P_{b_1}^{QPSK} = \frac{1}{2} \left( P \left\{ \Im[Y_i \hat{H}_i^*] < 0 | X_i^d = \frac{(1+j)\sqrt{E_s}}{\sqrt{2}} \right\} \right) + \frac{1}{2} \left( P \left\{ \Im[Y_i \hat{H}_i^*] < 0 | X_i^d = \frac{(-1+j)\sqrt{E_s}}{\sqrt{2}} \right\} \right) \quad (4.4.2.2)$$

Similarly, to compute the BER of the least significant bit (LSB) of the constellation symbol, we consider two constellation symbols  $\frac{(1+j)\sqrt{E_s}}{\sqrt{2}}$  and  $\frac{(1-j)\sqrt{E_s}}{\sqrt{2}}$  were sent since they have different BERs due to imperfect CSI. The decision boundary for the LSB of the QPSK symbol is the imaginary axis and the BER of the LSB of the subcarrier  $i$  is

$$P_{b_2}^{QPSK} = \frac{1}{2} \left( P \left\{ \Re[Y_i \hat{H}_i^*] < 0 | X_i^d = \frac{(1+j)\sqrt{E_s}}{\sqrt{2}} \right\} \right) + \frac{1}{2} \left( P \left\{ \Re[Y_i \hat{H}_i^*] < 0 | X_i^d = \frac{(1-j)\sqrt{E_s}}{\sqrt{2}} \right\} \right) \quad (4.4.2.3)$$

Finally the average BER over  $N$  subcarriers is

$$P_b = \frac{1}{2N} \sum_{i=0}^{N-1} [P_{b_1}(i) + P_{b_2}(i)] \quad (4.4.2.4)$$

Conditioning on  $X_i$ , the random variables  $Y_i$  and  $\hat{H}_i$  are also Gaussian because they are the weighted sum of the Gaussian random variables. Therefore, we can use Lemma 1 to compute  $P_{b_1}(i)$  and  $P_{b_2}(i)$  where  $\mu_{Y_i \hat{H}_i | X_i^d}$ ,  $\mu_{Y_i Y_i | X_i^d}$  and  $\mu_{\hat{H}_i \hat{H}_i | X_i^d}$  are solved above with possible  $X_i^d$ .

When the CFO is perfectly compensated (i.e.  $\epsilon = 0$ ), we have  $\alpha = 1$ ,  $\mu_{Y_i \hat{H}_i | X_i^d} = X_i^d$ ,

$\mu_{Y_i Y_i | X_i^d} = |X_i^d|^2 + N_0 = E_s + N_0$ ,  $\mu_{\hat{H}_i \hat{H}_i | X_i^d} = 1 + \frac{N_0}{PE_b}$ . In this case, the subcarrier BER  $P_b^{QPSK}(i)$  is independent of the index of the subcarrier  $i$  and the average BER is given by

$$P_b^{QPSK} = \frac{1}{2} \left( 1 - \frac{1}{\sqrt{\left(2 + \frac{2N_0}{E_s}\right) \left(1 + \frac{N_0}{PE_b} - 1\right)}} \right) \quad (4.4.2.5)$$

#### 4.4.3. 16-QAM Modulation Scheme

The 16-QAM constellation with Gray encoding is shown in Fig. 4.4.1(b). The first and the third bits correspond to the In phase(I) bits, while the second and fourth bits correspond to the quadrature (Q) bits. The I and Q components of the 16-QAM are Gray encoded by assigning the bits 11, 10, 00 and 01 to the levels  $-3d, -d, d$  and  $3d$  where  $d = \sqrt{E_s/10}$ .

Since we are interested in the evaluation of BER, we need to determine the decision boundary for each bit first. In Fig. 4.4.2, the decision boundaries for the MSB and LSB of the I/Q components are depicted. Due to the symmetry of the I and Q components, we only need to calculate the BER for I components.

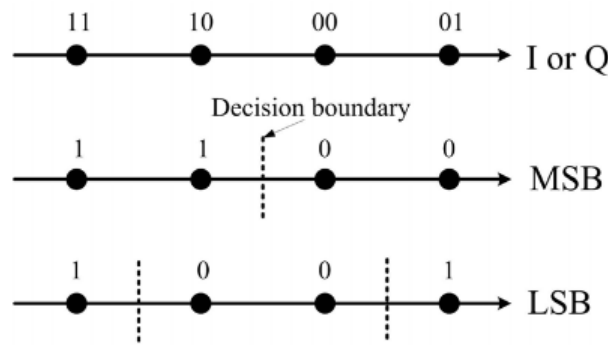


Figure 4.4.2: 16-QAM bit by bit demapping

Let  $\kappa$  be the constellation of 16-QAM where each constellation point has the same probability to be sent,  $\kappa_1$  be the set of the four 16-QAM constellation symbols having  $d$  as their I-component, i.e.  $\kappa_2$  be the set of four 16-QAM constellation symbols having  $3d$  as their I-component, i.e.  $\kappa_2 = \{x \in \kappa : \Re[x] = 3d\}$ . Since the decision boundary for the MSB bit is the imaginary axis, for the subcarrier  $i$ , the BER of the MSB bit of the I component is given by :

$$P_b^{MSB}(i) = \frac{1}{8} \sum_{X_i^d \in \kappa_1 \cup \kappa_2} P\{\Re[Y_i \hat{H}_i^*] < 0 | X_i^d\} \tag{4.4.3.1}$$

On the other hand, the decision boundaries for the LSB bit are  $I = -2d$  and  $I = 2d$  on the I-Q plane. For the subcarrier  $i$ , the BER of the LSB bit of I components is

$$\begin{aligned}
 P_b^{LSB}(i) = & \frac{1}{8} \left\{ \sum_{X_i^d \in \kappa_1} \left[ 1 - P \left( -2d < \frac{\Re[Y_i \hat{H}_i^*]}{|\hat{H}_i|^2} < 2d |X_i^d \right) \right] \right. \\
 & \left. + \sum_{X_i^d \in \kappa_2} \left[ 1 - P \left( -2d < \frac{\Re[Y_i \hat{H}_i^*]}{|\hat{H}_i|^2} < 2d |X_i^d \right) \right] \right\}
 \end{aligned}
 \tag{4.4.3.2}$$

The average BER of the 16-QAM with imperfect CSI is

$$P_b^{16QAM} = \frac{1}{2N} \sum_{i=0}^{N-1} [P_b^{MSB}(i) + P_b^{LSB}(i)]
 \tag{4.4.3.3}$$

Conditioned on the transmitted data symbol  $X_i^d$ ,  $Y_i$  and  $\hat{H}_i$  are both Gaussian. Therefore, we can use Lemma 1 to compute  $P_b^{MSB}(i)$  directly where  $\mu_{Y_i \hat{H}_i | X_i^d}$ ,  $\mu_{Y_i Y_i | X_i^d}$  and  $\mu_{\hat{H}_i \hat{H}_i | X_i^d}$  are given above with  $X_i^d \in \kappa_1 \cup \kappa_2$ . However, the BER formula of  $P_b^{LSB}(i)$  is not in exact form of Lemma 1. To apply Lemma 1 to compute  $P_b^{LSB}(i)$ , we need to transform the random variable  $Y_i$  into a new random variable  $\hat{Y}_i$  so that Lemma 1 is applicable for  $\hat{Y}_i$  and  $\hat{H}_i$ . To be more specific, following probability is computed:

$$f(X_i^d, D) = P \left( \Re[Y_i \hat{H}_i^*] < |\hat{H}_i|^2 D X_i^d \right),$$

where  $D$  is a real number. Let  $\hat{Y}_i = Y_i - \hat{H}_i D = H_i X_i^d + W_i - \hat{H}_i D$ , then

$$f(X_i^d, D) = P(\Re[\hat{Y}_i \hat{H}_i^*] < 0 | X_i^d) = \frac{1}{2} \left( 1 - \frac{\Re[\mu_{Y_i \hat{H}_i | X_i^d}]}{\sqrt{\mu_{Y_i Y_i | X_i^d} \mu_{\hat{H}_i \hat{H}_i | X_i^d} - (\Im[\mu_{Y_i \hat{H}_i | X_i^d}])^2}} \right)
 \tag{4.4.3.4}$$

Where the second equality is a direct consequence of applying Lemma 1. Finally, we can express  $P_b^{LSB}(i)$  in terms of  $f(X_i^d, D)$  as

$$P_b^{LSB}(i) = \frac{1}{8} \left\{ \sum_{X_i^d \in \kappa_1} [1 - f(X_i^d, 2d) + f(X_i^d, -2d)] + \sum_{X_i^d \in \kappa_2} [f(X_i^d, 2d) + f(X_i^d, -2d)] \right\}
 \tag{4.4.3.5}$$

To evaluate  $f(X_i^d, D)$ , we first compute  $\mu_{Y_i \hat{H}_i | X_i^d} = \mathbb{E}[H_i \hat{H}_i^*] X_i^d - \mathbb{E}[\hat{H}_i \hat{H}_i^*] D$ , where  $\mathbb{E}[H_i \hat{H}_i^*] = \mathbb{E}[H_i(\alpha H_i + I_i + \hat{W}_i)^*] = \alpha + \mathbb{E}[H_i \hat{I}_i^*]$ , where  $\mathbb{E}[H_i \hat{I}_i^*]$  and  $\mathbb{E}[H_i \hat{H}_i^*]$  have been given above.

Then  $\mu_{Y_i Y_i | X_i^d}$  is computed:

$$\begin{aligned} \mu_{Y_i Y_i | X_i^d} &= \mathbb{E}[(Y_i - \hat{H}_i D)(Y_i - \hat{H}_i D)^* | X_i^d] \\ &= |X_i^d|^2 + N_0 + \mathbb{E}[H_i \hat{H}_i^*] D^2 - 2\Re(\mathbb{E}[\hat{H}_i D (H_i X_i^d)^*]) \end{aligned} \quad (4.4.3.6)$$

When the CFO is perfectly compensated (i.e.  $\epsilon = 0$ ), we have  $\alpha = 1$ ,  $\hat{I}_i = 0$  and new values of  $\mu_{Y_i \hat{H}_i | X_i^d}$ ,  $\mu_{Y_i Y_i | X_i^d}$  and  $\mu_{\hat{H}_i \hat{H}_i | X_i^d}$  become:

$$\begin{aligned} \mu_{Y_i \hat{H}_i | X_i^d} &= X_i^d - \left(1 + \frac{N_0}{PE_b}\right) D, \\ \mu_{Y_i Y_i | X_i^d} &= |X_i^d|^2 + N_0 + \left(1 + \frac{N_0}{PE_b}\right) D^2 - 2D\Re[X_i^d], \\ \mu_{\hat{H}_i \hat{H}_i | X_i^d} &= 1 + \frac{N_0}{PE_b}. \end{aligned}$$

In this situation, the function  $f(X_i^d, D)$  can be simplified to the expression given below :

$$f(X_i^d, D) = \frac{1}{2} \left( 1 - \frac{\Re[X_i^d] - \left(1 + \frac{N_0}{PE_b}\right) D}{\sqrt{\left[\Re[X_i^d] - \left(1 + \frac{N_0}{PE_b}\right) D\right]^2 + |X_i^d|^2 \frac{N_0}{PE_b} + N_0 \left(1 + \frac{N_0}{PE_b}\right)}} \right) \quad (4.4.3.7)$$

## 4.5. SIMULATION RESULTS

OFDM system with  $N = 64$  subcarriers has been considered. The effective OFDM symbol period is  $T = 3.2\mu s$  and the subcarrier frequency spacing  $f_s$  is  $312.5 kHz$ . The received signal is sampled at the rate of  $20MHz$ . The power delay profile of the multipath Rayleigh is exponentially decaying and the root mean square(rms) delay spread is equal to  $100 ns$ . It is assumed that the channel is fixed for the whole frame and is independent from frame to frame. These parameters and assumptions are typical for the indoor WLAN applications.

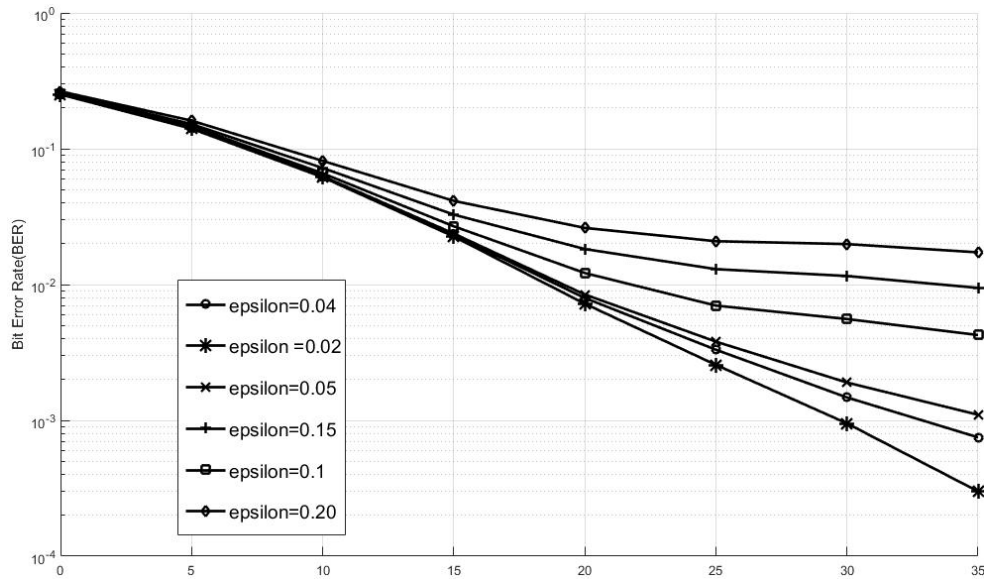
The OFDM training symbol consists of 64 subcarriers, which are modulated by the BPSK symbol of the sequence  $X^p = [X_0^p X_1^p \dots X_{N-1}^p] = \sqrt{E_b}[X_1^p X_2^p X_3^p X_4^p]$  where one of the pilot sequences are used since optimization of the pilot sequences has not been considered as of now. The training sequence is selected under the peak to average power ratio (PAPR) constraint [1].

$$X_1^p = [-1, -1, 1, 1, -1, 1, 1, -1, ]$$

Figures 4.5.1-4.5.6 show the effects of the channel estimation error and Carrier Frequency offset (CFO, epsilon- $\epsilon$ ) on the Bit Error Rate performance of BPSK, QPSK, 16 QAM modulated OFDM signals in multipath Rayleigh fading channels, respectively. Here two types of channel taps have been considered and the simulations are depicted according for channel tap values of 3 and 5 . Accordingly the results have been compared by varying the CFO values and checking the BER performance with the signal to noise ratio (SNR). The solid lines are obtained from the computer simulation and the markers are computed from the theoretical results. The horizontal axis represents the modulated data symbol SNR  $E_s / N_0$  . It is assumed that the number of the OFDM data symbols are much greater than that of the OFDM training symbols in one frame, hence the loss of power in the OFDM training symbols is negligible.

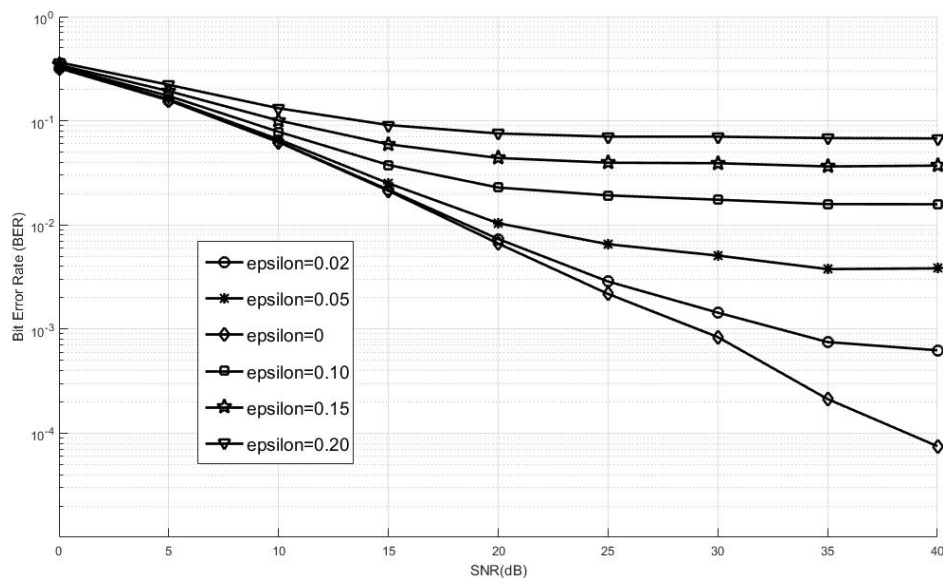
Figure 4.5.1 depicts the Bit Error Rate performance of OFDM based system with training pilot sequence in presence of carrier frequency offset and channel estimation error for BPSK modulation. The plot is over different values of the CFO ranging in residual /fractional quantities. The filter tap considered for this simulation is a three tap filter, so the cyclic prefix length is taken as  $N_{CP} = 4$ .

## OFDM SYSTEM IN PRESENCE OF CHANNEL ESTIMATION ERROR AND CFO



**Figure4.5.1:** BER expression of FFT based- OFDM system in presence of CFO and channel estimation error for BPSK in Rayleigh channel with  $N = 8$ .

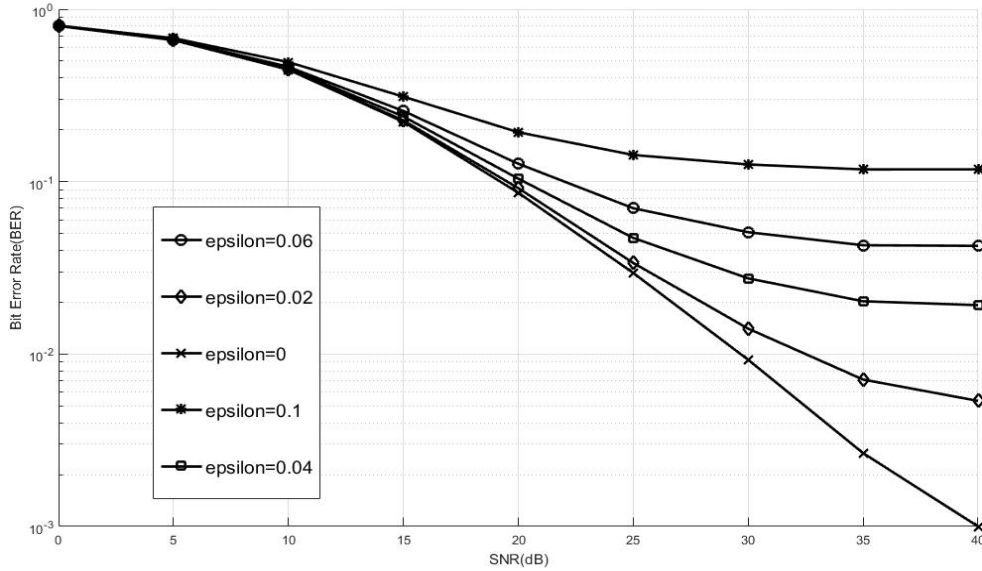
Figure 4.5.2 depicts the Bit Error Rate performance of OFDM based system with training pilot sequence in presence of carrier frequency offset and channel estimation error for QPSK modulation. The filter tap considered for this simulation is a three tap filter, so the cyclic prefix length is taken as  $N_{CP} = 4$ . The plot is over different values of the CFO ranging in residual /fractional quantities.



**Figure4.5.2:** BER expression of FFT based- OFDM system in presence of CFO and channel estimation error for QPSK in Rayleigh channel with  $N = 8$

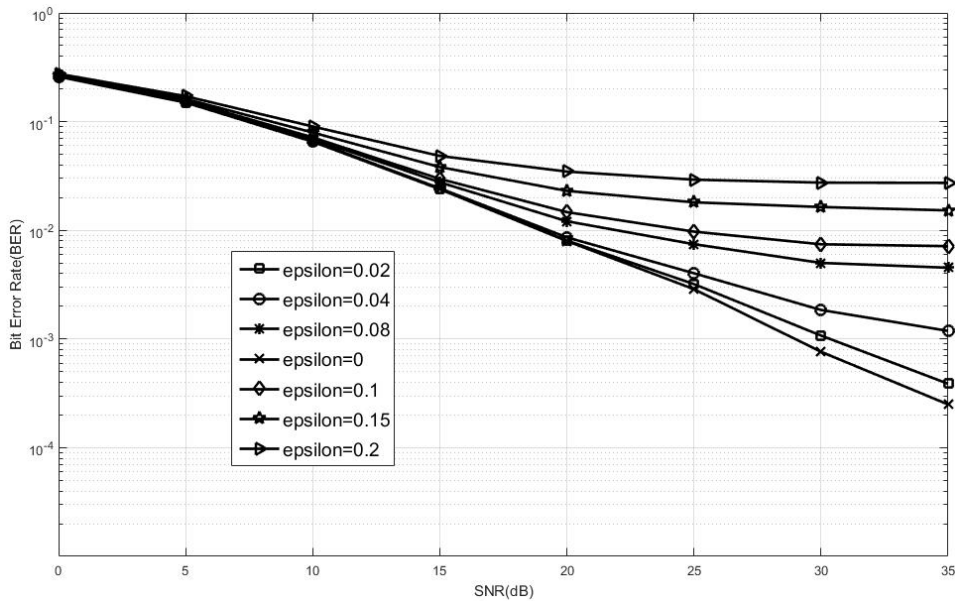
Figure 4.5.2 depicts the Bit Error Rate performance of OFDM based system with training pilot sequence in presence of carrier frequency offset and channel estimation error for QPSK

modulation. The filter tap considered for this simulation is a three tap filter, so the cyclic prefix length is taken as  $N_{CP} = 4$ . The plot is over different values of the CFO ranging in residual /fractional quantities.



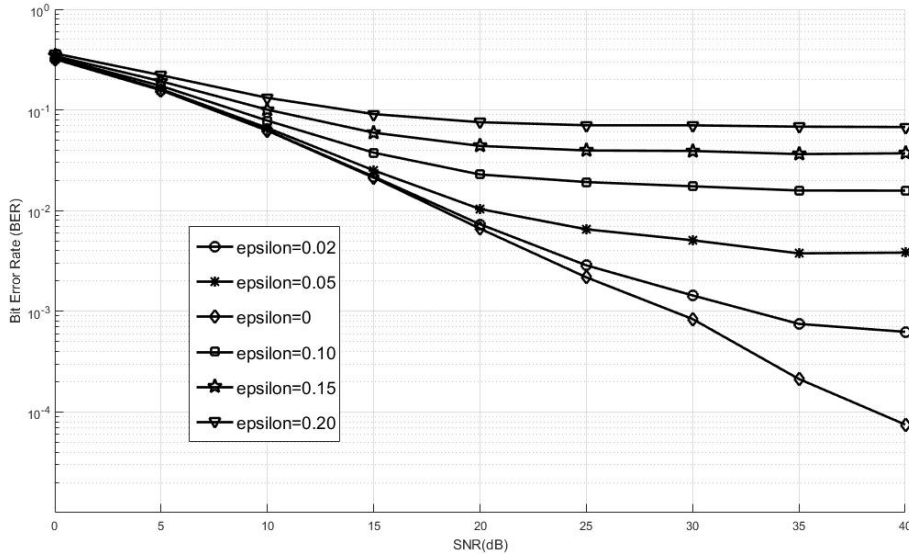
**Figure4.5.3.:** BER expression of FFT based- OFDM system in presence of CFO and channel estimation error for 16 QAM in Rayleigh channel with  $N = 8$ .

Figure 4.5.3 depicts the Bit Error Rate performance of OFDM based system with training pilot sequence in presence of carrier frequency offset and channel estimation error for 16 QAM modulation. The filter tap considered for this simulation is a three tap filter, so the cyclic prefix length is taken as  $N_{CP} = 4$ .



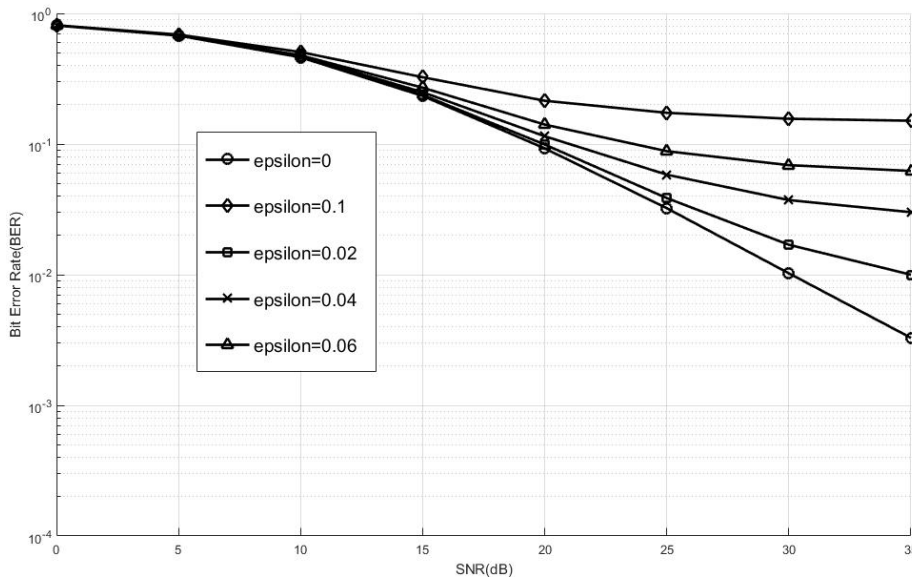
**Figure4.5.4:** BER expression of FFT based- OFDM system in presence of CFO and channel estimation error for BPSK in Rayleigh channel with tap filter length=5.

Figure 4.5.4 depicts the Bit Error Rate performance of OFDM based system with training pilot sequence in presence of carrier frequency offset and channel estimation error for BPSK modulation. The filter tap considered for this simulation is a five tap filter, so the cyclic prefix length is taken as  $N_{CP} = 5$ .



**Figure4.5.5.:** BER expression of FFT based- OFDM system in presence of CFO and channel estimation error for QPSK in Rayleigh channel with tap filter length=5.

Figure 4.5.5 depicts the Bit Error Rate performance of OFDM based system with training pilot sequence in presence of carrier frequency offset and channel estimation error for QPSK modulation. The filter tap considered for this simulation is a three tap filter, so the cyclic prefix length is taken as  $N_{CP} = 5$ .



**Figure4.5.6.:** BER expression of FFT based- OFDM system in presence of CFO and channel estimation error for 16-QAM in Rayleigh channel with tap filter length=5.

Figure 4.5.6 depicts the Bit Error Rate performance of OFDM based system with training pilot sequence in presence of carrier frequency offset and channel estimation error for 16 QAM modulation. The filter tap considered for this simulation is a three tap filter, so the cyclic prefix length is taken as  $N_{CP} = 5$ .

#### 4.6. DISCUSSION OF SIMULATED RESULTS

From Figures it is evident the theoretical analysis exactly match with the simulation results for different normalized CFO  $\epsilon$ . When the CFO is perfectly compensated in the channel estimation stage (i.e.  $\epsilon = 0$ ), the performance loss due to imperfect Channel state information is about 3 dB, 5dB,7dB (for channel tap = 3) for BPSK , QPSK, 16-QAM respectively.

As the normalized CFO,  $\epsilon$  increases, the channel estimate becomes less reliable and the BER performance becomes worse. Due to the effect of ICI created by CFO, there exist error floors when  $E_s/N_0$  is large. Finally, it is examined that performance degradation due to channel estimation is more severe in high-order modulation than in BPSK. That implies the high order modulation like 16 QAM needs much more accurate CFO and channel estimation to avoid performance loss.

The influence of number of channel taps on the BER performance for BPSK, QPSK, 16-QAM modulated OFDM signals in Rayleigh fading channel is depicted in Figures. When  $E_s/N_0$  is small, the BER is mainly dominated by AWGN and the increase in channel tap, does not provide a performance gain. On the other hand when  $E_s/N_0$  is large, the BER is mainly governed by the ICI and the increase of the channel tap does not have much performance gain.

Since 16-QAM is more sensitive to channel estimation error compared to BPSK,QPS, a large value of the number of training symbols can benefit 16-QAM more than the other two types of the modulation.

\*\*\*\*\*

# CHAPTER-V

---

## CONCLUSION & FUTURE SCOPE

Topics:

5.1. Conclusion

5.2. Future Scope

**REFERENCES**

---

This chapter is organised as: In first section, the Thesis report is concluded regarding the “Analytical Performance Evaluation of OFDM in Presence of Channel Estimation Errors and Carrier Frequency Offset”. In second section, the further scope of this work is decided through the problem formulation for readers over the use of Generalized Frequency Division Multiplexing (GFDM) over OFDM . The use of GFDM in 5th Generation Non-Orthogonal Waveforms for Asynchronous Signalling (5GNOW) based on GFDM. After discussing the further scope of this work, future plan can easily be formulated.

## 5.1. CONCLUSION

OFDM is a special case of wideband multicarrier modulation in which multiple symbols are transmitted in parallel using different sub-carriers with overlapping frequency bands that are mutually orthogonal. An equivalent wideband frequency bandwidth is separated into a number of narrowband signals. The time dispersion caused by multipath delay is reduced because the symbol duration of a narrowband signal will be larger than that of a wideband transmission scheme. The overlapping multicarrier techniques can implement the same number of channels as conventional FDM system but with a reduced amount of bandwidth. In conventional FDM, adjacent channels are separated using guard band.

In OFDM, each subcarrier has integer number of cycles within a given time interval  $T$ , and the number of cycles by which each adjacent subcarrier differs is exactly one. This implementation adds orthogonality to the subcarriers. Because of these inherent properties (orthogonal subcarriers) it saves the bandwidth during the transmission. In OFDM system the bandwidth is divided into  $N$  slots and then data rate is increased by  $N$ -times.

In 3<sup>rd</sup> generation WCDMA and OFDM was used. Just because of these OFDM (multicarrier system) a large number of high data rate applications became possible like-

- DAB
- HDTV
- Wireless LAN networks
- IEEE 802.16 Broadband Wireless Access System
- Multimedia applications e.g. video games etc.

In this thesis the predominant feature of any communication system, i.e. channel estimation techniques have been summarized using both conventional ways and using soft computing. It is observed that the block-type pilot channel estimation schemes are more suitable for the slow fading channels, and the comb-type pilot channel estimation schemes are more suitable for the middle and fast fading channels. In addition, block-type pilot schemes are used over middle or fast fading channels, the channel estimation error may vary considerably as a function of the location of the data blocks with respect to the pilot block. The result may be a periodic variation of the decoding error rates for different OFDM blocks. On the other hand, the comb-type pilot schemes can eliminate this variation, and therefore all OFDM data symbols experience a similar error rate. Because the error rate of the comb-type pilot schemes is higher than the lowest error rate that can be achieved by the block-type pilot schemes, the block-type pilot schemes provide the opportunity to protect the data with high importance/priority by transmitting them at the positions where the error rate is low. Therefore, comb-type pilot schemes are more suitable for generic data transmission, while the block-type pilot schemes are more suitable for transmission over slow fading channels or transmission with unequal error protection (UEP).

It is well known that synchronization is a major issue of Multi carrier communication systems are competing well with single carrier systems, also suffer from a serious drawback i.e. high peak-to-average power ratio (PAPR). Various alternative solutions have been proposed, but each one of them has its own advantages and drawbacks. For instance, clipping is the simplest technique for reducing the PAPR; being a linear process it causes both in band and out-of-band distortion. The out-of-band distortions can be reduced by filtering but peak re-growth can be its consequence. Moreover, repetition of clipping and filtering process may lead to degradation in bit error rate (BER) performance. Among distortionless methods of PAPR reduction the PTS and SLM methods are the most attractive and significant probabilistic techniques due to their good performance in terms of PAPR reduction. The main drawback of these techniques is the requirement to send side information at receiver to recover original data. Obviously, when the side information is corrupted, the original data cannot be correctly recovered. Therefore, some extra protection bits have to be employed for the protective transmission of the side information to guarantee a reasonable BER performance, resulting in a decrease in spectrum efficiency.

Nowadays, soft computing based schemes are also being successfully applied to reduce PAPR in OFDM system due to their inherent qualities like adaptive in nature, no

requirement of physical behavior of model and importantly the less complexity. In this report, a neural network based switching of null subcarrier and data subcarrier technique is adapted to reduce the PAPR of the multicarrier system. The described scheme allows no side information with low complexity.

After developing a link between the OFDM based systems and Artificial neural networks, an attempt was made to compare the conventional channel estimation with those implemented using neural networks. To increase OFDM system performance under frequency selective channels, channel estimation is required before demodulation of OFDM signals. Among the techniques of channel estimation both pilot- based channel estimation and blind channel estimation are most popular. An ANN based channel estimation technique as an alternative to pilot based channel estimation technique for OFDM systems over Rayleigh fading channels has been described. There are no pilot symbols which are added to OFDM ,therefor this technique is more bandwidth efficient and makes full use of the learning property of neural network so very less complex than pilot based techniques. Using Levenberg-Marquardt there is no need of any matrix computation.

Due to the additive white Gaussian noise (AWGN) and the intercarrier interference(ICI) caused by the residual carrier offset (CFO), the channel estimation based on the training symbols is not perfect. The BER analysis and performance degradation has been observed resulting from imperfect channel state information(CSI). An exact BER analysis for BPSK,QPSK and 16-QAM modulated OFDM signals in frequency selective Rayleigh fading channels without any assumption on the correlation between the channel estimate and the channel estimation error. The depicted results are accurate even for large CFO and channel estimation error.

Finally a Matlab based transceiver section of OFDM based Long Term Evolution(LTE) has been made, with varying the fading channel, namely EVA,EPA and ETU. Using various frequency and time averaging window for channel estimation the performance analysis has been considered.

Based on the results of this work the following papers have been generated

1. Sarvraj Singh Ranhotra, Atul Kumar, Maurizio Magarini: “*Comparison of Performance of Blind and Non Blind Channel Equalizers using Neural Networks*”,submitted at ICC.
2. Sarvraj Singh Ranhotra, Atul Kumar, Maurizio Magarini: “*Exact Error Probability Analysis of DFrFT-based 16-QAM OFDM Systems over the Frequency Selective*

*Rayleigh and Nakagami-M fading Channel in presence of CFO*” (in preparation)

3. Sarvraj Singh Ranhotra, Atul Kumar, Maurizio Magarini: “*Exact BER analysis of FRFT-OFDM system over frequency selective Rayleigh fading channel with CFO and Channel Estimation Error*”. (in preparation)

## 5.2. FUTURE SCOPE

Apart from OFDM another multi-carrier modulation scheme, called General frequency division multiplexing(GFDM) provides major contribution to 5G communication. In contrast to OFDM, it can benefit from transmitting multiple symbols per sub- carrier. GFDM targets block based transmission which is enabled by circular pulse shaping of the individual sub carriers. Current market trends and future projections indicate that one of the major challenges in next generation mobile communications systems will be to support massive wireless connectivity of machine- type communication and tactile internet, in wider sense Internet of Things devices. This vision can be implemented by designing an additional wireless communication standard. OFDM is known to produce severe interference when frequency offsets occur, which can limit efficiency when aggregating fragmented spectrum resources. With the proposal of GFDM against OFDM, it provides reduced out of band radiation. Like Filter banks multi carrier(FBMC) approach[], GFDM has the capability to shape spectrum in a favourable way.

### ➤ Channel Estimation in OFDM based systems

With the upcoming new multicarrier modulation scheme, the channel estimation techniques in OFDM can be extended to GFDM. The interpolation techniques need to be re thought since the block based structure in GFDM accounts for multiple symbols and multiple sub carriers.

### ❖ Artificial Neural Networks-

Similarly to OFDM based on replacement of null subcarriers with data sub carriers, and implementing using Artificial Neural Networks, showcasing improvements in PAPR, GFDM based systems can also be implemented using Neural Networks, with conceived advantages. Also channel estimation using ANN in this thesis report has been limited to OFDM systems, however can be extended to MC-CDMA systems too.

➤ **OFDM System In Presence Of Channel Estimation Error & CFO**

Further this can be extended to Performance analysis of OFDM system in presence of channel estimation error, CFO and integer /residual symbol timing offset.

❖ **BER expression for BPSK modulation scheme in following environments-**

- AWGN channel
- Flat Fading channel
- Frequency Selective Fading channel

❖ **BER expression of QPSK modulation scheme-**

- AWGN channel
- Flat Fading channel
- Frequency fading channel

❖ **BER expression of QAM modulation scheme-**

- AWGN channel
- Flat Fading channel
- Frequency Fading channel

These above results have not been given yet. So, anyone can take step from here for further “*performance Analysis of OFDM system in presence of non linearities*” Apart from these many scopes based on the performance evaluation, if anyone is interested in **Error Control Coding** subject then the performance can be improved to a better extent by using different coding system. So, a better scope is there by using coding system.

Also the BER analysis can be extended to frequency- selective Rician fading channels by generalizing Lemma 1 (chapter 4), to the case of non-zero mean complex valued Gaussian random variables. From the BER expression, it is evident that BER depends on the patterns of training sequences. The design of optimal training sequence in the sense of minimizing the average BER subject to the PAPR constraint is quite valuable topic to study for future scope.

**❖ One additional aspect with this work “*LTE transceiver section*”**

The LTE physical layer, or PHY, is tasked with the transportation of signals between the base stations and the mobile users, with high spectral efficiency. The two key enablers to achieve such results are the Orthogonal Frequency Division Multiplexing (OFDM) and the multiple-antenna technology (MIMO). OFDM consists in dividing the available spectrum into equally spaced, mutually orthogonal, narrow band sub-carriers. This brings the advantages, among others, of an absent inter symbol interference as each sub-carrier is orthogonal to the other ones, and simple receiver structures as each sub-carrier witnesses flat fading [26]. The LTE PHY layer makes use of OFDM in two different flavours for uplink and downlink. Orthogonal Frequency Division Multiple Access (OFDMA) is the key radio access technology for the downlink while Single Carrier Frequency Division Multiple Access (SC-FDMA) is used for the uplink.

The introduction of LTE release 10, also known as LTE-Advanced, has brought some technological modifications in order to improve the overall capacity [33]. With the exception of carrier aggregation (CA), which is outside the scope of this dissertation, the PHY layer remains largely unchanged. Heterogeneous base stations have been introduced to the E-UTRAN to improve the overall spectral efficiency [34, 35]. LTE-A includes small cells to the existing e-NodeB network to increase the network capacity and to remove indoor and outdoor coverage holes. These small cells have to operate in co-channel deployment, sharing the spectrum with the pre-existing e-NodeBs [36]. The implementation of such a multi-tiered network presents complex challenges in terms of coordination between the entities, in order to avoid interference and to maximise the downlink performance. The following sections describe the properties of the different base station types discussed in this work and present the set of advantages and challenges they impose.

There are many more problems and scope of innovation in future mobile systems to improve the performance of systems based on the use of non-orthogonal multicarrier waveforms. The main hypothesis of this proposal is that the underlying design principles-synchronism and orthogonality of the physical layer of mobile radio systems constitute a major obstacle for the envisioned service architecture. Hence, there is a clear motivation for an innovative and in part disruptive re-design of the physical layer from scratch. In this project we will explore the inherent trade-offs between possible relaxation in orthogonality and synchronism and their corresponding impact on performance versus the required signal processing capabilities. The

## CONCLUSION & FUTURE SCOPE

project proposal will focus on implementation aspects of emerging MCM technologies suitable for future wireless multicarrier systems.

One of the main future scope of this work is the development of a flexible and dynamic resource allocation for the physical signals and verify if optimized pilot symbols placed at different locations in the resource grid give a variance in the performance. The features of LTE-A like carrier aggregation can also be carried out . This will allow for the definition of the fundamental building blocks and the related parameters including spectrum, bandwidth, multiple access schemes, waveform generation for LTE/LTE-A standards.

\*\*\*\*\*

## REFERENCES

- [1] Y. Wu and W. Y. Zou, "Orthogonal frequency division multiplexing: a multi-carrier modulation scheme," *IEEE Trans. Consum. Electron.*, vol. 41, no. 3, pp. 392-399, Aug. 1995.
- [2] S. Hara and R. Prasad, "*Multi-Carrier Techniques for 4G Mobile Communications*", 1<sup>st</sup> Edition, Artech House, Boston, 2003.
- [3] L. Hanzo, M. Munster, B. J. Chol, and T. Keller, "*OFDM and MC- CDMA for Broadband Multi-user Communications, WLANs and Broadcasting*," John Wiley & Sons, 2003.
- [4] Peled, A. and Ruiz, A.; "Frequency domain in data transmission using reduced computational complexity algorithms", Acoustics, Speech, and Signal Processing, IEEE International Conference on ICASSP '80, vol. 5, pp.964 –967, Apr. 1980.
- [5] T. Keller and L. Hanzo, "Adaptive multicarrier modulation: A convenient framework for time-frequency processing in wireless communications," *Proc. IEEE*, vol. 88, no. 5, pp. 611–640, May 2000.
- [6] L.J. Cimini, "Analysis and simulation of a digital mobile channel using orthogonal frequency division multiplexing," *IEEE Trans. Commun.* , vol. COM-33, pp. 665-675 July 1985.
- [7] Kalet, "The multitone channel," *IEEE Trans. Commun.* vol. 37, pp.119-124. Feb.1989.
- [8] ETSI EN 300 744 v1.4.1 (2001-01), "Digital video broadcasting (DVB-T); framing structure, channel coding and modulation for digital terrestrial television," 2001.
- [9] M. L. Dolez, E.T. Heald, and D.L. Martin, "Binary data transmission techniques for linear systems," *Proc. I.R.E*; vol. 45, pp. 656-661, May 1957.
- [10] <http://standards.ieee.org/getieee802/802.11.html>
- [11] P. A. Bello, "Selective fading limitations of the KATHRYN modem and some system design considerations," *IEEE Trans. Commun. Technol.*, vol. COM-13, pp. 320–333, Sept. 1965.
- [12] M. S. Zimmerman and A. L. Kirsch, "The AN/GSC-10 (KATHRYN) variable rate data modem for HF radio," *IEEE Trans. Commun. Technol.*, vol. COM-15, pp.197–205, April 1967.
- [13] P. A. Bello, "Selective fading limitations of the KATHRYN modem and some system design considerations," *IEEE Trans. Commun. Technol.*, vol. COM-13, pp. 320–333, Sept. 1965.
- [14] M. S. Zimmerman and A. L. Kirsch, "The AN/GSC-10 (KATHRYN) variable rate data modem for HF radio," *IEEE Trans. Commun. Technol.*, vol. COM-15, pp.197–205, April 1967.
- [15] R.W. Chang and R. A. Gibby, "A theoretical study of performance of an orthogonal multiplexing data transmission scheme," *IEEE Trans. Commun. Tech.*, vol. COM-16, pp. 529–540, Aug. 1968.
- [16] Orthogonal Frequency Division Multiplexing," U.S. Patent No. 3,488,445, Filed Nov. 14, 1966, Issued Jan. 6, 1970.

- [17] S. B. Weinstein and P. M. Ebert, "Data Transmission by Frequency-Division Multiplexing Using the Discrete Fourier Transform," *IEEE Trans. Commun. Tech.*, vol. COM-19, pp. 628–634, October 1971.
- [18] B. R. Saltzberg, "Performance of an efficient parallel data transmission system," *IEEE Trans. Commun. Tech.*, vol. COM-15, pp.805–813, Dec. 1967.
- [19] H. F. Marmuth, "On the Transmission of Information by Orthogonal Time Functions," *AIEE Trans; (communication and Electronics)*, vol. 79, pp. 248–255, July 1960.
- [20] S. B. Weinstein and P. M. Ebert, "Data Transmission by Frequency-Division Multiplexing Using the Discrete Fourier Transform," *IEEE Trans. Commun. Tech.*, vol. COM-19, pp. 628–634, October 1971.
- [21] J. S. Chow, J. C. Tu, and J. M. Cioffi, "A Discrete multitone transceiver System for HDSL applications," *IEEE J. Select. Areas Commun.*, vol. 9, no. 6, pp 895–908, August 1991.
- [22] P. S. Chow, J. C. Tu and J. M. Cioffi, "Performance evaluation of a multichannel transceiver system for ADSL and VHDSL services," *IEEE J. Selected Area*, vol., SAC-9, no.6, pp. 909-919, Aug. 1991.
- [23] R.V. Paiement, "Evaluation of single carrier and multicarrier modulation techniques for digital ATV terrestrial broadcasting," *CRC Report, no. CRC-RP-004*, Ottawa, Dec. 1994.
- [24] European Telecommunications Standards Institute (ETSI), *Radio Broadcasting Systems; Digital Audio Broadcasting (DAB) to Mobile, Portable and Fixed Receivers*, European Telecommunication Standard ETS 300 401, February 1995.
- [25] V. Engels and H. Rohling, 'Multilevel differential modulation techniques (64-DAPSK) for multicarrier transmission systems', *European Transactions on Telecommunications*, vol. 6, no. 6, pp. 633-640, November/December 1995.
- [26] G. Wornell, "Emerging applications of multirate signal processing and wavelets in digital communications", *Proceedings of the IEEE*, vol. 84, no. 4, pp. 586-603, April 1996.
- [27] A.J. Jones, T.A. Wilkinson, and S.K. Barton, 'Block coding scheme for reduction of peak to mean envelop power ratio of multicarrier transmission schemes', *Electronics Letters*, vol. 30, no. 25, pp. 2098{2099, 1994.
- [28] M.L. Moher and J.H. Lodge, "TCMP { A Modulation and Coding Strategy for Rician-Fading Channels", *IEEE Journal on Selected Areas in Communications*, vol. 7, no. 9, pp. 1347-1355, December 1989.
- [29] P. Höher, "TCM on frequency-selective land-mobile fading channels", in *Proceedings of the Tirrenia International Workshop on Digital Communications*, Tirrenia, Italy, September 1991, pp. 317-328.
- [30] O. Edfors, M. Sandell, J.J. van de Beek, S.K. Wilson, and P.O. Börjesson, "OFDM channel estimation by singular value decomposition", *IEEE Transactions on Communications*, vol. 46, no. 7, pp. 931-939, July 1998.

- [31] Y. Li, L.J. Cimini, Jr., and N.R. Sollenberger, "Robust channel estimation for OFDM systems with rapid dispersive fading channels", *IEEE Transactions on Communications*, vol. 46, no. 7, pp. 902-915, July 1998.
- [32] S.K. Wilson, R.E. Khayata, and J.M. Cio, "16-QAM modulation with orthogonal frequency-division multiplexing in a Rayleigh-fading environment", in *Proceedings of the IEEE Vehicular Technology Conference (VTC'94)*, Stockholm, Sweden, June 1994, pp. 1660-1664.
- [33] Jiang, T., & Wu, Y. (2008). An overview: Peak-to-average power ratio reduction techniques for OFDM signals. *IEEE Transactions on Broadcasting*, 54(2), 257–268.
- [34] Han, S. H., & Lee, J. H. (2005). An overview of peak-to-average power ratio reduction techniques for multicarrier transmission. *IEEE Wireless Communications*, 12(2), 56–65.
- [35] Marc, D., Behravan, A., Eriksson, T., & Pijoan, J. L. (2008). Evaluation of performance improvement capabilities of PAPR-reducing methods. *Wireless Personal Communications*, 47(1), 137–147.
- [36] Armstrong, J. (2002). Peak-to-average power reduction for OFDM by repeated clipping and frequency domain filtering. *IEEE Electronics Letters*, 38(8), 246–247.
- [37] Cimini, L. J., & Sollenberger, N. R. (2000). Peak-to-average power ratio reduction of an OFDM signal using partial transmit sequences. *IEEE Communication Letters*, 4(3), 86–88.
- [38] Yong, W., Ge, J., Wang, L., & Li, J. (2012). Reduction of PAPR of OFDM signals using nonlinear companding transform. *Wireless Personal Communications*. doi:[10.1007/s11277-012-0820-2](https://doi.org/10.1007/s11277-012-0820-2).
- [39] Yong, W., Ge, J., Wang, L., & Li, J. (2012). Reduction of PAPR of OFDM signals using nonlinear companding transform. *Wireless Personal Communications*. doi:[10.1007/s11277-012-0820-2](https://doi.org/10.1007/s11277-012-0820-2).
- [40] Davis, J. A., & Jedwab, J. (1999). Peak-to-mean power control in OFDM, Golay complementary sequences, and Reed-Muller codes. *IEEE Transactions on Information Theory*, 45(7), 2397–2417.
- [41] Yang, K., & Chang, S. (2003). Peak-to-average power control in OFDM using standard arrays of linear block codes. *IEEE Communication Letters*, 7(4), 174–176.
- [42] Ryu, H. G., Lee, J. E., & Park, J. S. (2004). Dummy sequence insertion (DSI) for PAPR reduction in the OFDM communication system. *IEEE Transactions on Consumer Electronics*, 50(1), 89–94.
- [43] Devlin, C. A., Zhu, A., & Brazil, T. J. (2008). Peak to average power ratio reduction technique for OFDM using pilot tones and unused carriers. In *IEEE radio and wireless symposium* (pp. 33–36).
- [44] Wen, J. H., Lee, S. H., Huang, Y. F., & Hung, H. L. (2008). A suboptimal PTS algorithm based on particle swarm optimization technique for PAPR reduction in OFDM systems. *EURASIP Journal on Wireless Communications and Networking*, 601346, 1–8.

- [45] Weng, C. E, Chang, C.W, Chen, C.H, & Hung, H.L. (2012). "Novel low-complexity partial transmit sequences scheme for PAPR reduction in OFDM systems using adaptive differential evolution algorithm," *Wireless Personal Communications*,. doi:[10.1007/s11277-012-0836-7](https://doi.org/10.1007/s11277-012-0836-7).
- [46] Lain, J. K., Wu, S. Y., & Yang, P. H. (2011). PAPR reduction of OFDM signals using PTS: A real-valued genetic approach, *EURASIP Journal on Wireless Communications and Networking*, 126, 1–8.
- [47] Jiang, T., & Wu, Y. (2008). An overview: Peak-to-average power ratio reduction techniques for OFDM signals. *IEEE Transactions on Broadcasting*, 54(2), 257–268
- [48] Wong, K. T., Wang, B., & Chen, J.-C. (2011). OFDM PAPR reduction by switching null subcarriers and data subcarriers. *IEEE Electronics Letters*, 47(1), 62–63.
- [49] Tolochko, I., & Faulkner, M. (2002). Real time LMMSE channel estimation for wireless OFDM systems with transmitter diversity. In *Proceedings of the 56th IEEE VTC*, Vancouver, Canada (pp. 1555–1559).
- [50] Patra, J. C., Pal, R. N., Baliarsingh, R., & Panda, G. (1999). Nonlinear channel equalization for QAM signal constellation using artificial neural networks. *IEEE Transactions on Systems, Man, and Cybernetics*, 29(2), 254–262.
- [51] Siu, S., Gibson, G. J., & Cowan, C. F. N. (1990). Decision feedback equalization using neural network structures and performance comparison with standard architecture. *Proceedings of the Institution of Electrical Engineers*, 137(pt. 1), 221–225.
- [52] Zhang, L., & Zhang, X. (2007). MIMO channel estimation and equalization using three-layer neural network with feedback. *Tsinghua Science and Technology*, 12(6), 658–662.
- [53] Sun, J., & Yuan, D. F. (2006). Neural network channel estimation based on least mean error algorithm in the OFDM systems. *Advances in Neural Networks*. Berlin: Springer.
- [54] 3rd Generation Partnership Project (2013) 3GPP – Releases, [www.3gpp.org/releases](http://www.3gpp.org/releases) (accessed 15 October 2013).
- [55] T. Pollet, M. Van Bladel, and M. Moeneclaey, "BER sensitivity of OFDM to carrier frequency offset and Wiener phase noise," *IEEE Trans. Commun.*, vol. 43, no. 2, pp. 191–193, Feb. 1995
- [56] P. Tan and N. C. Beaulieu, "Reduced ICI in OFDM systems using the 'better than' raised-cosine pulse," *IEEE Commun. Lett.*, vol. 8, no. 3, pp. 135–137, Mar. 2004.
- [57] Y. Wang, Z. Zhang, and Y. Chen, "BER analysis of BPSK OFDM systems with residual frequency and timing offsets over frequency selective Rayleigh fading channels," *J. Comput. Inform. Syst.*, vol. 8, no. 24, pp. 10349–10357, Dec. 15, 2012.
- [58] K. Sathanathan and C. Tellambura, "Probability of Error Calculation of OFDM Systems with Frequency Offset," *IEEE Trans. on Commun.* vol. 49, no. 11, pp. 1884–1888, Nov 2001.

- [59] L. Rugini and P. Banelli, "BER of OFDM systems impaired by carrier frequency offset in multipath fading channels," *IEEE Trans. on Wireless Commun.*, vol 4, no. 5, pp.2279-2288, Sep 2005.
- [60] N. C. Beaulieu and P. Tan, "On the effects of receiver windowing on OFDM performance in the presence of carrier frequency offset," *IEEE Trans Wireless Commun.* vol. 6, no.1, pp. 202-209, Jan 2007.
- [61] P. Dharmawansa, N. Rajatheva, and H. Minn, "An exact error probability analysis of OFDM systems with frequency offset," *IEEE Trans. Commun.*, vol. 57, no. 1, pp. 26-31, Jan. 2009.
- [62] R. Uma Mahesh and A. K. Chaturvedi, "Closed form ber expressions for BPSK OFDM systems with frequency offset", *IEEE Trans. on Commun.* vol. 14, no. 8, pp. 731-733, Aug 2010.
- [63] Wang et al, "BER analysis of BPSK OFDM systems with CFO and STO over frequency selective fading channels", *IEEE Trans. on Commun.* vol. 29, no. 8, pp. 137-142, Aug 2008.
- [64] U. Mahesh and A. K. Chatuvedi, "Closed form BER expressions for BPSK OFDM systems with fractional timing offset and carrier frequency offset," in *Proc. Nat. Conf. Commun.*, Kharagpur, India, 2012, pp. 1-4.
- [65] A. Kumar, M. Magarini, H. D. Joshi, and R. Saxena: "Exact SER Analysis of FrFT-based QPSK OFDM system over Frequency Selective Rayleigh Fading Channel with CFO", submitted to *Electron. Lett.*, May 2015